Solar and Space Physics (Heliophysics) Decadal Survey 2024-2033

Coronal Microscale Observatory

Mission Concept Study Final Report

February 2023

Study Leads/POC: D. M. Rabin and Anne-Marie Novo-Gradac
NASA Goddard Space Flight Center

Study Team

A. Winebarger[1], N. Viall[2], N. Reginald[2,3], D. Rabin[2], J. Parker[2], A. Novo-Gradac[2], J. Newmark[2], J. Klimchuk[2], G. Kerr[2], A. Inglis[2], L. Golub[4], K. Denis[2], I. De Moortel[5], A. Daw[2], P. Chamberlin[6], P. Calhoun[2]

[1] NASA Marshall Space Flight Center
[2] NASA Goddard Space Flight Center
[3] The Catholic University of America
[4] Harvard-Smithsonian Center for Astrophysics
[5] University of St. Andrews and University of Oslo
[6] Laboratory for Atmospheric and Space Physics, University of Colorado Boulder

Study Engineering Support Institutions

GSFC Mission Design Laboratory
GSFC Cost Estimating, Modeling, and Analysis Office
GSFC Optical Communications Team
University of Illinois Urbana-Champaign
University of Colorado Laboratory for Atmospheric and Space Physics
Harvard-Smithsonian Center for Astrophysics
GSFC Science Proposal Support Office

Table of Contents

Executive Summary

The Coronal Microscale Observatory (CMO) addresses the following program-level science objective of the Solar-Terrestrial Probes (STP) program: “Understand the fundamental physical processes of the space environment from the Sun to Earth, to other planets, and beyond to the interstellar medium.” The goals of CMO are:

- Determine the physical mechanisms that drive primary heating events (nanoflares and wave heating) in the solar corona.
- Determine the physical conditions that produce clusters of primary heating events and bright coronal loops.
- Determine how fine-scale substructure influences the initiation and evolution of flares of sizes ranging from nanoflares to small flares.
- Understand the formation of the solar wind, particularly the slow wind.

CMO’s mission science objectives in pursuit of these goals are:

- Determine the relative importance of magnetic reconnection, wave heating, or other mechanisms in producing primary heating events.
- Measure the spatial and temporal properties of primary heating events.
- Determine what causes primary heating events that manifest as coronal loops.
- Measure fine-scale substructure in flares of various sizes.
- Determine and compare the energy releases accompanying weak and strong guide-field reconnection.
- Determine how much solar wind originates from different source regions on the Sun, particularly from active regions, quiet Sun, and coronal hole boundaries.
- Determine how much solar wind is released through magnetic reconnection, and the height of the reconnection.
- Measure how much thermal and kinetic energy is associated with the reconnection events that release closed-magnetic-field plasma into the solar wind.
- Determine the relationship between primary heating events and the thermal and kinetic energy of the solar wind on intermediate and global scales.

CMO’s high-level measurement requirements are:

- Image coronal plasma with spatial resolution as high as 20 km (0.03 as).
- Understand the nanoflare heating and cooling process by measuring the evolution of plasma properties over a wide range of temperature (0.2–10 MK) and column density with time resolution (~10 s) sufficient to capture rapid heating.
- Measure plasma flow, temperature, and density from the low corona (down to 1.05 Rs) into the middle corona (to 5 Rs) with angular resolution high enough (5 as) to determine the pervasiveness and influence of small-scale structure and to image wind released through reconnection events.
- Measure the mesoscale coronal structure at overlapping heights to connect the small-scale processes through the mesoscales to the global-solar wind.

To accomplish its science objectives, CMO positions three spacecraft and three instruments near the Sun-Earth L1 Lagrange point. One instrument is a cluster of 6 extreme ultraviolet (EUV) “microscopes”, each imaging a small field of view on the Sun with very high angular resolution in a narrow wavelength band sensitive to emission from plasma in a limited temperature range. The second instrument is a multiband, full-disk coronagraph. The third instrument is a finescale EUV imager that is a bridge between the microscale field and full-disk

EUV imagers on other missions as well as the CMO coronagraph (for near- and off-limb EUV targets). The craft nearest the Sun houses diffractive lenses (photon sieves) that form images on the intermediate craft 100 m away, which carries 6 EUV detectors. The intermediate craft also carries an external occulting disk for the third craft, 200 m farther away, that carries the internally occulted coronagraph.

The three CMO craft fly in precise formation to ensure that the EUV imagers point to a desired target on the Sun and the external occulter accurately blocks the solar disk. The novel mission architecture arises from the intrinsically long EUV focal length of the photon sieves, which are uniquely capable of achieving nearly diffraction-limited EUV imaging, and the distant external occulter, which enables visible-light imaging of the corona very close to the solar limb with undiminished angular resolution.

The GSFC Mission Design Laboratory concluded that CMO's mission-level requirements—including spacecraft buses, launch vehicle, trajectory, orbit, propulsion, power, onboard data storage, communications, and concept of operations—can be met with existing technology.

CMO's key technologies are photon sieves, which have been demonstrated in the laboratory and are slated to fly on the VISORS CubeSat mission in 2024; and a suite of metrology instruments that provide information to a guidance, navigation, and control (GNC) system that directs liquid ionic thrusters to maintain formation. Although based on relatively conventional technology and VISORS software, the metrology/GNC subsystem is considered to be the most significant technology risk because of its challenging precision requirements.

1. Science Investigation

A white paper for the 2024 Decadal Survey of Solar and Space Physics, “Observing Coronal Microscales and their Connection with Mesoscales,” discusses the scientific motivation for the Coronal Microscale Observatory (CMO) and the principal questions it is designed to address [1]. This report therefore provides only a thumbnail sketch of the CMO science investigation in §§1.1-1.2 but includes a preliminary Science Traceability Matrix in §1.3 that could not be included in the white paper.

1.1. Solar Terrestrial Probes Science Objectives

CMO addresses the following program-level science objective of the Solar Terrestrial Probes (STP) program: “Understand the fundamental physical processes of the space environment from the Sun to Earth, to other planets, and beyond to the interstellar medium” [2]. In the STP program, “Successive missions target the ‘weakest links’ in the chain of understanding” [2]. CMO targets three major knowledge gaps in our understanding of the solar corona and the solar wind.

Why the Sun has a tenuous upper atmosphere some 1000 times hotter than the photosphere is a fundamental open problem in space plasma physics despite decades of study. Observations by soft x-ray and extreme ultraviolet (EUV) imagers, which remotely sense spectral lines emitted from highly ionized coronal elements, have provided important clues regarding the nature of the heating. However, current instrumentation cannot resolve the structure of the heated regions, and the heating mechanisms remain unknown. A leading hypothesis is that, in most of the corona, heating is confined to narrow current sheets in which energy is dissipated despite the low resistivity of the coronal plasma. The characteristic width of these dissipation regions is estimated to be on the order of 100 km [3] [4]. We call time-variable energy releases on these scales *primary heating events* without limiting the physical mechanism(s) that cause them. Observing the heating substructure will prove to be key in testing reconnection and wave heating theories as they are refined in response to new data. Thus, **the first knowledge gap (KG1) to be filled is direct observational knowledge of primary heating events on spatial scales significantly smaller than 100 km**.

The consensus view on the solar wind is that there are many types of solar wind that exhibit different plasma characteristics—e.g., plasma density, elemental composition, velocity, temperature, variability, and mesoscale structures—that encode how those types of solar wind were likely formed. Different types of solar wind result from the time-history of solar wind formation [5], how it was heated in the low corona, how it was released into the heliosphere, and how it continues to be accelerated and heated through the middle and high corona. Thus, **the second targeted knowledge gap (KG2) is the formation of the solar wind and the resulting mesoscale solar wind structures**.

The third knowledge gap (KG3) is the relationship of primary heating events, singly or collectively, to the formation of solar wind in specific environments, particularly active regions, quiet Sun, and coronal hole boundaries. The answers to the objectives addressed by CMO involve the fundamental physics of turbulence, waves, and magnetic reconnection, and how they occur in the unique solar environment. This has implications for how the Sun forms the heliosphere, Sun-Earth interactions (including space weather), and stellar environments.

It has been fifty years since Parker [6] postulated the inevitability of current sheets in the corona and their centrality to coronal heating in active regions. Since then, theory, simulations, and space-based observations have advanced dramatically; but observation has still not directly confronted theory—we have not seen “inside the machine.” We must break that barrier to move

the field of coronal heating definitively forward. At the same time, as emphasized in white papers by Klimchuk et al. [7], Vourlidas et al. [8], Kepko et al. [9], and others, major advances in understanding the Sun-heliosphere system depend on linking fine-scale observations and modeling to mesoscale and large-scale counterparts. Thus, the Coronal Microscale Observatory includes a coronagraphic instrument that, in combination with other space-based assets, will forge that connection for the solar corona.

1.2. Mission Concept Science Objectives

1.2.1. Microscales: Primary Coronal Heating Events

Observations by soft x-ray and extreme ultraviolet (EUV) imagers have provided important clues to the nature of coronal heating. However, current instrumentation cannot resolve the structure of the heated regions, and so the properties and mechanisms of heating remain poorly determined. Definitive progress will require a quantum improvement in spatial resolution, which the CMO mission will provide.

It is widely believed that coronal heating takes two basic forms: (1) the sudden release of stored magnetic energy by fast magnetic reconnection (Figure 1) [10], and (2) the nonlinear dissipation of wave energy (Figure 2) [11]. These are often referred to as DC and AC mechanisms, respectively, with the first also being called nanoflare heating. Both mechanisms are impulsive in nature, and wave heating is sometimes put in the nanoflare category. Here we reserve the term “nanoflare” for reconnection-based heating.

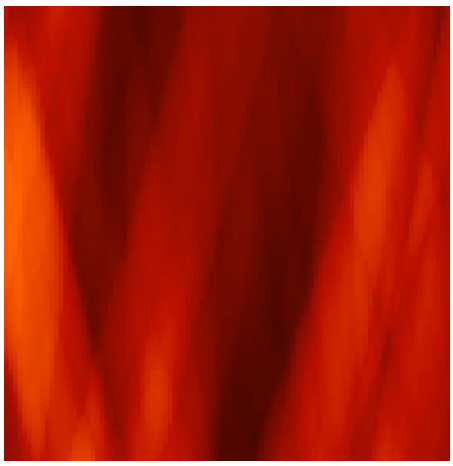

Figure 1. Physics-based simulated image of nanoflare heated strands as observed in Fe XVIII 9.39 nm (T= 5–10 MK) (Klimchuk 2021). The field of view is 1000 x 1000 km^2. Because impulsively heated nanoflare strands cool quicky, the line-of-sight confusion is smaller, and the contrast higher, for high-temperature lines.

Nanoflare and wave heating both occur on the Sun, but their relative importance in different solar regions has not been established. Likely, nanoflares dominate in active regions, and waves dominate in coronal holes and the solar wind. Which is more important in the quiet Sun is an open question. CMO will establish definitively the roles of nanoflares and waves in all these regions.

The more extensive discussion in the CMO white paper [1] identifies the following key science objectives related to coronal microscales:

SO1. Determine the relative importance of magnetic reconnection, wave heating, or other mechanisms in producing primary heating events.

SO2. Measure the spatial and temporal properties of primary heating events.

SO3. Determine the cause of concentrations of primary heating events that manifest as coronal loops.

SO4. Measure fine-scale substructure in flares of various sizes.

SO5. Determine how the energy release associated with strong guide-field reconnection compares with weak guide-field reconnection in the corona.

1.2.2. Connecting Microscales to the Solar Atmospheric System

The regions of the solar atmosphere—photosphere, chromosphere, transition region, low-middle-high corona, and solar wind—comprise a system of systems with cross-regional and

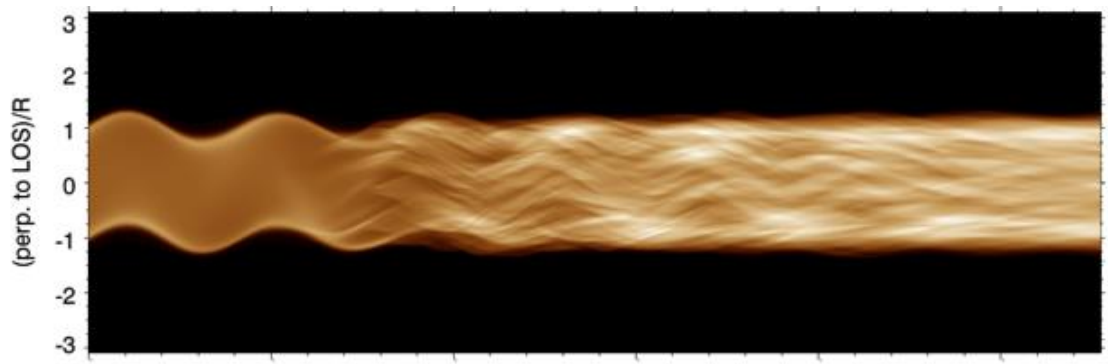

Figure 2. Simulated observation in Fe XII (193 Å) of a loop heated by the resonant absorption of Alfvén waves [11]. Each tick on the horizontal axis is a minute of time. The vertical axis is relative intensity as a function of position across the loop axis.

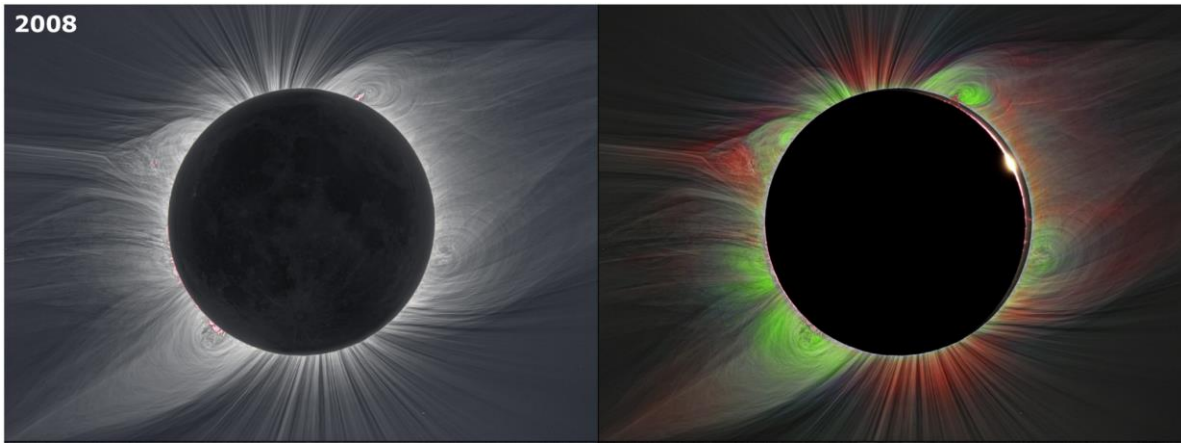

Figure 3. Eclipse images [12]. Left: white light emission, a proxy for density. Right: overlay of white light with Fe XI 789.2 nm (red) and Fe XIV 530.3 nm (green) emission, proxies for coronal temperature. This image illustrates the complex structure of the corona. The CMO coronagraph will measure radial flow speed as well as temperature and density.

cross-scale coupling. Emergent phenomena, i.e., physical behaviors that emerge only when the parts interact in a wider whole, are revealed when studying cross-scale and cross-regional parts of the solar atmospheric system. CMO also incorporates a coronagraph that will measure the speed, temperature and density of the coronal plasma (Figure 3) to connect microscale primary heating events to mesoscale and larger system scales. The discussion in the CMO white paper [1] leads to the following key science objectives related to the formation and structure of the solar wind and their relationships to primary heating events.

SO6. Determine from where on the Sun the solar wind is released. This is achieved by tracking the connectivity of structures through the corona and comparing with the speed.

SO7. Determine how much solar wind mass is released through reconnection events and at what height reconnection events occur. This is achieved by measuring density structures and the associated velocities as a function of time for closed magnetic field structures.

SO8. Measure how much thermal and kinetic energy is associated with the reconnection events that release closed-magnetic-field plasma into the solar wind.

SO9. Determine the relationship between primary heating events in the low corona (measured by the EUV imager) and the kinetic and thermal energy of the inner solar wind (density, temperature, and speed). Determine the scales at which global energy relationships break down.

1.3. Mission Concept Science Traceability

1.3.1. Measurement Requirements and STM

CMO's high-level measurement requirements, as derived from the science requirements in §1.1 and §1.2 are:

M1. Image coronal plasma with spatial resolution as high as 20 km (0.03 as).
M2. Understand the nanoflare heating and cooling process by measuring the evolution of plasma properties over a wide range of temperature (0.2–10 MK) and column density with time resolution (~10 s) sufficient to capture rapid heating.
M3. Measure plasma flow, temperature and density from the low corona (down to 1.05 Rs) into the middle corona (to 5 Rs) with angular resolution high enough (<5 as) to determine the pervasiveness and influence of small-scale structure and to image wind released through reconnection events.
M4. Measure the mesoscale coronal structure at sufficient overlapping heights (to 2 Rs) to connect the small-scale processes through the mesoscales to the global-solar wind.

The CMO spectral lines are given in Table 1. A high-level CMO Mission Concept Science Traceability Matrix (STM) is shown in Table 2 (foldout, p. 5).

1.3.2. Science Closure

In accordance with the guidance received for this report, science closure is interpreted as closing a program-level knowledge gap (KG1–3, §1.1) to the degree that key associated science objectives (SO1–9 above) are achieved or, as often happens, transformed in response to new and unexpected findings.

Ion	Wavelength (nm)	Temperature (MK)	Diffraction Limit (mas)
Fe XXI	12.88	7 - 11 - 19	19
Fe XVIII	9.39	3 - 7 - 13	14
Fe XV	28.42	1.5 - 2.2 - 4	42
Fe IX	17.11	0.4 - 0.8 - 1.5	25
Ne VII	46.52	0.3 - 0.5 - 0.8	69
He II	30.38	0.05 - 1	45

Table 1. CMO carries 6 EUV "microscopes" with broad temperature coverage. Temperatures are given at the peak of the contribution function and at 10% of peak on either side. Only a crude range is given for He II 30.4 nm because the line formation is complex. 1 mas = 0.001 arc second (as).

If the EUV telescope cluster performs nominally (M1–M2) for three years, SO1 and SO3 will be fully achieved. SO2 will be substantially achieved and likely transformed in some respects, as both wave heating and reconnection heating are complex mechanisms with many possible variants. SO4 should be achieved with a three-year (nominal) or longer mission to catch GOES C-class or larger flares. If the challenging alignment stability of the two spacecraft that constitute the photon sieve telescope system is subnominal, even by a factor of three, SO1–4 may still be largely achieved with a three-year mission because the imagers frame rapidly (5 Hz), so image smear caused by formation drift can be removed post-facto with some loss of signal-to-noise ratio.

Table 2. Mission Concept Science Traceability Matrix

Science Objective	Science Requirement	Measurement	Instrument	Functional Requirement

Determine the relative importance of microscale reconnection heating and wave heating in the solar corona.	Determine the magnitudes, durations, and frequencies of primary heating events. Distinguish drifting heating (waves) from spreading heating (reconnection). Compare reconnection heating in different magnetic environments (plasmoids vs. turbulence)	Measure the amount of very hot (>5 MK) and hot (1–5 MK) plasma with spatial resolution <100 km on the Sun. Measure the spatial distribution and temporal distribution of temperature increases and density structures as a function of many heating and cooling cycles at a given location. Measure this at flux tube apices (coronal temperatures 1–10 MK) and at flux tube footpoints (transition region, 0.2–1 MK).	• Six co-aligned, narrowband EUV microscale imagers (EMIT instrument)
			  • Temperature sensitivity spanning 0.2–10 MK
			  • Angular resolution 0.02–0.06 as
			  • Field of view 20x20 as^2
			  • Cadence 10–30 s
			  • Duration of observation sequence ~1 hr
				• Halo orbit at Sun-Earth Lagrange Point 1
				• Two spacecraft separated by 100 m holding precise formation
				• Mission duration of 3 yr to sample quiet regions and active regions of different types

Determine the properties of primary coronal heating events.	Measure the sizes, shapes, and evolution of primary heating events. Observe how these structures interact to produce nanoflares and how the structures are in turn modified and rearranged by nanoflare reconnection. Measure the conditions that result in clusters of primary heating events that produce bright coronal loops.	Measure density and temperature structures and compare to inferred <100 km elementary structure scale. Measure the relationship of structures in temperatures and density with groups of heating events (increases in temperature), and avalanches of heating events over several heating and cooling cycles. Measure this at flux tube apices (coronal temperatures 1–10 MK) and at flux tube footpoints (transition region, 0.2–1 MK).	• EMIT instrument
			
			• EUV finescale imager (EFI instrument) *
			  • Two narrow bands (T~1 MK, T~3 MK)
			  • Angular resolution 0.25 as
			  • Field of view 3x3 arcmin^2
			  • Cadence 10 s	

Determine the importance of substructures in solar flares of different magnitudes	Determine the prevalence and size distribution of reconnection plasmoids. Determine similarities and differences among events spanning many orders of magnitude (full, micro, nano flares). Measure how the energy release accompanying strong guide-field reconnection compares with weak guide-field reconnection.	Measure the spatial and temporal distributions of temperature and density structures during individual flare events spanning several orders of magnitude. Measure this at flux tube apices (coronal temperatures 1-10 MK) and at flux tube footpoints (transition region, 0.2–1 MK).		• Halo orbit at Sun-Earth Lagrange Point 1 • Two spacecraft separated by 100 m holding precise formation • Mission duration of 3 yr to observe flares at least as large as C-class

Determine how the solar wind is formed.	Determine from where on the Sun the solar wind is released.	Measure plasma flow via brightness enhancements (density structures) and their optical motion. Measure the nonradial connectivity continuously from the low corona through the transition to the upper corona where radial flows/structure dominate.	• Externally occulted, multiband and emission line coronagraph (MBC instrument)
			  • Continuous observations
			  • Field of view 1.05–5 Rs
			  • Cadence ≤10 s
			  • Angular resolution 5.5 as
				• Halo orbit at Sun-Earth Lagrange Point 1
				• Two spacecraft separated by 200 m holding precise formation
				• Mission duration of 3 yr to observe a sufficient range of global solar magnetic configurations

	Determine how much solar wind is released through magnetic reconnection and at what heights.	Image the time-dependent increases of T and N when hotter, denser plasma from closed-fields is released onto cooler, more tenuous open field lines. Measure the density and temperature structures as they advect outward.		
	Determine how much thermal and kinetic energy is associated with reconnection events that release closed-field plasma into the solar wind. Measure the solar wind acceleration and temperature as a function of distance from the Sun and solar latitude.	Globally measure N, V, and T as a function of latitude and distance from Sun. Determine global distribution of acceleration energy and thermal energy.		
	Determine the relationship between primary heating events in the low corona and the kinetic and thermal energy of the solar wind on mesoscales.	Measure the physical properties and evolution of primary heating events in a near-limb field of view. Follow the structural evolution of the 1–3 MK corona in a larger, overlapping field of view that extends farther off the limb. Measure N, V, and T in the low- and mid-corona above those fields of view.	• EMIT • EFI • MBC	• Halo orbit at Sun-Earth Lagrange Point 1 • Three spacecraft separated by 100–300 m holding precise formation • Mission duration of 3 yr to sample multiple quiet and active regions and to observe a sufficient range of global solar magnetic configurations.

* The EFI instrument was not included in the Mission Design Lab study but has since been judged to be an important component of the mission concept. The estimated cost of adding EFI is included in the mission cost estimate (§5.2).

If the coronagraph and the EUV telescopes perform nominally (M1–4) for one year, SO5 (as well as SO1–4) will be largely achieved. SO6–8 should be achieved with a three-year nominal mission; SO9 is a broad objective that will be greatly advanced but not to full closure. If the EUV telescopes fail, progress on SO6–9 can be made with the coronagraph and data from other space-based EUV imagers.

Descopes

In terms of both science and cost, by far the most consequential descope would be the coronagraph instrument. Some progress could be made on SO5 with the CMO EUV telescopes and data from a ground-based multi-band coronagraph that observes close to the solar limb [13], but SO6–9 would not be achieved. The consequence would be a dramatic reduction in the scope and cross-systems focus of CMO science. SC3 and the occulter on SC2 (see Figure 4) would be eliminated. Data volume would be reduced by 30-40%. The metrology system would be modestly (but not dramatically) simplified.

Neither reducing the number of photon sieves (wavelength channels) nor descoping the EUV finescale imagers would have a significant effect on total mission cost.

2. Mission Concept Investigation

2.1. Overview

To accomplish its science objectives, CMO positions three spacecraft and three instruments in a quasi-halo orbit around the Sun-Earth L1 Lagrange point (Figure 4). The Extreme Ultraviolet Microscale Telescopes (EMIT) instrument comprises 6 EUV “microscopes”, each imaging a small field of view on the Sun with very high angular resolution in a narrow wavelength band sensitive to emission from plasma in a limited temperature range. The second instrument is a multi-band, externally occulted coronagraph (MBC). The third instrument is the EUV Finescale Imager (EFI). EFI is a powerful instrument for studying active region structure and dynamics; it also functions as a bridge between the EMIT field of view and full-disk EUV imagers on other missions as well as the CMO coronagraph (for near- and off-limb EUV targets). The craft nearest the Sun (SC1) houses diffractive lenses (photon sieves) that form images on the intermediate craft 100 m away (SC2), which carries 6 EUV detectors. A fixed 2.5-m diameter sunshade on SC1 blocks solar light outside the field of view of the microscale imagers from reaching the EUV detectors. SC2 carries a fixed external occulting disk for the third craft (SC3), 200 m farther away, that carries the internally occulted coronagraph.

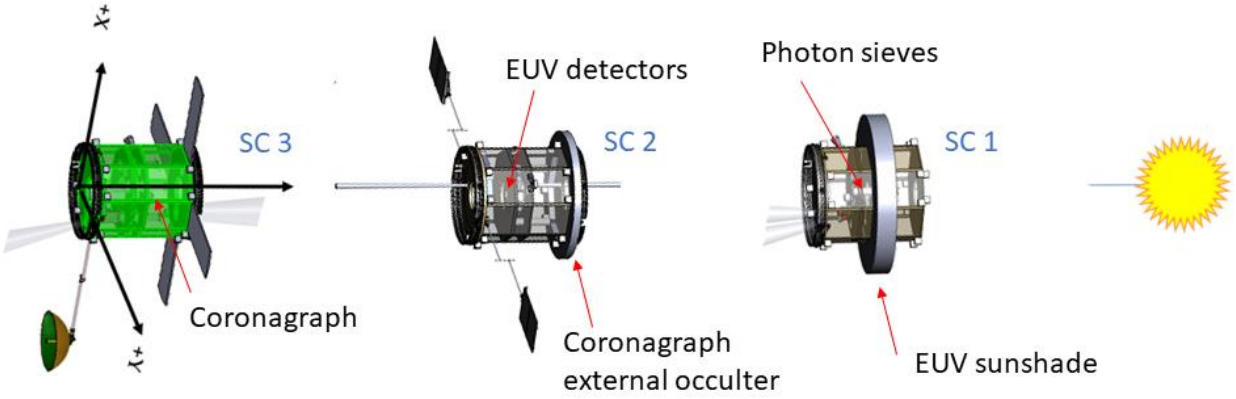

Figure 4. Schematic illustration of the Coronal Microscale Observatory.

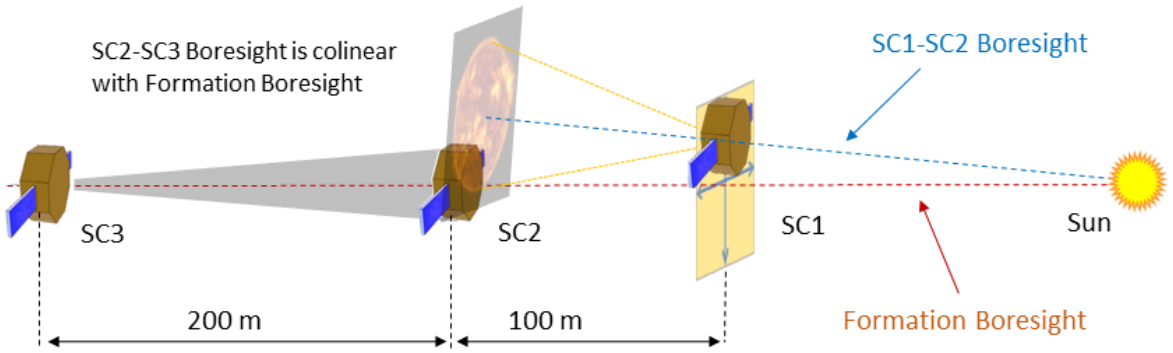

Figure 5. CMO's precise formation requires both position and attitude control to achieve and maintain the boresight desired for each instrument.

The three craft fly in precise formation to ensure that EMIT points to a desired target on the Sun and the external occulter accurately blocks the solar disk. To achieve and maintain precise formation, the relative position between each spacecraft pair is measured continuously by a Relative Position Sensing System (RPSS). Data from the RPSS are ingested by a guidance, navigation, and control (GNC) algorithm, based on software developed for the RPSS and for the VISORS mission, that commands low-force thrusters to adjust the position of each spacecraft.

The novel mission architecture arises from (1) the intrinsically long EUV focal length of the photon sieves, which are uniquely capable of achieving nearly diffraction-limited EUV imaging; and (2) the distant external occulter, which enables visible-light imaging of the corona very close to the solar limb with undiminished angular resolution. The L1 location provides an uninterrupted view of the Sun and a low gravity-gradient environment that enables CMO to maintain formation for at least 5 years.

EMIT and MBC are "distributed" instruments that require cooperative placement of two spacecraft. For instruments mounted on a single spacecraft, the attitude of the spacecraft (or an independent pointing mechanism) defines the center of the field of view (instrument boresight). In contrast, an EMIT photon sieve acts much like an ideal thin lens. Tilting the lens on SC1 with respect to incoming parallel rays does not move the focal point in the image plane on SC2, which is taken for simplicity as a fixed reference. Rather, the line connecting the vertex of the lens to the center of the image sensor must be changed by moving SC1 transversely to that line (Figure 5). For MBC, the boresight of the camera on SC3 must point to the center of the Sun *and* pass through the center of the external occulter. SC3 may need to move transversely to SC2 to achieve and maintain this singular "formation boresight". The SC1-SC2 separation is small enough that EMIT can point anywhere on the Sun by translating SC1 off the formation boresight without SC1 appearing in the MBC field of view. SC1 and SC3 have conventional requirements for 3-axis attitude stabilization because they carry self-contained cameras (for EFI and MBC) that maintain individual boresights. The attitude requirements on SC2 are loose, although in practice it makes more sense to implement the same attitude system on each spacecraft. CMO's formation alignment requirements are summarized in Table 3. Figure 6 illustrates the relative sizes of the EMIT and EFI fields of view as seen against a portion of the MBC field of view.

Primary propulsion for large scale maneuvers and orbit insertion is provided by a hydrazine monopropellant system. Fine positioning and attitude adjustments will be made using ionic liquid thrusters. Each ionic thruster provides up to 0.45 mN of thrust and is a fully independent unit with its own fuel reserve. Each spacecraft carries 24 separate ionic thrusters distributed over the body of the spacecraft. The number of thrusters ensures reliability and graceful degradation as

the fuel in each thruster is consumed over the life of the mission. There are no reaction wheels on the three spacecraft because the ionic thrusters provide all attitude adjustments.

Table 3. Formation alignment requirements

		SC1	SC2	SC3
Longitudinal separation relative to SC2 along formation boresight	Requirement (m)	100	N/A	-200
	Knowledge (mm)	5	N/A	5
	Control (mm)	15	N/A	15
	Stability (mm s^{-1})	0.5	N/A	0.5
Transverse linear offset from formation boresight	Requirement (mm)	Variable	N/A	0
	Knowledge (mm)	0.01	N/A	0.3
	Control (mm)	0.3	N/A	1
	Stability (mm s^{-1})	0.03	N/A	0.1
Attitude relative to formation boresight	Requirement (as)	Variable	0	0
	Knowledge (as)	2	20	2
	Control (as)	7	60	7
	Stability (smear) (as s^{-1})	0.1	1	0.1

CMO is a Class C+ mission with selective redundancy. Mission life is 3 years with a goal of 5 years. The three spacecraft buses are designed with high commonality. CMO can be launched by several existing vehicles (including Falcon 9FT) and is compatible with the ESPA ring payload adapter.

The baseline communications design provides for approximately 12Tb/day to be transmitted via Ka-band to ground stations of the NASA Near Space Network. A preferred optical communications enhancement (Appendix F) would triple the data rate while reducing mass and power.

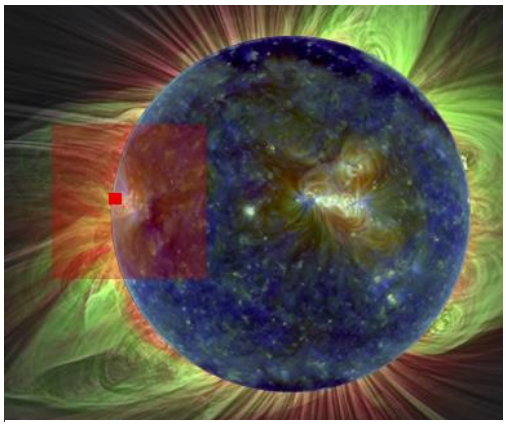

Figure 6. EMIT (solid red square) and EFI (transparent orange square) fields of view against a portion of the MBC field of view, which extends to 5 Rs. The composite eclipse image [12] is from 2017 August 2021. The cotemporal EUV disk image is a composite of three SDO AIA channels (21.1/19.3/17.1 nm).

Organization Chart

An organization chart is shown in Figure 7. Because of the present maturity level of the mission concept (§2.2), some key personnel are not named. The present Science Team, which is expected to grow considerably as science and instrument partnerships are established, is shown in Table 4.

2.2. Concept Maturity Level

CMO is an early-stage “stretch” mission concept. The scientific objectives presented in §1 are bold—far from incremental—yet fully motivated by well-defined knowledge gaps. To enable space-based photon sieve imaging, CMO requires significant but incremental technology development as described in §2.3.1.The other two CMO instruments are adaptations of existing instruments.

The MDL (Mission Design Lab)study of CMO concluded that mission-level requirements—including spacecraft buses, launch vehicle, trajectory, orbit, propulsion, power, onboard data storage, communications, and concept of operations—can be met with existing technology. Under ordinary circumstances, the instruments would have been studied by the Instrument Design Lab (IDL) before proceeding to the MDL. The schedule of the ROSES solicitation did not permit this in the case of CMO.

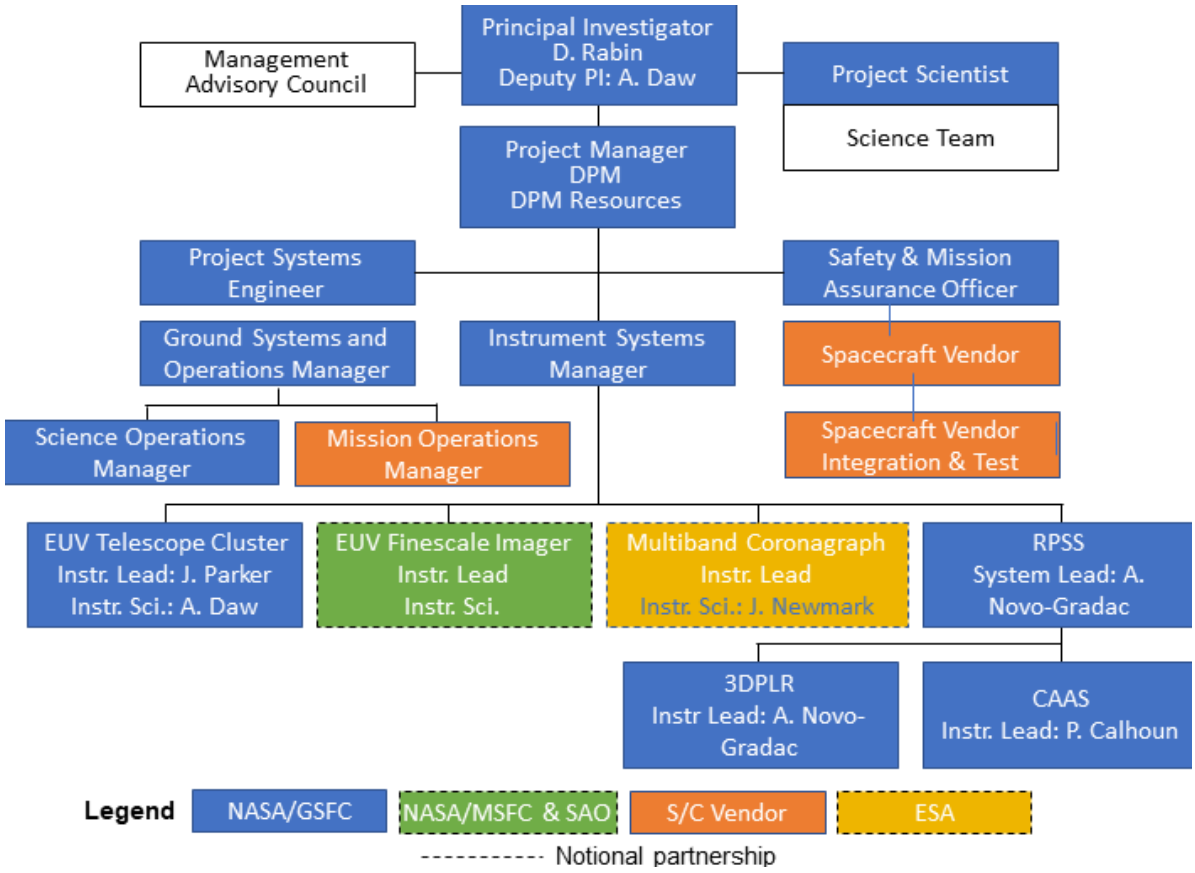

Figure 7. CMO organization chart.

The CMO concept is judged to be at Concept Maturity Level 3–4 based on the following considerations:

1. The study by the GSFC Mission Design Laboratory (MDL) produced a point design that satisfies the high-level Mission Concept Science Traceability Matrix in §1.3.1. The design
   - is specified to the subsystem level with respect to volume, mass and power;
   - includes high-level CAD for the spacecraft buses and the placement within them of instruments as well as avionics, propulsion, power, and communications components;
   - identifies a suitable orbit and launch vehicles capable of delivering the full payload to that orbit;

Table 4. CMO Science Team.

Nicholeen Viall	GSFC (Team Lead)
Adrian Daw	GSFC
Amy Winebarger	MSFC
Andrew Inglis	The Catholic University of America
Anne-Marie Novo-Gradac	GSFC
Daniel Seaton	Southwest Research Institute
Douglas Rabin	GSFC
Eliad Peretz	GSFC
Emily Mason	Predictive Science, Inc.
Farzad Kamalabadi	U. Illinois Urbana-Champaign
Graham Kerr	The Catholic University of America
Ineke de Moortel	U. St. Andrews, U. Oslo
James Klimchuk	GSFC
Jeffrey Newmark	GSFC
Joel Allred	GSFC
Leon Golub	Harvard -Smithsonian Center for Astrophysics
Matthew West	Southwest Research Institute
Natchimuthuk Gopalswamy	GSFC
Nelson Reginald	The Catholic University of America
Philip Chamberlin	U. Colorado Laboratory for Atmospheric and Space Physics
Steven Christe	GSFC

- presents a concept of operations from commissioning to end of mission;
- specifies a baseline communications system that meets minimum mission requirements;
- has been subjected to cost-risk analysis by the GSFC Cost Estimating, Modeling and Analysis (CEMA) Office;

2. The MDL point design satisfies basic attributes of CML 4 but cannot be considered a Preferred Design Point because:

   - The STM is still developing and requires a higher level of detail.
   - The instruments are not designed at the CAD level.
   - One instrument (EUV finescale imager) is currently judged to be an important component of the mission concept but was not included in the MDL study.
   - A key tradeoff (radio versus optical communications) was not considered by the MDL study, although a subsequent independent study of the optical communications option was conducted.

2.3. Technology Maturity

2.3.1. Enabling Technologies

Reference has been made to NASA's Technology Readiness Assessment Best Practices Guide [14] to estimate Technology Readiness Level (TRL). The three lowest TRL technologies required for CMO are:

1. Photon sieve. A photon sieve satisfying all CMO baseline requirements is TRL 4. However, a sieve of half the needed diameter and lower efficiency is TRL 5–6 and is slated for flight demonstration in 2024 by the VISORS (VIrtual Super-resolution Optics with Reconfigurable Swarms) mission [15].
2. 3D Precision Laser Ranger (3DPLR). The least-developed component of the 3DPLR is TRL 4.
3. Compact Astrometric Alignment Sensor (CAAS). The CAAS is TRL 4–5.

The 3DPLR and CAAS are components of the Relative Position Sensing System (RPSS). The following sections summarize the bases of the TRL assessments and the sensitivity of mission performance to technology performance.

2.3.1.1 Photon Sieve

A photon sieve [16] is a flat diffractive optic (Figure 8) that forms nearly diffraction-limited images at EUV and x-ray wavelengths where conventional focusing mirrors with aperture

Figure 8. Photon sieves photolithographically fabricated in silicon wafers at GSFC. Left: photograph of an 80-mm diameter sieve with 1,666 zones comprising 17,591,294 holes ranging in size from 290 µm to 7 µm in diameter. Left Inset: micrograph of innermost zones. Center and right: micrographs of the center and edge of an 80-mm diameter arc sieve with 4,999 zones comprising 52,352,407 slots ranging from 144 µm to 2 µm in width.

≳20 cm are challenging to manufacture cost effectively (or at all) with the accuracy needed to approach the diffraction limit. Similar to a Fresnel zone plate, which comprises alternating opaque and transmissive annular zones, a photon sieve replaces the annular rings with concentric rings of holes or arcs for structural integrity and finer control of the point spread function. A sieve, like a zone plate, may be characterized as binary amplitude, binary phase, or multiphase. Binary amplitude means that the sieve material is opaque to EUV light, so that transmission is either 1 (holes) or 0; the efficiency is about 7%. Binary phase means that the sieve material imparts a half-wave phase shift to reinforce constructive interference at focus and improve efficiency to >20%. Multiphase means that the phase change is controlled within each Fresnel zone, potentially yielding efficiency as high as 80% depending on the sieve material. CMO baseline performance requires a 17-cm diameter binary phase sieve. The VISORS sieve is binary amplitude, 8 cm diameter. It has survived vibration testing and has been demonstrated in the laboratory to produce EUV images consistent with analytical predictions (TRL 5–6). A 17-cm binary amplitude sieve is currently TRL 4, as is an 8-cm binary phase sieve; the combined TRL for the CMO sieve is rated TRL 4 on that basis. A 17-cm binary amplitude sieve would satisfy the angular resolution requirements of the STM in individual exposures, but the ultimate resolution of faint features could be degraded by a factor of two because of residual blurring after the coalignment and addition of successive images.

The photon sieve technology maturation plan is given in §4.2.1; more detail on the technology is given in Appendix C.

2.3.1.2 Relative Position Sensing System (RPSS)

The RPSS provides relative position sensing between pairs of spacecraft. One RPSS suite ensures that SC1 and SC2 provide a stable field of view for the EUV microscale imagers. A second RPSS suite ensures that the external occulter on SC2 is accurately centered on the Sun as seen from the coronagraph on SC3. Data from the RPSS is processed by the guidance system, which will command the ionic thrusters to make fine corrections in attitude and position. Each RPSS comprises three major subsystems. Coarse relative position and attitude sensing is achieved using a Radio Direction Finder (RDF); fine relative position sensing is achieved with a 3D Precision Laser Ranger (3DPLR); fine attitude sensing is provided by a Compact Astrometric and Alignment Sensor (CAAS). Figure 9 is a map of how the two RPSS suites are distributed among the three spacecraft. The RPSS technology maturation plan is given in §4.2.2; Appendix D gives a more comprehensive description of the RPSS components.

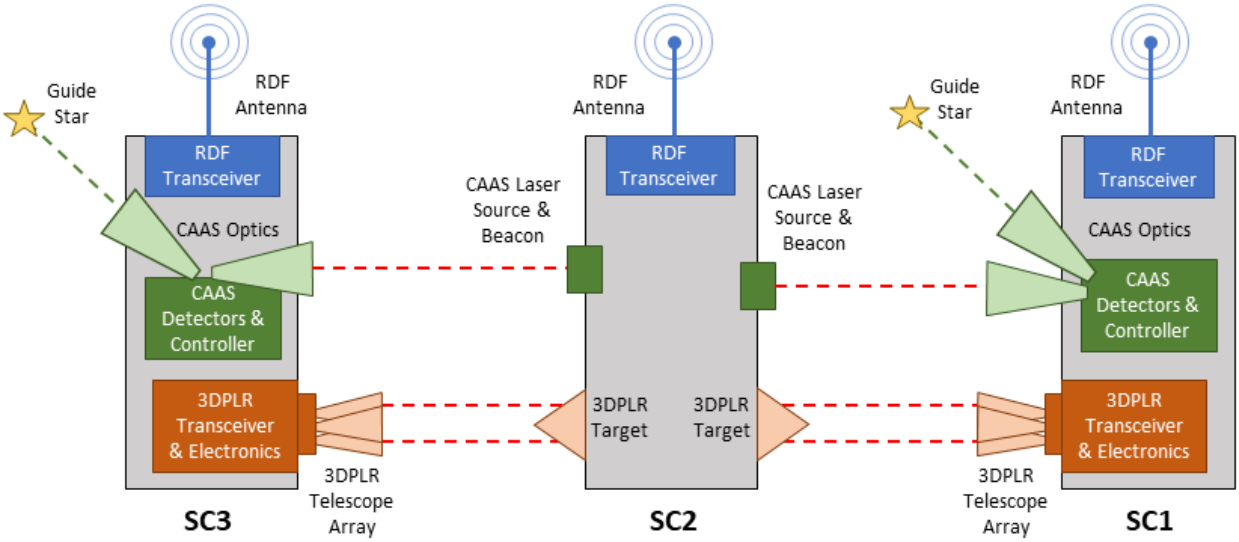

Figure 9. Distribution of components of the Relative Position Sensing System.

Radio Direction Finder (RDF)

Radio Direction Finding is a well-established technology in ground-based applications, widely used in military and search and rescue applications. To adapt this technology to the space environment, it is necessary to identify appropriate space qualified radio transceivers/antennas and to develop software that is customized to the equipment selected. At least one provider of space-qualified S-band radio systems has developed a prototype of an RDF system that would meet CMO requirements. The CMO team is currently communicating with that provider to understand their requirements for adapting their prototype system to CMO. The prototype system is judged to be TLR 4.

3D Precision Laser Ranger (3DPLR)

The 3DPLR employs heterodyne phase analysis on periodic laser pulses to achieve sub-mm range resolution, which is finer than what is achieved with typical time-of-flight laser rangers. A single ranger of this type provides high resolution longitudinal ranging between two spacecraft. To achieve transverse ranging, an array of six laser beams is directed from one spacecraft to a three-dimensional target on a second spacecraft. The target is a six-sided pyramid with 45° elevation faces coated with retroreflective material. The retroreflective material ensures that the laser light is returned to the source even though the surface is inclined to the beams. If the second spacecraft translates off the line of sight between the two spacecraft, one beam ascends a pyramid surface while a second laser beam descends a pyramid surface. The first ranger detects a shorter range while the seconds detects a longer range. Correlating the data from all six rangers provides a full data set to describe the relative position between the two spacecraft. In effect, the six laser beams are like the strings that provide the link between a puppeteer and a marionette. The 3DPLR is currently TRL 4.

Compact Astrometric Alignment Sensor (CAAS)

The CAAS provides attitude sensing between two spacecraft and to inertial space. The CAAS combines guide star measurements with focused light from a laser beacon mounted on the opposing spacecraft using a novel beam combining/dividing detector assembly to achieve ultra-precise performance in a compact package. Receiver telescopes focus the images of the guide star and the laser beacon onto a knife-edged prism. The prism directs a fraction of each image to separate sensors. When alignment is optimum, the images are split evenly and each sensor records an equal intensity. Any shift in attitude or transverse offset results in the image translating relative to the knife edge and the two sensors receiving unequal fractions of the image. Two sets of prism/sensors ensures that both perpendicular axes are monitored. In addition to relative sensing, the CAAS provides near milli-arcsecond inertial attitude sensing. The CAAS is currently TRL 4–5.

2.3.2. Instruments

2.3.2.1 EUV Microscale Telescopes (EMIT)

The components of EMIT are photon sieves (TRL 4 based on §2.3.1.1) and detector assemblies (TRL 5–6 based on the VISORS engineering model shown in Figure 11). The overall TRL is 4; technology maturation is confined to the photon sieve component (§4.2.1).

2.3.2.2 EUV Finescale Imager (EFI)

The EFI design concept is based on the EUV imager being developed for MUSE (Multi-Slit Solar Explorer), a NASA mission in development. The MUSE imager (TRL 6) derives from the

highly successful Hi-C sounding rocket instrument (TRL 9). EFI is judged to be TRL 5 overall because accommodating the MUSE instrument on CMO SC1 has not yet been studied.

2.3.2.3 Multiband Coronagraph (MBC)

The ASPIICS (Association of Spacecraft for Polarimetric and Imaging Investigation of the Corona of the Sun) instrument, on which the MBC design concept is based (§3.1.3), is TRL 8. However, the complex ASPIICS instrument was designed and fabricated by a multinational consortium. Even if a partnership is established, it is unlikely that MBC can be a build-to-print copy of ASPIICS. MBC is therefore judged to be TRL 6.

2.4. Key Trades

Launch Vehicle

A launch energy (C3) of −0.7 $km^2\ s^{-2}$ is needed to achieve the desired L1 quasi-halo orbit (Figure 15). The MDL study estimated the wet launch mass of CMO to be about 1500 kg. Thus, a vehicle such as Antares (1705 kg capability), Falcon 9FT (1830 kg), or Vulcan VCO (2160 kg) would meet the requirement; each of these vehicles has a fairing large enough to accommodate the launch stack. As the design team had the greatest experience with Falcon 9 FT, that vehicle was baselined. With the addition of a third instrument, the mission mass has increased somewhat, so the launch vehicle is an open trade.

Relative Position Sensing System

The layered spacecraft metrology system of the ESA (European Space Agency) PROBA-3 (Project for On-Board Autonomy 3) mission is similar in concept to the RPSS system described in this study [17]. The specifications of the PROBA-3 system meet CMO requirements except for the extremely accurate (~0.02 as 1σ) transverse position knowledge between SC1 and SC2 that in CMO is provided by CAAS. The VISORS mission relies on cross-correlation of successive short (0.2–0.5 s) exposures to create coadded images that be downlinked without exceeding the capabilities of the downlink system. CAAS enables more accurate coaddition based on a priori knowledge.

The MDL study baselined the RPSS system for three reasons: (1) RPSS does not require two components of the PROBA-3 system, the Vision Based Sensor (VBS) [18] and the Shadow Position Sensor (SPS) [19]; (2) RPSS is projected to require less SWaP; (3) The PROBA-3 system is a multi-country collaboration that would require a similarly complex international partnership for CMO. It was judged that a US-based solution should be studied to mitigate that risk. However, the PROBA-3 system (omitting VBS and SPS), with the addition of CAAS, is considered to be a viable trade.

Low Force Thrusters

Several low force thrusters have been developed to support small satellites as well as gravitational wave research. The MDL study considered five different classes of low force thrusters, including Hall effect thrusters, radio frequency ion thrusters, electrospray thrusters, green propulsion, and cold gas thrusters. At least three of these technologies have flight heritage. Xenon Hall effect thrusters were found to have too-high thrust. RF ion thrusters, which have flight heritage, were judged to be more complicated than the TILE (Tiled Ionic Liquid Electrospray) thrusters adopted. Green propulsion was judged to be too early in technological development. Cold gas thrusters have flight heritage but are considerably heavier. Two electrospray thrusters were considered, from Busek Propulsion and Accion Systems (TILE). Both have flight heritage. At the time of study, the team had greater access to detailed

information about the TILE thrusters. The Busek electrospray and RF ion thrusters are considered to be viable alternatives.

Direct-to-Earth Communications

The baseline plan for communicating science data to Earth is via the Ka-band radio system. This is a well established solution with Near Space Network (NSN) stations located around the globe. Recent developments indicate that optical communications would enable a much higher duty cycle for EMIT. The MDL study conservatively baselined a proven Ka-band system. However, as optical communications are likely to be available in a time frame relevant to CMO, Appendix F explores this option.

3. Technical Overview

3.1. Instrument Payload Description

As addressed in §2.2, the CMO instruments are not fully designed. Therefore, this section presents functional descriptions together with information on analogous instruments. EMI, based on photon sieve optics, is a novel instrument. EFI and MBC will be closely based on existing instruments and proven technology. Nevertheless, in developing a mission life-cycle cost estimate for CMO (§5), *all three instruments were considered as ground-up design efforts* making use of subsystem heritage to the maximum extent possible.

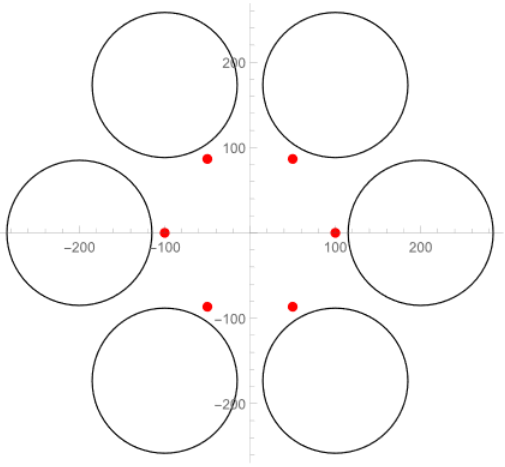

Figure 10. Geometrical arrangement of photon sieves on SC1. A red dot marks the optical axis of each sieve. Distances are in mm.

3.1.1. EUV Microscale Telescopes

Each telescope is simple in concept: a photon sieve on SC1 (see Figure 4) is fabricated to focus a particular EUV emission line at the common focal length of 100 m. The image sensor, located on SC2, is in a vacuum chamber that includes a small multilayer-coated flat mirror to limit the bandpass. The six sensor assemblies are identical except for their multilayer coatings. Figure 10 shows the geometrical arrangement of the sieves on SC1; the red dots mark the optical axes, which are outside the sieves themselves (eccentric pupil) so that the images are formed within 100 mm of the center of mass of SC2 to limit the blurring caused by SC1 attitude jitter to <1 pixel. Radiometric calculations were adapted from VISORS.

The baseline sensor is a space-qualified 2Kx2K CMOS array similar to the Teledyne CIS115 sensor used on VISORS. A photon-counting 4Kx4K

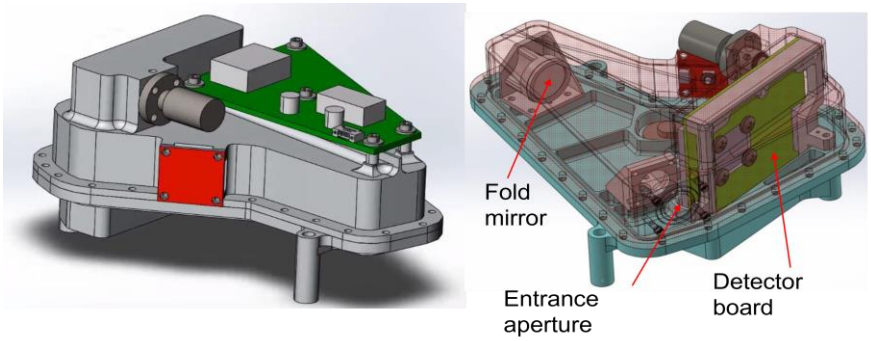

Figure 11. The VISORS vacuum detector chamber is the template for the detector assembly of each CMO EUV Telescope. The longest dimension of the chamber is about 15 cm.

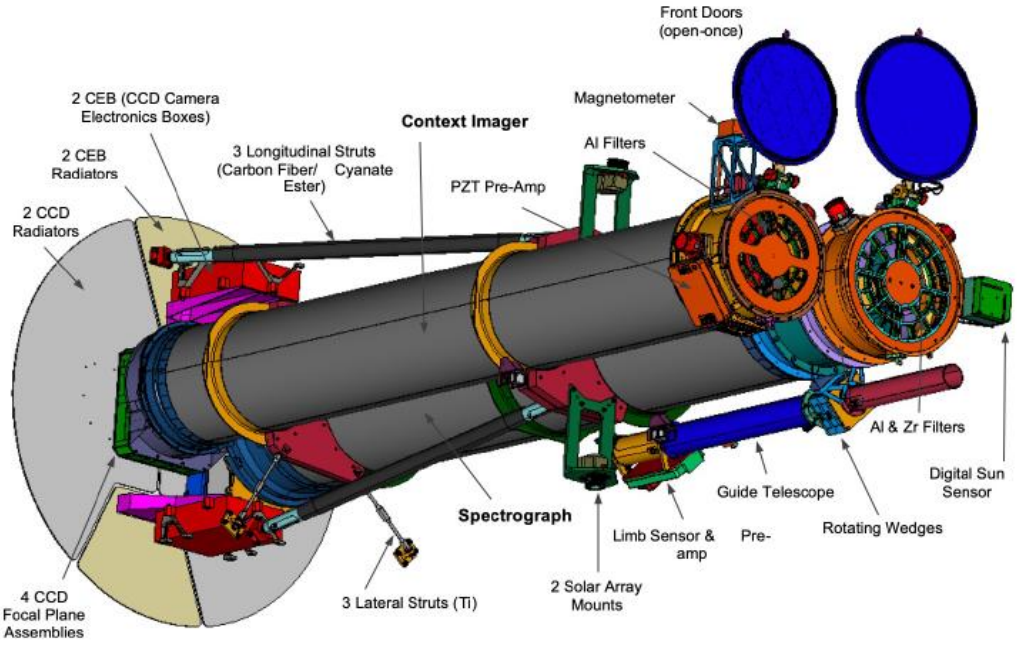

Figure 12. CAD view of the MUSE spacecraft [22]. The EUV imager is labeled Context Imager.

CMOS sensor [20] is now commercially available and is a potentially superior alternative that could be investigated during pre-formulation. Figure 11 shows the VISORS detector chamber. The SWaP requirements of the CMO chambers have been estimated from the VISORS design; they are not much larger than for the VISORS chamber.

3.1.2. EUV Finescale Imager

The EFI design concept is based on the EUV imager being developed for the MUSE mission [21] [22] (Figure 12). That instrument in turn derives from the highly successful Hi-C sounding rocket instrument [23] [24]. CMO will adopt as much heritage as possible from the MUSE imager, as it meets the requirements of the CMO STM. As noted in §2.2, a finescale imager was not included in the MDL study. Two principals of the MUSE and Hi-C teams are members of the CMO study team.

The MUSE instrument provides images in two narrow bands around 30.4 nm (including He II) and 19.5 nm (including Fe XII, Fe XXIV). A pair of images, one for each channel, is recorded every 4 s with a common field of view, 580 x 290 as^2.

SC1 as currently designed has more than enough SWaP to accommodate the addition of EFI. This is not surprising given that the three spacecraft have a common architecture, but the photon sieve optical package on SC1 is quite light compared to the EUV detector package on SC2 and the coronagraph on SC3, and the photon sieves use no power.

3.1.3. Multiband Coronagraph

The MBC design concept is based on the ASPIICS coronagraph [25] [26] [27] expected to fly on the ESA PROBA-3 mission in 2024. Apart from its external occulter on a separate spacecraft (as in CMO), ASPIICS is a classical Lyot coronagraph (Figure 13). ASPIICS measures coronal linear polarization in the 540-570 nm band using three polarizers (each coupled to a wideband filter) in its filter/polarizer wheel as well as two emission lines, Fe XIV 530.3 nm (the coronal green line) and He I 587.6 nm (the D3 line), using narrowband (2.0 nm) filters. CMO will add a

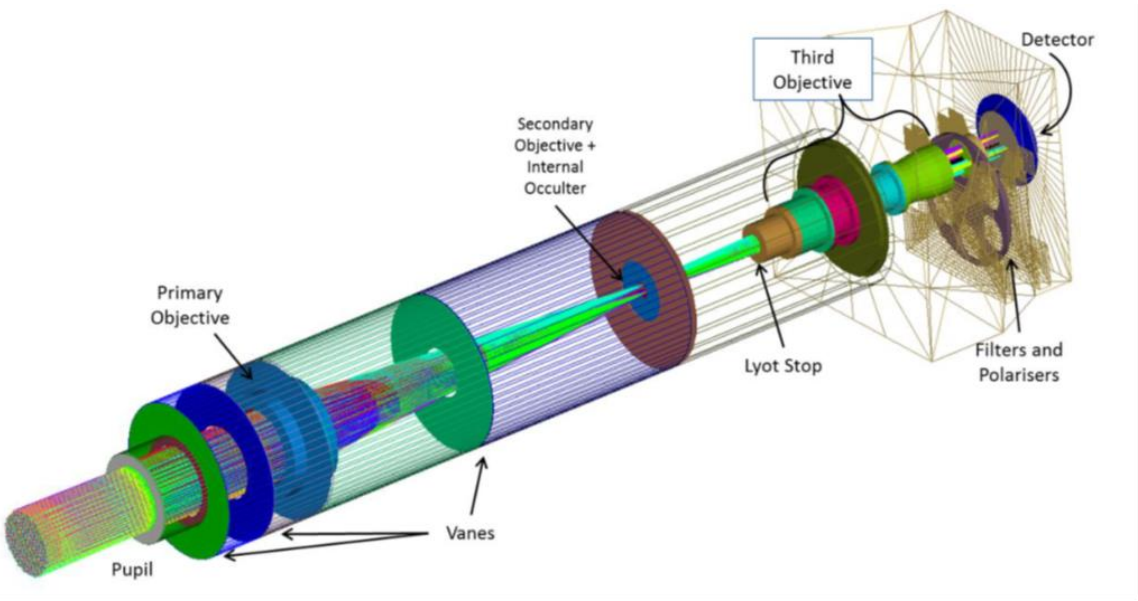

Figure 13. Optomechanical model of the ASPIICS coronagraph *[26]*.

second filter wheel carrying four narrowband filters in the wavelength region 394−423 nm that enable the measurement of coronal temperature and radial flow speed using the bandpass ratio method demonstrated by eclipse observations and the BITSE (Balloon-Born Investigation of Temperature and Speed of Electrons in the Corona) experiment [28] [29].

SWaP estimates for MBC were derived from ASPIICS [25].

3.1.4. Instrument Tables

Table 5–Table 8 summarize the space, weight, power, and data generation characteristics of the CMO instruments. The tables reflect the fact that EMIT and MBC are distributed across two spacecraft.

Table 5. Instrument distribution and space requirements

Instrument	Component	Enclosing Volume on SC1 (mm^3)	Enclosing Volume on SC2 (mn^3)	Enclosing Volume on SC3 (mm^3)
EMIT	Photon sieves	1600 x 600 x 600	0	0
	Sunshade	Integral to spacecraft structure	0	0
	Detector subsystem	0	700 x 680 x 310	0
MBC	External occulter	0	Integral to spacecraft structure	0
	Coronagraph	0	0	900 x 400 x 300
EFI	Entire instrument	1450 x 420 x 420	0	0

Table 6. Payload mass, power, and science data rate for SC1

SC1	Mass			Average Power			Science Data Rate		
	CBE (kg)	% Cont.	MEV (kg)	CBE (W)	% Cont.	MEV (W)	Mbps	% Cont.	Mbps
EMIT (sieves and sunshade)	12.9	28%	16.5	0.0	0%	0.0	0	0%	0
MBC	0.0	0%	0.0	0.0	0%	0.0	0	0%	0
EFI	60.0	30%	78.0	40.0	30%	52.0	13.4	10%	14.7
Totals	72.9		94.5	40.0		52.0	13.4		14.7

Table 7. Payload mass, power, and science data rate for SC2

SC2	Mass			Average Power			Science Data Rate		
	CBE (kg)	% Cont.	MEV (kg)	CBE (W)	% Cont.	MEV (W)	Mbps	% Cont.	Mbps
EMIT (detector assembly)	36.0	25%	45.0	60.0	25%	75.0	16.1	10	17.7
MBC (occulter)	15.0	30%	19.5	0.0	0%	0.0	0	0%	0
EFI	0.0	0%	0.0	0.0	0%	0.0	0	0%	0
Totals	51.0		64.5	60.0		75.0	16.1		17.7

Table 8. Payload mass, power, and science data rate for SC3

SC3	Mass			Average Power			Science Data Rate		
	CBE (kg)	% Cont.	MEV (kg)	CBE (W)	% Cont.	MEV (W)	Mbps	% Cont.	Mbps
EMIT	0.0	0%	0.0	0.0	0%	0.0	0	0%	0
MBC (detector)	30.0	25%	37.5	50.0	25%	62.5	26.8	10%	29.5
EFI	0.0	0%	0.0	0.0	0%	0.0	0	0%	0
Totals	30.0		37.5	50.0		62.5	26.8		29.5

3.2. Flight System

3.2.1. Description

The three CMO spacecraft are designed to share a common bus, reducing complexity and cost. The common bus includes most of the flight subsystems and the superstructure of the spacecraft. The backbone of the structure is an octagonal frame with top and bottom decks for additional stiffness. Each spacecraft has a 1-in thick honeycomb deck to support the propellant tanks and a second honeycomb deck to serve as an optical bench to support the various customized elements of the science instruments and RPSS. Detailed mechanical views and block diagrams of the three spacecraft are given in Appendix E.

Primary propulsion is chemical and is responsible for deployment, cruise, and course positioning. All spacecraft have a hydrazine monopropellant system. SC1 and SC2 each have two hydrazine tanks while SC3 has four so that it has sufficient fuel to provide propulsion for the stack during maneuvers executed prior to separation from the other two spacecraft..

Secondary propulsion allows fine adjustments in position and is accomplished using a set of low-force thrusters distributed about the spacecraft. Attitude control is also accomplished using secondary propulsion, eliminating the need for reaction wheels. TILE liquid ionic thrusters from Accion Systems are baselined as the low force-thrusters due to their overall simplicity and low consumption of resources. Each thruster pod provides a maximum thrust of 0.45 mN, has a specific impulse of 1650 s, and includes a self-contained tank of ionic fluid. Each spacecraft has a total of 24 separate TILE thrusters: four each on the top and bottom decks, and four each on perpendicular side faces. The locations of 12 of the thrusters are shown in Figure 14. A maneuver requires a subset of the thrusters to operate while the remaining ones are on standby.

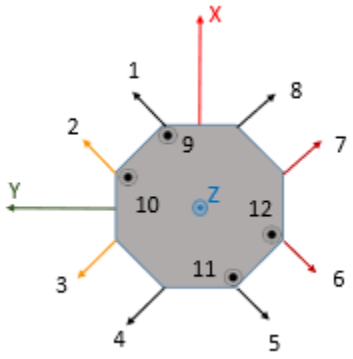

Figure 14. Location of 12 of the 24 liquid ionic thrusters on each spacecraft.

Because the three spacecraft will be located near one another and maintain the same attitude, the thermal design is common to all three. The thermal environment is relatively simple given the L1 halo orbit (0.99 AU) with no infrared or albedo effects from Earth. The bottom deck of the spacecraft serves as the principal radiator; multilayer insulation (MLI) will cover most of the spacecraft. Thermal control is achieved passively using mechanical thermostats and Kapton film heaters. Similarly, the radiation environment for all three spacecraft is identical and simple. The 5-year mission dose is estimated to be 23.4 krad for 2.5 mm of aluminum shielding with 95% confidence.

The sequential formation impacts the size and shape of solar panels and therefore available power for each spacecraft (see Figure 4). When on or near the formation boresight, SC1 is a potential optical obstruction in the fields of view of EMIT and MBC; thus, SC1's solar panels are body mounted and distributed around a narrow fixed circular collar that also serves as the EMIT sunshade. Unlike EMIT, MBC can tolerate narrow radial obstructions similar to telescope spider vanes; thus, SC2 has deployable solar panels supported by arms that hold them out of the MBC field of view. However, the solar panels are still limited in size because the supporting arms must be thin to minimize their impact on MBC. SC3, last in the formation, has no unusual limits on solar panel size and shape. The four deployable solar panels are hinged at the spacecraft body and have a total area that is large in comparison to the other two spacecraft.

Communications are conducted on two frequency bands. General housekeeping, navigation, commanding, and other spacecraft relevant data are communicated between the individual spacecraft and to ground stations via S-band. The same S-band system provides the RDF component of the RPSS. All three spacecraft have identical S-band transceivers and antennas. Science data are handled on Ka-band. Each spacecraft has a Ka-band transceiver and omnidirectional antenna for communication with the other spacecraft as well as a 16 Tb solid state recorder to accumulate science data. Direct-to-Earth (DTE) communication for science data originates from SC3 due to its greater power generation. Communications are conducted as "hub and spoke" between SC3 and the other two spacecraft. A deployable high gain antenna and 100 W amplifier are added to the Ka-band system on SC3, as well as a gimbal control system for pointing the antenna toward Earth. A potentially superior DTE system using laser communications is explored in §3.3.1 and Appendix F.

3.2.2. Flight System Components

As discussed in §2.3.1.2, each spacecraft carries individualized components of the RPSS as well as components of the science instruments.

Table 9 gives a breakdown of how the various flight system components are distributed among the three spacecraft.

Table 9. Distribution of spacecraft-specific flight system components

Category	System	Component	Description/Comment	SC1	SC2	SC3
Science Instrument	EMIT	Imaging optics	Array of six photon sieves	✶		
		Sunshade	Circular panel around SC1	✶		
		Sensors	EUV sensors		✶	
Science Instrument	MBC	Occulter	Circular panel around SC2		✶	
		Camera	Visible light camera			✶
Science Instrument	EFI	Entire Instrument	EUV camera	✶		
Flight System RPSS	RDF	Transceivers	Identical S-band systems	✶	✶	✶
		Antenna Array	Identical array on all 3 spacecraft	✶	✶	✶
	3DPLR (1/2)	Transceiver	Sensing SC1/SC2	✶		
		Retroreflective target	Sensing SC1/SC2		✶	
	3DPLR (2/3)	Transceiver	Sensing SC2/SC3			✶
		Retroreflective target	Sensing SC2/SC3		✶	
	CAAS (1/2)	Telescopes & Detectors	Sensing SC1/SC2	✶		
		Laser Source & Beacon	Sensing SC1/SC2		✶	
	CAAS (2/3)	Telescopes & Detectors	Sensing SC2/SC3			✶
		Laser Source & Beacon	Sensing SC2/SC3		✶	
Flight System	Primary Propulsion	Hydrazine Tanks	SC1 & SC2 have 2 tanks.	✶	✶	
			SC3 has 4 tanks to support stack maneuvers			✶
Flight System	Power	Solar Panels	Body mounted, 1.9 m^2	✶		
			Deployable (2) on slender folding arms. Net area = 2.4 m^2		✶	
			Deployable (4), hinged at SC body. Total area = 3.4 m^2			✶
Flight System	DTE Comm.	Ka-band System for DTE	Transceiver for DTE			✶
			Deployable high gain antenna for DTE			✶
			Gimbal Control for Ka-band DTE antenna			✶

Table 10 shows the flight system mass and power properties for elements common to all three spacecraft. Table 11–Table 13 then show flight system mass properties for each spacecraft including both unique and common elements.

Table 10. Mass and power for flight system components common to all spacecraft

	Mass			Average Power		
Common Elements	**CBE (kg)**	**% Cont.**	**MEV (kg)**	**CBE (W)**	**% Cont.**	**MEV (W)**
Structures & Mechanisms	164.0	27%	208.2	0.0	0%	0.0
Thermal Control	12.1	23%	14.8	0.0	0%	0.0
Primary Propulsion (Dry Mass)	10.1	28%	12.9	14.8	30%	19.3
Secondary Propulsion	48.0	25%	60.0	36.0	25%	45.0
Attitude Control & Avionics	12.3	6%	13.1	68.8	15%	79.5
Rel. Pos. Sen. Sys. (RPSS)	3.1	21%	3.8	12.9	5%	13.6
Command & Data Handling	8.9	30%	11.6	17.5	30%	22.8
Telecom: Interspacecraft	12.1	21%	14.7	10.0	10%	11.0
Telecom: Direct to Earth	0.0	0%	0.0	0.0	0%	0.0
Power	30.6	30%	39.7	15.2	30%	19.8
Total COMMON Flight Elements Dry Bus Mass	300.5	26%	377.9	175.3	20%	210.8

Table 11. Mass and power for flight system components of SC1

	Mass			Average Power		
SC1	**CBE (kg)**	**% Cont.**	**MEV (kg)**	**CBE (W)**	**% Cont.**	**MEV (W)**
Common Flight Elements	300.5	26%	377.9	175.3	20%	210.8
SC1 Unique Structures & Mechanisms	0.0	0%	0.0	0.0	0%	0.0
SC1 Unique Thermal Control	0.0	0%	0.0	0.0	0%	0.0
SC1 Unique Primary Propulsion (Dry Mass)	3.9	5%	4.1	0.0	0%	0.0
SC1 Unique Secondary Propulsion	0.0	0%	0.0	0.0	0%	0.0
SC1 Unique Attitude Control & Avionics	0.0	0%	0.0	0.0	0%	0.0
SC1 Unique RPSS	28.4	25%	35.5	16.0	25%	20.0
SC1 Unique Command & Data Handling	0.0	0%	0.0	0.0	0%	0.0
SC1 Unique Telecom: Interspacecraft	0.0	0%	0.0	0.0	0%	0.0
SC1 Unique Telecom: Direct to Earth	0.0	0%	0.0	0.0	0%	0.0
SC1 Unique Power	13.6	30%	17.7	0.0	0%	0.0
Total Flight Element Dry Bus Mass for SC1	346.3	26%	435.1	191.3	21%	230.8

Table 12. Mass and power for flight system components of SC2

	Mass			Average Power		
SC2	**CBE (kg)**	**% Cont.**	**MEV (kg)**	**CBE (W)**	**% Cont.**	**MEV (W)**
Common Flight Elements	300.5	0%	377.9	175.3	0%	210.8
SC2 Unique Structures & Mechanisms	45.4	30%	59.0	0.0	0%	0.0
SC2 Unique Thermal Control	0.0	0%	0.0	0.0	0%	0.0
SC2 Unique Primary Propulsion (Dry Mass)	3.9	5%	4.1	0.0	0%	0.0
SC2 Unique Secondary Propulsion	0.0	0%	0.0	0.0	0%	0.0
SC2 Unique Attitude Control & Avionics	0.0	0%	0.0	0.0	0%	0.0
SC2 Unique RPSS	4.9	25%	6.1	13.0	25%	16.3
SC2 Unique Command & Data Handling (image processing single board computer)	2.0	30%	2.6	8.0	30%	10.4
SC2 Unique Telecom: Interspacecraft	0.0	0%	0.0	0.0	0%	0.0
SC2 Unique Telecom: Direct to Earth	0.0	0%	0.0	0.0	0%	0.0
SC2 Unique Power	17.6	30%	22.8	0.0	0%	0.0
Total Flight Element Dry Bus Mass for SC2	374.2	26%	472.5	196.3	21%	237.5

Table 13. Mass and power for flight system components of SC3

	Mass			Average Power		
SC3	**CBE (kg)**	**% Cont.**	**MEV (kg)**	**CBE (W)**	**% Cont.**	**MEV (W)**
Common Flight Elements	300.5	0%	377.9	175.3	0%	210.8
SC3 Unique Structures & Mechanisms	42.1	30%	54.7	15.0	30%	19.5
SC3 Unique Thermal Control	0.0	0%	0.0	0.0	0%	0.0
SC3 Unique Primary Propulsion (Dry Mass)	7.7	5%	8.1	0.0	0%	0.0
SC3 Unique Secondary Propulsion	0.0	0%	0.0	0.0	0%	0.0
SC3 Unique Attitude Control & Avionics	0.0	0%	0.0	0.0	0%	0.0
SC3 Unique RPSS	28.4	25%	35.5	16.0	25%	20.0
SC3 Unique Command & Data Handling	0.0	0%	0.0	0.0	0%	0.0
SC3 Unique Telecom: Interspacecraft	0.0	0%	0.0	0.0	0%	0.0
SC3 Unique Telecom: Direct to Earth	19.1	20%	22.9	48.0	22%	58.7
SC3 Unique Power	32.4	30%	42.1	0.0	0%	0.0
Total Flight Element Dry Bus Mass for SC3	430.2	26%	541.2	254.3	22%	309.0

3.2.3. Flight System Characteristics

Table 14 gives the flight system characteristics of SC1, SC2, and SC3.

Table 14. Flight system characteristics common to all spacecraft

Flight System Element	Value/ Summary, units	SC1	SC2	SC3
Design Life, months	36 months (60 months goal)	✶	✶	✶
Structures	Machined Aluminum (housings), Aluminum Honeycomb (Optical bench), Composite & Composite Facesheets (Solar Array)	✶	✶	✶
Number of deployed structures	SC2: Solar Arrays (2) SC3: Solar Arrays (4), Ka-Band Antenna (1)	0	2	5
Thermal Control	Survival heaters controlled using thermostats All other elements are passive: MLI, radiator panels, coating, heat pipes	✶	✶	✶
Primary Propulsion (PP)				
PP: Estimated delta-V budget	SC3 drives stack for some maneuvers (m/s)	66	66	82
PP: Propulsion type	Mono-propellant Hydrazine thrusters	✶	✶	✶
PP: Number of thrusters	4 prime, 4 redundant	8	8	8
PP: Number of tanks		2	2	4
Secondary Propulsion (SP)	Used for Attitude control and fine positioning			
SP: Propulsion type	Electric Propulsion with ionic fluid propellant	✶	✶	✶
SP: Maximum thrust	0.45 mN for each thruster	✶	✶	✶
SP: Configuration of thrusters	4 per face on 6 orthogonal faces of spacecraft	✶	✶	✶
SP: Number of thrusters & tanks	One self-contained tank on each thruster pod	24	24	24
SP: Est. Impulse budget, Ns	15Ns per thruster, 24 thrusters per SC	360	360	360
Attitude sensors	Course Sun Sensors (8), Star Tracker, Inertial Measurement Unit, RPSS	✶	✶	✶
Attitude control actuators	Secondary Propulsion	✶	✶	✶
Attitude control method	3-axis stabilized, solar reference	✶	✶	✶
Attitude control	0.0007 deg (2.3 as) 1σ	✶	✶	✶
Attitude knowledge	0.000004 deg (0.015 as) 1σ	✶	✶	✶
Agility requirements	Maintain formation autonomously	✶	✶	✶
Housekeeping data rate	kbps	10	10	10
Data storage capacity	Solid state recorder on each SC (Tb)	16	16	16
Maximum storage record rate	Solid state recorder on each SC (Gbps)	2.0	2.0	2.0
Maximum storage playback rate	SC1 & SC2: transmit to SC3 (Gbps) SC3: transmit to Earth (Gbps)	0.105	0.105	0.315
Power: Type of s array structure	SC1: body mounted, SC2 & SC3: Deployed	Body	Depl	Depl
Solar Array size, square meters	Spacecraft specific	1.9	2.4	3.4
Solar cell type	TjGaAs (Triple Junction Gallium Arsenide)	✶	✶	✶
Expected power generation	Beginning of Life (BOL) (W)	509	658	912
Expected power generation	End of Life (EOL) (W)	427	550	762
On-orbit average power consumption	Includes 25% contingency (W) SC1 panels are enlarged to accommodate EFI	482	496	688
Battery type (NiCd, NiH, Li-ion)	20 amp hr Li-ion battery	✶	✶	✶

3.3. Concept of Operations and Mission Design

3.3.1. Description

Launch, Transfer and Science Orbit

During the launch and early transfer phases of the mission, the three spacecraft are held together as a stack. Several medium-lift launch vehicles (including Falcon 9 FT and Vulcan) can physically accommodate the stack and meet trajectory requirements. The trajectory transfer insertion (TTI) maneuver requires Δv = 3.2 km s^{-1}; the characteristic energy requirement is C3 = -0.7 km^2 s^{-2}. TTI is performed under the power of the launch vehicle upper stage, after which the stack separates from the upper stage. While still configured as a stack, SC3 deploys solar arrays, powers on, and undergoes a health and safety checkout. Next, SC3 executes a trajectory correction maneuver on behalf of the stack, after which the stack separates, and the other two spacecraft power on systems, establish communication, and SC2 deploys solar arrays (SC1 arrays are body mounted). The spacecraft are positioned approximately 500 m apart and cruise to L1 as a squadron. Approximately 6.5 months after launch, the squadron enter a quasi-halo orbit about L1 (Figure 15).

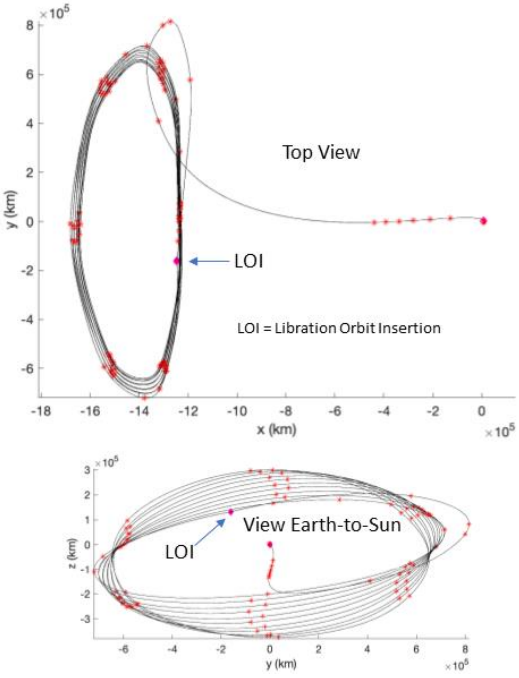

Figure 15. Transfer trajectory and L1 quasi-halo orbit.

Formation Alignment and Stationkeeping

Once in orbit around L1, the spacecraft execute a series of fine maneuvers to bring the formation into alignment. The fine maneuvers are executed under secondary propulsion (TILE thrusters). Alignment begins with the three spacecraft at their cruise separations of 500 m. First, all three spacecraft orient themselves toward the Sun using their course sun sensors. The line of sight between the center of the occulter on SC2 and the center of the Sun defines the formation boresight (see Figure 5). Under RDF guidance, SC1 maneuvers to take up a position 20 m (minimum safe distance) in front of S2 along the boresight. This close spacing ensures that the RPSS optical sensors have sufficient return signals to execute the remainder of the alignment procedure. Using the 3DPLR and CAAS subsytems of the RPSS, the attitude and transverse offset of SC1 are brought into full alignment with SC2 and the formation boresight. SC1 then translates along the boresight until it reaches its final station of 100 m in front of SC2. SC3 then undergoes the same alignment procedure and takes its position 200 m behind SC2. With the formation complete, instrument check-out can begin.

Stationkeeping is conducted with secondary propulsion only. The RPSS continuously provides position and attitude data to the GNC system, and the TILE thrusters are fired as needed to autonomously keep the formation in alignment. Each spacecraft must perform these small maneuvers to keep from diverging from the unstable quasi-halo orbit, due to gravitational perturbations, ground-based navigation errors, thrust errors, and other small perturbing forces. Nominally, each spacecraft performs the same stationkeeping maneuvers. Once per month a calibration slew maneuver is planned, which will require coarse formation.

Science Data Rates and Communications

CMO has two main science data modes, synoptic and high cadence, that differ only in the rate that EMIT generates data. Synoptic mode is the default mode and is used to address most of the STM science objectives (Table 2). High cadence mode is used to achieve the highest possible angular resolution (the least possible image smear) and to study rapidly evolving phenomena such as microflares and jets. The data generation rate in either mode is constrained by the speed of interspacecraft (ISC) data transfer, the speed of Direct-to-Earth (DTE) data transfer, and how much ground station contact time is available daily. Table 15 shows four feasible data generation scenarios according to data mode and communications protocol (radio or optical). For radio frequency communications, the ISC rate is 105 Mbps (S-band) and the DTE rate (Ka-band) is 315 Mbps. For optical communications, the ISC and DTE rates are the same, 1.07 Gbps. Optical communications would enable a much more flexible and frequent use of high-cadence mode. This mode is critical to pushing back the microscale frontier.

Operations

Science data communications are discussed in the preceding paragraph. Routine spacecraft and navigational data are communicated via S-band. Each spacecraft has an S-band radio system and can communicate DTE to uplink/downlink spacecraft tracking, telemetry, and commanding data. S-band uplinks/downlinks are planned to take place only during first shift (8 hr/day). Ground range commanding will be verified every other day. Updated commands will be uploaded once per week, and once per month the instruments will undergo a 1-hour calibration.

Given the high degree of autonomy for CMO, missions operations will be generally straightforward. The baseline plan is to use the GSFC virtual Multi-Mission Operations Center (MMOC). This reduces the need for dedicated hardware and shares costs with other missions. The science operations center (SOC), also at GSFC, will manage science data processing, experiment planning and payload monitoring. Science operations are planned to last for five years with a minimum of three years. At end of mission, the spacecraft will exit the L1 orbit in the anti-Earth direction and be passivated.

Table 15. Data generation and downlink scenarios

Scenario	**Instrument**	**Cadence (s)**	**Duty Cycle**	**Data Generation**		**DTE Duration (hr)**	**ISC Duration (hr)**
				(Mb/s)	**(Tb/day)**		
RF Synoptic	EMIT	5	0.90	72.5	6.3	2.8	16.7
	EFI	5	1.00	13.4	1.2	1.0	6.1
	MBC	5	1.00	53.7	4.6	4.1	N/A
	Totals			**140.0**	**12.1**	**7.9**	**22.7**
RF High Cadence	EMIT	0.33	0.05	61.0	5.3	2.3	13.9
	EFI	5	1.00	13.4	1.2	1.0	6.1
	MBC	5	1.00	53.7	4.6	4.1	N/A
	Totals			**128.1**	**11.1**	**7.4**	**20.1**
Optical Synoptic	EMIT	1	1.00	402.7	34.8	4.5	N/A
	EFI	5	1.00	13.4	1.2	0.3	0.3
	MBC	5	1.00	53.7	4.6	1.2	1.2
	Totals			**470.0**	**40.6**	**6.0**	**1.5**
Optical High Cadence	EMIT	0.25	0.25	402.7	34.8	4.5	N/A
	EFI	5	1.00	13.4	1.2	0.3	0.3
	MBC	5	1.00	53.7	4.6	1.2	1.2
	Totals			**470.0**	**40.6**	**6.0**	**1.5**

3.3.2. Mission Design Tables

Table 16. Overall mission design

Parameter			
Orbit	Quasi-halo orbit around Sun-Earth L1 point		
Mission Lifetime	36 months (60 months goal)		
Maximum Eclipse Period	None		
Launch Site	Cape Canaveral		
Spacecraft	**SC1**	**SC2**	**SC3**
Total Mass **with** contingency, including instruments	530 kg	534 kg	579 kg
Propellant Mass **without** contingency	17 kg	17 kg	32 kg
Propellant contingency	5 kg	5 kg	10 kg
Propellant Mass **with** contingency	22 kg	22 kg	42 kg
Launch Adapter Mass **with** contingency	13 kg	0 kg	0 kg
Total Launch Mass	565 kg	556 kg	620 kg
Total Launch Mass, Stack of three	1741 kg		
Launch Vehicle	**Falcon 9FT**		**Vulcan**
Launch Vehicle Lift Capability High escape velocity, C3 = -0.7	1830 kg		2160 kg
Launch Vehicle Mass Margin	89		419
Launch Vehicle Mass Margin	5%		24%

Table 17. Mission modes

Mode	**Spacecraft Configuration**	**Payload Configuration**	**Spacecraft Configuration**
Data Taking (Not downlinking)	Precision Formation	Instruments ON and collecting data	Precision Formation and ACS control Comm cross link ON
Data Taking (Downlinking	Precision Formation	Instruments ON and collecting data	Precision Formation and ACS control Comm cross link ON Transmitter ON
ΔV Mode	Not in formation	Instrument in STBY	Prop System ON Transmitter ON
Coarse Alignment	Coarse formation	Instruments in STBY	Prop system ON Alignment system in capture mode
Calibration	Precision Formation	Instruments in CAL	Precision Alignment XY Offset in SC2
Safe	Collision Avoidance Safe Attitude	Instruments in SAFE	Sun Point Collision Avoidance Transmitter ON
Launch	Not in Formation	Instruments in SAFE	C&DH, ACS, Comm Receiver ON

Table 18. Mission Operations and Ground Data Systems

	Launch & Early Orbit Phase: Transfer to L1	**Launch & Early Orbit Phase: Detector Checkout at L1**	**Prime Science Mission**	**Extended Science Mission**
Number of Contacts per Week	TBD	TBD	168	168
Duration for Mission Phase	28 weeks	13 weeks	156 weeks	104 weeks
Downlink Information				
Downlink Frequency Band	S-Band	S-Band Ka-Band	S-Band Ka-Band	S-Band Ka-Band
Telemetry Data Rates	S: 10 kbps	S: 10 kbps Ka: 315 Mbps	S: 10 kbps Ka: 315 Mbps	S: 10 kbps Ka: 315 Mbps
Transmitting Antenna Types	S: Omni	S: Omni Ka: High Gain	S: Omni Ka: High Gain	S: Omni Ka: High Gain
Transmitter peak power	S: 40 W	S: 40 W Ka: 30 W	S: 40 W Ka: 30 W	S: 40 W Ka: 30 W
Transmitting Power Amplifier		Ka, 100 W	Ka, 100 W	Ka, 100 W
Total Daily Data Volume		Ka: 36 Tb/day	Ka: 36 Tb/day	Ka: 36 Tb/day
Uplink Information				
Number of Uplinks per Day	TBD	TBD	8	8
Uplink Frequency Band, GHz	S-Band	S-Band	S-Band	S-Band
Telecommand Data Rate, kbps	S: 1 kbps	S: 1 kbps	S: 1 kbps	S: 1 kbps
Receiving Antenna Type	S: Omni	S: Omni	S: Omni	S: Omni

3.3.3. Data Products

EMIT Data Products

The data products follow the processing scheme for the Atmospheric Imaging Assembly (AIA) on the Solar Dynamics Observatory (SDO).

Level 0 Raw data for each wavelength channel.
Level 1.0 Intensity images derived from Level 0 (raw) data. Replace bad pixels, de-spike, subtract bias and dark current, insert metadata in image header.
Level 1.5 Apply flat field, normalize to unit exposure, apply calibration to derive radiance (W m^{-2} sr^{-1}) at each pixel.
Level 2 Multi-temperature movies derived from co-aligned image sequences, differential emission measure (DEM) maps.

EFI Data Products

The data products follow the processing scheme for EMIT images for a single wavelength channel (no DEM maps).

MBC Data Products

The data products to Level 1.0 follow the processing scheme for EMIT images (also similar to ASPIICS processing [30]).

Level 1.5 Correct for stray light, apply flat field, normalize to unit exposure, apply calibration to derive radiance (W m^{-2} sr^{-1}) at each pixel.

Level 2 White light images and movies, polarized brightness and polarization angle images and movies, images and movies in Fe XIV 530.3 nm and He I D3 587.6 nm, temperature and radial flow maps.

Joint Data Products

Level 3 Coaligned images and movies for EMIT, EFI, and (for EUV fields extending beyond the limb) MBC.

Further joint products are anticipated that incorporate data from other spacecraft and ground-based observatories.

3.4. Ground-Based Observatories

CMO does not require specific data or support from ground-based observatories to achieve closure on its key scientific objectives (§1.3.2) but would be scientifically enhanced by ground-based capabilities, specifically including images, magnetograms, and spectra acquired with instruments coupled to adaptive optics. Existing instruments can observe the photosphere and chromosphere with angular resolution 0.05–0.3 as and field of view 30–120 as on a side, specifications that complement the 0.02–0.06 as resolution and 20 as field of view of the CMO EUV microscopes. Magnetograms will be particularly valuable for identifying the magnetic roots of flux tubes that exhibit primary heating events. Observatories with suitable instruments include the 4-m Daniel K. Inouye Solar Telescope (DKIST) [31], the 1.6-m Goode Solar Telescope (GST) [32], and the 1.5-m GREGOR telescope [33].

3.5. Risk List

The following are judged to be the top risks for the CMO mission concept at its present state of development. A standard risk chart is shown in Figure 16.

Risk 1

Statement: Given that the requirements for precision and stability of the CMO satellite formation exceed the demonstrated state of the art, there is a possibility that the performance of the EUV telescopes and coronagraph will be degraded, resulting in science data of lower quality.

Context and mitigation: Image smear (EMIT) or suboptimal external occultation (MBC) increases gradually with departure from nominal formation. The most challenging requirement, transverse alignment, can be violated by a factor of three and still yield EUV angular resolution better than the current state of the art and acceptable coronagraph occultation. Mitigation comprises demonstration of feasibility via the VISORS and PROBA-3 precision formation flying (PFF) missions [15] [34]; and technology development of RPSS (§4.2.2).This is a system-level risk encompassing subsystem-level risks 3 and 4.

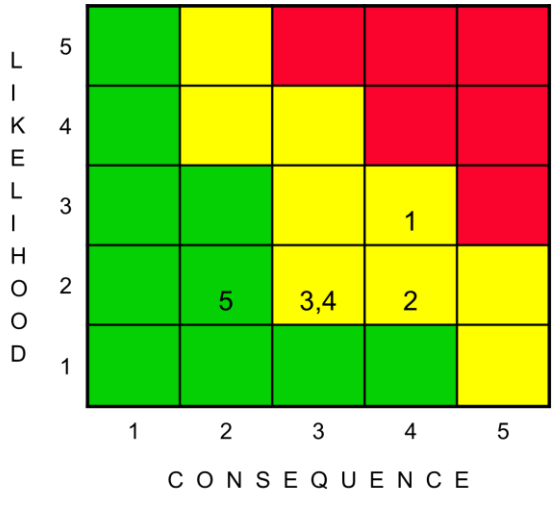

Figure 16. Top five CMO risks based on current technology and technology development plan.

Impact: Absent mitigation by flight demonstration of PFF to VISORS or PROBA-3 levels, it is doubtful that CMO, even with supporting PFF technology development to TRL 6, would be considered viable as a major mission.

Risk 2

Statement: Given that a photon sieve optic has not been demonstrated in space, there is a possibility that one or more of the CMO optics will be damaged during launch.

Context and mitigation: A silicon photon sieve similar in design to the CMO sieves except for having a smaller (80 mm) diameter has survived vibration testing to GEVS (General Environmental Verification Standard) levels. Vibration and acoustic testing of a CMO-spec sieve is expected to be completed in 2023. An 80-mm sieve will fly on the VISORS mission.

Impact: CMO carries six independent photon sieve telescopes. Any one telescope will provide observations of primary coronal heating events with unprecedented resolution. The loss of one or more photon sieves would decrease the scientific return from the mission by restricting temperature coverage. It is possible for a sieve to suffer tearing damage within only a portion of the aperture; such a tear would decrease the contrast of the image but may maintain nearly full angular resolution.

Risk 3

Statement: Given that neither the Compact Astrometric Alignment Sensor nor a closely similar sensor has reached TRL 5, there is a possibility that the CAAS will not perform to specifications.

Context and mitigation: A CAAS breadboard model has been fabricated and tested. A CAAS engineering model is designed and will be fabricated and tested under the RPSS technology development plan (§4.2.2).

Impact: CMO will be able to achieve most of its scientific objectives without the CAAS if the 3DPLR performs to its specifications. Objectives that relate to the evolution of individual fields of view over hours or longer will be adversely affected because CAAS provides the most accurate link to an absolute reference frame.

Risk 4

Statement: Given that neither the 3D Precision Laser Ranger nor a closely similar sensor has reached TRL 5, there is a possibility that the 3DPLR will not perform to specifications.

Context and mitigation: A 3DPLR engineering model will be designed, fabricated, and tested under the RPSS technology development plan (§4.2.2).

Impact: The 3DPLR lab prototype has demonstrated 400 μm resolution, which exceeds the requirement. Furthermore, each 3DPLR has six separate channels. Only one channel is required for longitudinal sensing that meets the requirement. With only one channel, transverse and attitude sensing may not perform to specifications, but CAAS is a parallel system that meets both attitude and transverse sensing requirements.

Risk 5

Statement: Given that the company developing the radio direction finder (RDF) considered by the MDL study is not presently planning to make the system commercially available, there is no identified RDF to achieve initial coarse formation of the three CMO satellites.

Context and mitigation: The company in question has indicated a willingness to study the cost of finishing the development of their RDF. This option, as well as market research to identify developers of similarly capable systems (including the one used by PROBA-3), will be explored as part of the RPSS development plan (§4.2.2).

Impact: Radio direction finding is the preferred method for CMO to acquire initial coarse formation. An analysis by Marr [35] indicates that intensive Deep Space Network (DSN) tracking over four days should be able to locate a spacecraft at L1 with a 3σ position error of 0.8 km and velocity error of 1.4 cm s^{-1}. Another option is a vision-based system as demonstrated on the PRISMA mission [36] [18].

4. Development Schedule and Schedule Constraints

4.1. High-Level Mission Schedule

Based on the technology development plan below (§4.2), it is estimated that 2-3 years of pre-formulation work will be necessary to reach Mission Concept Review.

Figure 17 shows the high-level CMO schedule for Phases B-F resulting from the MDL study. The duration of Phase A for a mission of this magnitude may be up to 2 years. Therefore, including time since MDL and pre-Phase A work, the timeline in the figure should realistically be delayed by about 3 years.

Table 19 summarizes the duration key mission phases.

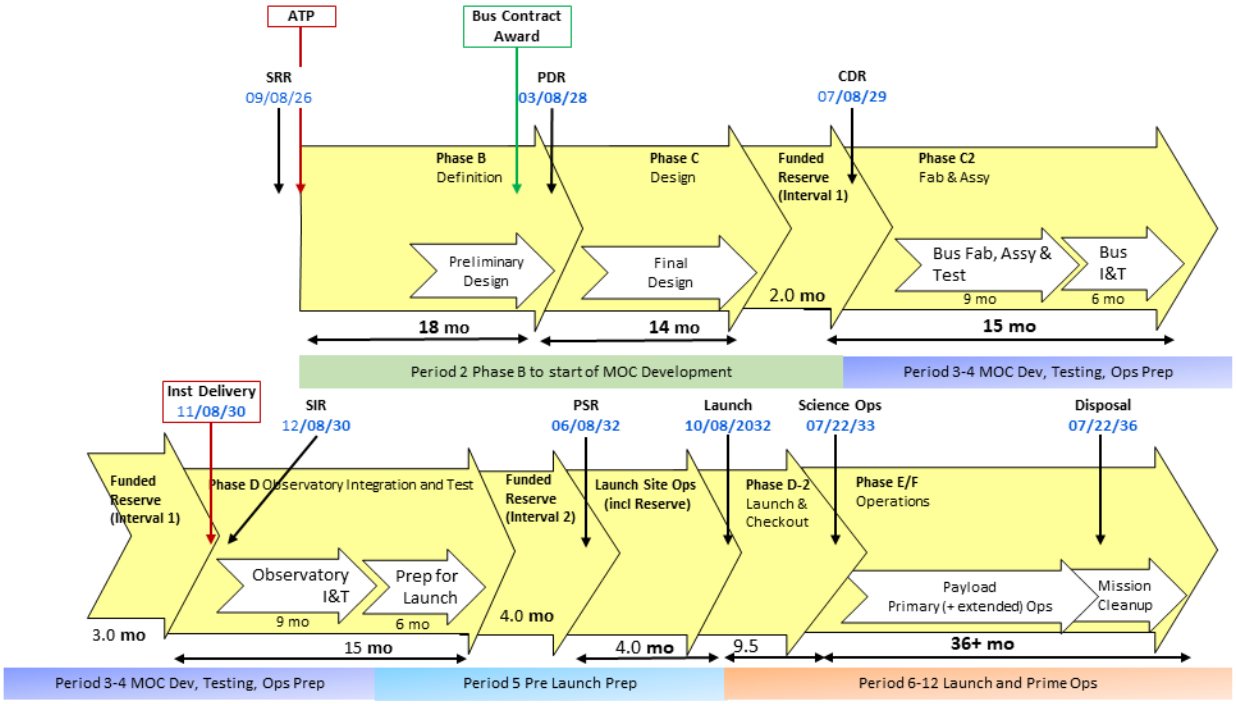

Figure 17. CMO high-level schedule for Phases B-F.

Table 19. Key Phase Durations

Project Phase	Duration (Months)
Phase A – Conceptual Design	24
Phase B – Preliminary Design	18
Phase C – Detailed Design	29
Phase D – Integration & Test	19
Phase E – Primary Mission Operations	36
Phase F – Extended Mission Operations	24
Start of Phase B to PDR	18
Start of Phase B to CDR	32
Start of Phase B to Delivery of EMIT Instrument	47
Start of Phase B to Delivery of EFI Instrument	47
Start of Phase B to Delivery of MBC Instrument	47
Start of Phase B to Delivery of RPSS	47
Start of Phase B to Delivery of Integrated SC1	56
Start of Phase B to Delivery of Integrated SC2	56
Start of Phase B to Delivery of Integrated SC3	56
System Level Integration & Test	10
Project Total Funded Schedule Reserve	9
Total Development Time Phase B - D (with reserve)	75

4.2. Science, Technology Development Plans

4.2.1. Photon Sieve Technology

Table *20* lays out the steps, activities, and resources needed to develop the photon sieves from the current state of the art to TRL 5 by project Phase A and to TRL 6 by Preliminary Design Review (PDR), ensuring that the EMIT instrument meets the scientific and programmatic requirements of CMO. The table can be interpreted with reference to §2.3.1.1 and Appendix C. The activities can proceed largely in parallel within a total development time of 3 years.

The cost of this effort was estimated using a standard GSFC budget tool that includes civil servant and contract labor (fully loaded rates), facility assessment (GSFC Detector Development Laboratory), equipment, materials, supplies, and projected inflation. The costs to achieve (cumulatively) the technology objectives are:

Objective 1	$261K
Objectives 1 and 2	$709K
Objectives 1, 2, and 3	$1149K

Table 20. Photon sieve development plan

Technology Objective	Starting Point for Objective	Description of Challenge	Development Effort	Need Date
1. Demonstrate binary amplitude photon sieves meeting CMO aperture requirement.	170 mm dia. with 7 μm (smallest) holes. TRL 4. 80 mm dia. with 2 μm arcs (5:1 aspect ratio). TRL 5.	Fabricate and test 170 mm dia. sieves with 4.7 μm minimum zone size and 10:1 aspect ratio arcs.	1 yr	Before MCR
2. Demonstrate binary phase sieves meeting CMO baseline requirements.	80 mm silicon with 2 μm holes. TRL 4.	Fabricate and test 170 mm dia. sieves with 4.7 μm minimum zone size and 10:1 aspect ratio arcs. Mounting solutions and environmental characterization (acoustic and vibration testing) for thin film phase sieves require specific attention.	2 yr	MCR
3. Demonstrate multi-phase sieves providing CMO optimal performance.	Laboratory proof of concept. TRL 3.	Fabricate and test 170 mm dia. sieves. Incorporate multiple phase zones to achieve >70% efficiency. Requires fine control of stress, oxidation and material interfaces. May require dedicated deposition equipment to ensure repeatable film quality.	3 yr	Mission PDR

4.2.2. Relative Position Sensing System

Each of component of the RPSS is currently at TRL 4.

Table *21* lays out the steps, activities, and resources needed to develop the RPSS to TRL 5 by project Phase A, and to TRL 6 by PDR. The table can be interpreted with reference to §2.3.1.2 and Appendix D.

The cost of this effort was estimated using the budget tool described in §4.2.1.

	RDF	3DPLR	CAAS	Total
Objectives 1, 2, 3	$946K	$673K	$559K	$2.18M
Objectives 4,5	0	$441K	$377K	$ 0.82M
		Total for all objectives		$ 3.00M

Table 21. Relative position sensing development plan

Technology Objectives	Starting point for Objective	Description of Challenge	Development Effort	Need Date
1. Demonstrate RDF subsystem using flight qualified components	DOD funded prototype (TRL4) developed ~2019, meets CMO requirements. Some hardware elements have	Work with vendor to update design and employ current model space qualified hardware Execute performance testing of updated design.	2 yr	MCR

	been discontinued by vendor.			
2. Refine hardware and software design of 3DPLR	Existing 3DPLR lab unit employs analog components & bench instruments. Telescopes/optical design employs COTS parts.	Transition analog components to digital components & software. Refine design of transmit/receive telescopes.	2 yr	MCR
3. Refine hardware and software design of CAAS	Existing CAAS lab unit employs bench instruments and COTS parts.	Refine optical and mechanical design. Develop software interface.	2 yr	MCR
4. Develop fully integrated robust packaged design for 3DPLR	Objective 2 achieved	Design and fabricate flight qualifiable packaging. Subject to environmental test. Demonstrate operation/sensing in vacuum environment.	1 yr	Mission PDR
5. Develop fully integrated robust packaged design for CAAS	Objective 3 achieved	Design and fabricate flight qualifiable packaging. Subject to environmental test. Demonstrate operation/sensing in vacuum environment.	1 yr	Mission PDR

4.3. Development Schedule and Constraints

Because of the maturity level of the mission (§2.2), only the high-level schedule (§4.1) has been estimated. The MDL study did not identify any unique facilities that would constrain Phases C/D development. Although the expertise necessary to make the photon sieves is presently unique, the associated facility at GSFC has no unique equipment and is expected to be available as needed. GSFC will also develop the RPSS. As to external dependencies, it is anticipated that the spacecraft and one of the three instruments (MBC) will be designed and fabricated outside NASA (Figure 7). The coronagraph may be supplied by an international partner.

The CMO mission has no science- or operations-based launch restrictions. All CMO's science requirements (§1.2) and measurement requirements (§1.3.1) can be accomplished during any phase of the solar cycle. CMO's trajectory and L1 halo orbit also place no restrictions on time of launch.

5. Mission Life-Cycle Cost

5.1. Costing Methodology and Basis of Estimate

A first-stage Cost Risk Analysis for CMO was carried out by the GSFC Cost Estimating, Modeling, and Analysis Office (CEMA). The CEMA process is shown schematically in Figure 18. The CMO analysis was carried out with the following procedures:

- CMO was assumed to be a Class C Observatory.
- Costs were reported in fiscal year (FY) 2027 constant year dollars.

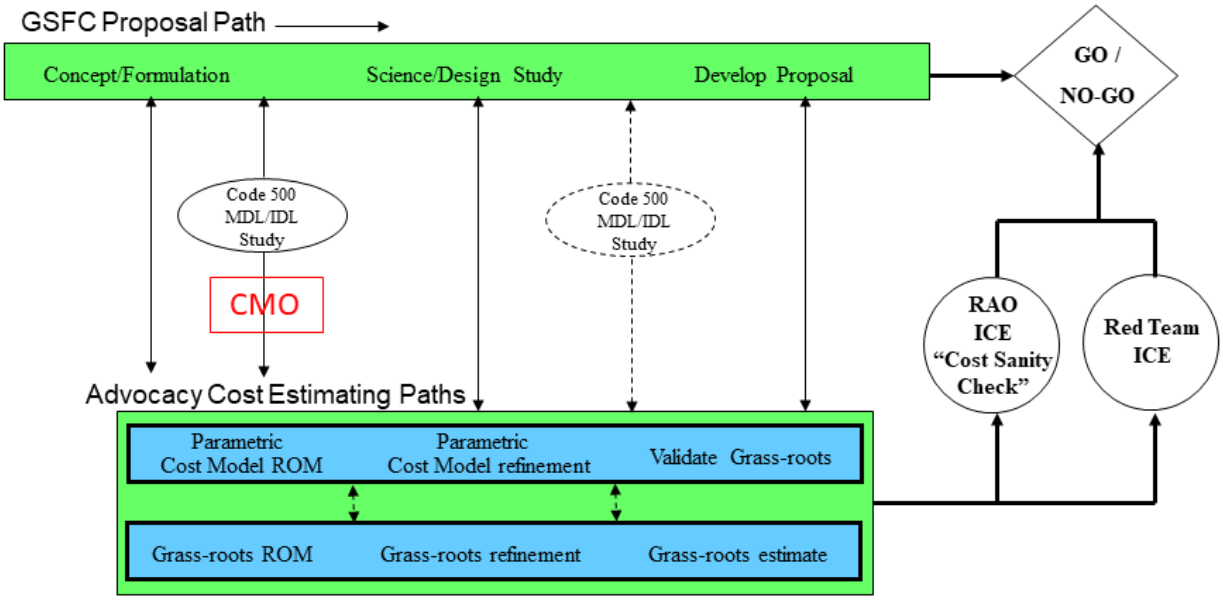

Figure 18. CMO is at an early stage of the iterative GSFC cost estimation process.

- Real year dollar (RY$) estimates were generated on the typical NASA assumption that 60% of total cost is expended at 50% schedule completion. This does not account for time-phasing of activities, long lead items, and funded schedule margin. *RY$ estimates do not constitute a GSFC cost estimate or a budget, which is integrally tied to an Integrated Master Schedule (not yet developed for CMO).*
- Component-level modeling was based on the MDL Master Equipment Lists (MELs) and final engineering presentations.
- Cost risk analysis incorporated mass contingency and margin, design, and modeling uncertainties. The analysis did not include cost associated with discrete risks; no discrete risks were identified during the MDL study. Appendix E describes the CEMA cost risk analysis procedure.
- Estimates for spacecraft covered WBS 6 costs from development through delivery to Observatory I&T (Integration and Test).
- Three spacecraft flight units (SC1–3) were modeled.
- Full non-recurring engineering (NRE) was applied to all subsystems of SC1 and a combination of shared and full NRE was applied to identical and unique subsystems of SC2 and SC3.
- Additional Costs were estimated for FPGA (Field Programmable Gate Array) Development, Flight Software and FSW Test Bed, Flight Spares and ETUs (Engineering Test Units), Ground Support Equipment, and Environmental Test.

5.2. Cost Estimate(s)

The CEMA-estimated cost profiles for the three CMO spacecraft are shown in Table 22. Cost summaries and S-curves are included in Appendix G.

CMO is not developed to the level necessary to complete a total mission cost funding profile by fiscal year. A mission cost summary based on the MDL study and the CEMA study for 70% confidence level is shown in Table 23 . All costs were estimated on the assumption that the mission is entirely NASA-funded and all significant work is performed in the US.

Pre-Phase A technology development costs are estimated in §4.2 but are excluded from total mission cost per NASA guidance.

Table 22. CEMA-estimated cost for the CMO spacecraft

SC1

60% Spread	50% CL		70% CL	
Year	Annual Cost FY27$M	Annual Cost RealYr$M	Annual Cost FY27$M	Annual Cost RealYr$M
2026	$1.1	$1.0	$1.2	$1.2
2027	$23.6	$23.6	$26.9	$26.9
2028	$42.9	$44.0	$48.9	$50.1
2029	$40.4	$42.6	$46.1	$48.5
2030	$20.8	$22.5	$23.7	$25.6
2031	$2.5	$2.7	$2.8	$3.1
Total	**$131.2**	**$136.4**	**$149.5**	**$155.4**

SC2

60% Spread	50% CL		70% CL	
Year	Annual Cost FY27$M	Annual Cost RealYr$M	Annual Cost FY27$M	Annual Cost RealYr$M
2026	$1.2	$1.2	$1.4	$1.3
2027	$27.0	$27.0	$30.7	$30.7
2028	$49.0	$50.3	$55.8	$57.3
2029	$46.2	$48.6	$52.6	$55.4
2030	$23.7	$25.7	$27.0	$29.2
2031	$2.8	$3.1	$3.2	$3.6
Total	**$149.9**	**$155.9**	**$170.7**	**$177.5**

SC3

60% Spread	50% CL		70% CL	
Year	Annual Cost FY27$M	Annual Cost RealYr$M	Annual Cost FY27$M	Annual Cost RealYr$M
2026	$1.4	$1.4	$1.6	$1.5
2027	$31.1	$31.1	$35.4	$35.4
2028	$56.6	$58.1	$64.4	$66.1
2029	$53.4	$56.2	$60.7	$63.9
2030	$27.4	$29.6	$31.2	$33.7
2031	$3.3	$3.6	$3.7	$4.1
Total	**$173.2**	**$180.0**	**$197.0**	**$204.8**

Summary (FY27$M)

Spacecraft	50% CL	70% CL
SC1	131.2	149.5
SC2	149.9	170.7
SC3	173.2	197.0
Total	454.3	517.2

Table 23. Estimate of CMO mission cost incorporating CEMA cost estimate for three spacecraft at 70% confidence level.

This summary is intended only for rough estimation and strategic planning. It is not a GSFC cost estimate or budget.

	Coronal Microscale Observatory		**Parametric Derived Point Estimate Mission Wraps applied to Parametric Estimate for Payload (WBS 5.0) and SC Bus (WBS 6.0)** ($M FY27)					
Line Item	**Top-Level WBS (per NASA Cost Analysis Working Group Cost Analysis Data Requirement)**	**Point Estimate Source**	**Percent of Flight Hardware (WBS 5.0+6.0)**	**Reference ROM Multipliers**	**WBS Point Estimate**	**Percent Reserves**	**Reserves**	**WBS Point Estimate (with Reserves)**
1.0	**Project Management**	Wrap	7.0%	7.0%	53.5	30.0%	16.0	69.5
2.0	**Systems Engineering**	Wrap	5.0%	5.0%	38.2	30.0%	11.5	49.6
3.0	**Safety and Mission Assurance**	Wrap	4.0%	4.0%	30.5	30.0%	9.2	39.7
4.0	**Science/Technology (Note 1)**	Wrap	7.0%	7.0%	53.5	30.0%	16.0	69.5
5.0	**Payload(s) (including I&T prior to S/C I&T)**				84.0	30.0%	25.2	109.2
	SC1 - Photon Sieves				7.0			
	SC1 - EUV Finescale Imager				22.0			
	SC2 - EUV Detectors				17.0			
	SC3 - Coronagraph				30.0			
	CAAS and 3DPLR Systems				8.0			
6.0	**Spacecraft**				679.7	30.0%	203.9	883.6
	SC Bus 1 (70% cost risk)	CEMA			*149.5*			
	SC Bus 2 (70% cost risk)	CEMA			*170.7*			
	SC Bus 3 (70% cost risk)	CEMA			*197.0*			
	Flt S/W	Wrap	10.0%		*51.7*			
	10 Unique FPGA Development Efforts	Wrap	$0.5		*4.8*			
	FlatSat (FSW Testbed)	Wrap	5.0%		*2.6*			
	GSE	Wrap	5.0%		*25.9*			
	Subsystem Environ. Testing	Wrap	5.0%		*25.9*			
	Flt spares & ETUs	Wrap	10.0%		*51.7*			
7.0	**Mission Operations System (MOS) (Note 2)**	MDL	16.5%	16.5%	16.5	30.0%	4.9	21.4
	Downlink costs (Note 3)				*0.0*			
	MOS (Phases E & F)				*16.5*			
9.0	**Ground System(s) (Notes 2, 4)**	MDL	6.5%	6.5%	24.7	30.0%	7.4	32.2
10.0	**Systems Integration and Test (Note 5)**	Wrap	7.0%	7.0%	53.5	30.0%	16.0	69.5
11.0	**Education & Public Outreach (science partner provided)**	Wrap	0.0%	0.0%	0.0	30.0%	0.0	0.0
	Project Level Reserve (science partner provided)						0.0	0.0
	Total without Launch Vehicle Services				1034.1	30.0%	310.2	1344.3
	Phase A (science partner provided)							6.0
8.0	**Launch Vehicle/Services (Note 6)**							0.0
	Total NASA Phase A-E							**1350.3**

Reference ROM Multipliers: WBS 1.0, 2.0, 3.0 based on TMC feedback and GSFC Code 101 historical data. Other WBS multipliers based on analysis of prior proposal estimates and additional feedback from TMC reviews. The Basis for Reference ROM Multipliers have not been verified with the grass-roots estimating organization and should be used with caution.
IDC includes subsystem and systems level contingency and margin per the GSFC Gold Rules.

Notes for Mission Summary:

1 Science partner provides this Wrap or Point Estimate. Should include any costs for developing Science Ops Centers as the MDL does not provide this estimate, along with science team during mission operations.
2 Includes Phase E cost of use of downlinks (not charged to NASA missions) and MOS costs
3 Note (if applicable) that "Downlink Costs will not actually be charged to NASA missions but must be reported in the proposal"
4 Includes MOS costs during Phase A,B,C,D
5 Includes S/C I&T and integration of S/C to LV, but not Payload and S/C subsystem I&T prior to S/C integration. (S/C subsystem I&T prior to S/C I&T is in WBS 6
6 Customer provided estimate

Appendix A. Acknowledgments

The Study Team is indebted to the GSFC Mission Design Laboratory Team, the GSFC Cost Estimating, Modeling, and Analysis Office, and the GSFC Optical Communications Team for their essential contributions to this study. We are grateful to the GSFC Heliophysics Science Division and the GSFC New Opportunities Office for their support. We thank Muzar Jah for her extensive help in adapting MDL figures and tables to the format required for the study.

Appendix B. Acronyms and Abbreviations

3DPLR	3D Precision Laser Ranger
AIA	Atmospheric Imaging Assembly on SDO
ASPIICS	Association of Spacecraft for Polarimetric and Imaging Investigation of the Corona of the Sun (PROBA-3)
CAAS	Compact Astrometric Alignment Sensor
CAL	Calibration Mode
CBE	Current Best Estimate
CDR	Critical Design Review
CEMA	Cost Estimating, Modeling, and Analysis Office (GSFC)
CL	Confidence Level
CMO	Coronal Microscale Observatory
DDL	Detector Development Laboratory (GSFC)
DEM	Differential Emission Measure
DKIST	Daniel K. Inouye Solar Telescope
DRIE	Dry Reactive Ion Etching
DSN	Deep Space Network
DTE	Direct to Earth
EFI	EUV Finescale Imager
EMIT	EUV Microscale Telescopes
EOL	End of Life
ETU	Engineering Test Unit
EUV	Extreme Ultraviolet
FPGA	Field Programmable Gate Array
FTE	Full Time Equivalent
GEVS	General Environmental Verification Specification
GNC	Guidance, Navigation, and Control
GOES	Geostationary Operational Environmental Satellite
GST	Goode Solar Telescope
I&T	Integration and Test
IDL	Instrument Design Laboratory (GSFC)
ISC	Intersatellite Communications
KG	Knowledge Gap
L1	Sun-Earth Lagrange Point 1
LOI	Lissajous Orbit Insertion
MBC	Multiband Coronagraph
MDL	Mission Design Laboratory (GSFC)
MEL	Master Equipment List
MMOC	Multi-Mission Operations Center
MUSE	Multi-Slit Solar Explorer
NRE	Non-Recurring Engineering

NSN	Near Space Network
OCSS	Optical Communications Sustainment Study
OGS	Optical Ground Station
OST	Optical Space Terminal
PDR	Preliminary Design Review
PFF	Precision Formation Flying
PLR	Precision Laser Ranger
PP	Primary Propulsion
RDF	Radio Direction Finder
RF	Radio Frequency
ROSES	Research Opportunities in Space and Earth Sciences
RPSS	Relative Position Sensing System
SAFE	Safe Mode
SC1	Spacecraft 1
SC2	Spacecraft 2
SC3	Spacecraft 3
SDO	Solar Dynamics Observatory
SEL1	Sun-Earth Lagrange Point 1
SNSPD	Superconducting Nanowire Single Photon Detector
SO	Science Objective
SP	Secondary Propulsion
SPS	Shadow Position Sensor (PROBA-3)
STBY	Standby
STP	Solar Terrestrial Probes
STM	Science Traceability Matrix
SWaP	Space, Weight, and Power
TBD	To Be Determined
TILE	Tiled Ionic Liquid Electrospray
TRL	Technology Readiness Level
TTI	Transfer Trajectory Insertion
VBS	Vision Based System (PROBA-3)
VISORS	VIrtual Super-resolution Optics with Reconfigurable Swarms
WBS	Work Breakdown Structure
WDM	Wavelength Division Multiplexing

Appendix C. Photon Sieve Technology

A photon sieve [16] is a flat diffractive optic that can be used to form nearly diffraction-limited images at EUV and x-ray wavelengths where conventional focusing mirrors with aperture ≳20 cm are challenging to manufacture cost effectively (if at all) with the accuracy needed to approach the diffraction limit. Similar to a Fresnel zone plate, which consists of alternating opaque and transmissive annular zones, the photon sieve replaces the annular rings by concentric rings of holes. The binary amplitude Fresnel zone plate offers an efficiency of up to 10% while the binary amplitude hole-based photon sieve is only about 4% efficient due to the smaller effective clear aperture area. Efficiency is improved if the holes are replaced with arcs. Binary amplitude photon sieves have been fabricated by lithographically patterning an opaque film on a transparent substrate [37] [38].

The photon sieve architecture enables the creation of membrane-based structures with through-holes for the transmissive sections. In the EUV, where almost all materials are highly absorbing, this architecture lends itself to a compelling solution for high resolution imaging with moderate efficiency. The GSFC Detector Development Laboratory (DDL) has developed large-area membrane-based photon sieves using process based on Micro-Electro-Mechanical Systems. Silicon-based membrane structures are fabricated with a combination of contact lithography and deep reactive ion etching [39].

CMO consists of a collection of the six photon sieves, each optimized for a wavelength of interest (Table 1).

The photon sieves are manufactured using silicon on insulator (SOI) wafers. The device layer of the SOI serves as the membrane material, while the handle layer serves as the frame. See “Photon sieve fabrication” below for further information on fabrication methodology.

A hole based binary amplitude sieve is the simplest form of photon sieve with the most mature process development. These sieves are baselined for CMO as risk reduction. Membrane based sieves 80 mm in diameter have been demonstrated and will be implemented for the NSF-funded VISORS mission (Figure 19). These sieves are currently approaching TRL 6 with completion of acoustic and vibration testing. They consist of annular arrays of 5:1 aspect ratio arcs achieving a theoretical efficiency of 7%. Aspect ratios of up to 15:1, enabling an efficiency of 9%, have been demonstrated in the laboratory.

Additional technology development is required for larger diameter photon sieves. At present, proof-of-concept 170-mm hole-based sieves have been demonstrated with 8-μm minimum zone size, meeting the requirements of 4 of 6 sieves for CMO but at limited efficiency. Intermediate diameter 140-mm sieves with 2 μm outer zones are under development at GSFC to serve as ground support equipment for the Multi-Slit Solar Explorer (MUSE) MIDEX mission. Sieve fabrication development for MUSE is well aligned to the proposed CMO mission with 140-mm diameter sieves planned to be demonstrated in 2023–2024. The Fe XVIII and Fe XIX sieves for CMO require less aggressive outer zones of 4.7 μm and 5.5 μm respectively but scaled to 170-mm diameter. An effort to extend 170 mm the diameter of sieves with 5-μm outer zones and

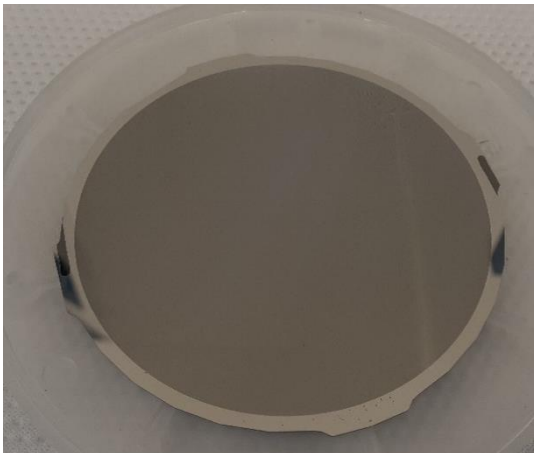

Figure 19. Example of 80-mm diameter binary amplitude sieve for the VISORS mission. Smallest holes are 8 μm diameter with 5.6 μm spaces.

15:1 arcs is recommended early in the technology development program. This will double the efficiency of currently available sieves and provide risk reduction for all the CMO sieves.

Advanced technology development for 170-mm diameter sieves with outer zones down to 2 μm will require additional fabrication development and process maturation and are mainly limited by achievable aspect ratios for relatively thick membranes on the order of 60 μm (Figure 20). Smaller zones to submicron level would require more advanced lithography approaches from standard 1x contact photomasks currently employed. Stepper lithography systems typically limit field sizes to 10's of millimeters on a side and would require splitting up a large area sieve design to dozens of photomasks to cover the full 170-mm diameter structure. This approach may be cost prohibitive. Another option is maskless direct write laser-based lithography. Systems are available that can pattern 200 mm wafers with feature sizes down to 0.5 μm. However, laser lithography systems have slow write-times due to the required rastering of the pattern. Further, submicron structures are limited to thinner membranes due to the requirement of thinner photoresists to meet the lateral dimensions and the challenge of making high aspect ratio structures. High aspect ratio etch masks with minimal lateral etch rate are also required to enable submicron high density, high aspect ratio structures. Binary amplitude sieve development has been focused on maximizing the membrane thickness to enable large apertures without mechanical support structures within the effective area. For zone sizes approaching 2 μm and below, the compatible thinner membranes would likely require membrane rib support structures for mechanical integrity further reducing efficiency.

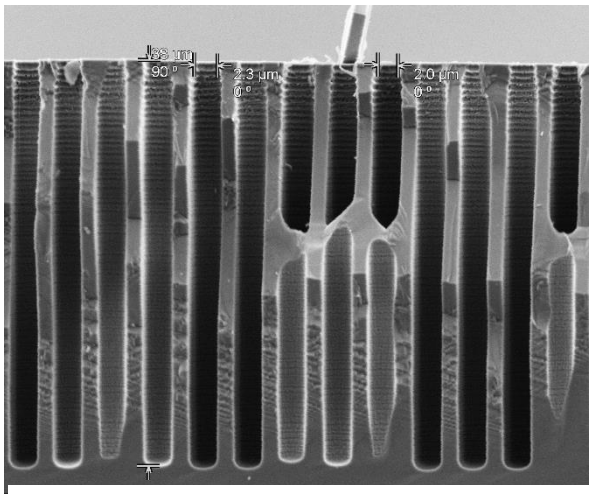

Figure 20. Cross section of high aspect ratio silicon. The apparent "connections" between cylinders are artifacts of the cleaving used to expose the cross section.

Binary Amplitude Sieve Summary

At present, 170 mm binary amplitude sieves are at TRL 3 and will require optical, acoustic and vibration testing for further TRL maturation. Further process development is required to demonstrate higher efficiency arcs with moderately smaller outer zones. The technology is currently available to demonstrate these sieves. We estimate that 1 year will be required to complete demonstration of all six CMO binary amplitude sieves. Additional support will be required for optical testing, mechanical packaging, acoustic and vibration testing.

Binary Phase Sieves

EUV Phase sieves must be very thin because they have no through holes. Ultra-thin transmissive films have recently been demonstrated for the production of pellicles for 13.5 nm EUV lithography applications [40]. The pellicles are used in semiconductor manufacturing to protect photomasks from particulate contamination. Free standing silicon nitride membranes as thin as 16 nm and demonstrated areas as large as 113 x 145 mm^2 have been shown to provide transmission approaching 90%. For a photon sieve or zone plate, such a structure could be modified to add the opaque zones with a second absorbing layer, creating a thin membrane binary amplitude sieve or binary amplitude zone plate. Here, the thin absorbing films will be compatible with very high-resolution submicron lithography. Alternatively, the opaque zones could be replaced with a phase shifting material designed such that transmission is maintained

but with a 180-deg phase shift with respect to the substrate. This technique has been demonstrated on quartz substrates or with dimpled polymer membranes for visible applications [41]. The primary challenge for EUV applications is the very thin materials required. A binary phase sieve increases the efficiency over the binary amplitude sieve by a factor of 2.5.

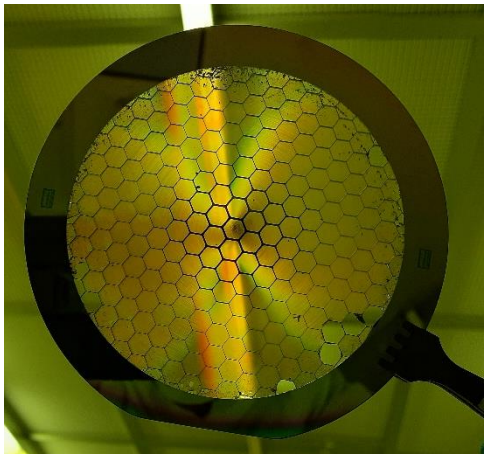

Figure 21. Prototype 80-mm diameter silicon binary phase sieve (100-nm thick silicon membrane)

At the GSFC DDL, silicon-based binary phase pinhole sieves with 2 mm outer zones have been demonstrated with diameters of up to 80 mm and silicon perforated membranes down to 100 nm thick, thus enabling phase shifting for the Ne VII and Fe XVIII and He I, He II lines. Current prototypes of silicon-based binary phase sieve membranes are supported by a hexagonal packed support grid machined into the silicon frame to improve mechanical integrity and are fabricated with the same fundamental processes as the binary amplitude sieves (Figure 21). Further increases in efficiency are enabled through development of phase shifting arc designs. Development of a binary phase sieve based on 5:1 arcs would have a theoretical efficiency of 17.5 percent. For CMO, another factor of two increase in area is required. 170-mm diameter polymer phase sieves 300 nm thick have been demonstrated at GSFC, but effects of polymer exposure to EUV along with dielectric charging and damage due to atomic oxygen need to be further investigated. For the Fe IX and Fe XV lines, further development of alternative thin films such as zirconium or aluminum for phase shifting is indicated, including procedures to control oxidation through thin film caping, and control film morphology and as-deposited stress. Demonstration of 170-mm diameter monolithic structures will require further development of procedures for handling the thin membrane materials. 80-mm diameter binary phase sieves are currently at TRL 3 with optical, vibration and acoustic testing being planned.

170-mm diameter binary phase sieves are estimated to require 3 years of development.

Multi-phase sieves

The binary phase sieve approximates the change in phase across a zone as a constant. However, as the path length changes across a zone-width, the effective phase also changes, so perfect phase compensation is not achieved. Ideally, the thickness of the membrane would increase across the zone to provide a phase shift progressing from 0 deg to 180 deg . A type of kinoform, such a structure can provide efficiency approaching 100% if material absorption and reflection is low. In the optical range, these structures have been demonstrated using gray scale lithography and tailored etching to create a silicon stamp which is then used as a master to imprint the desired topography into a polymer sheet [42] [43]. For CMO, a polymer solution will be challenging due to the effects of EUV exposure on the optical properties, along with the effects of exposure to atomic oxygen, radiation and dielectric charging in the space environment. The large apertures required for CMO and very high control of thickness uniformity required for full phase compensation have not been attempted and are at a low TRL. However, an approximate design based on a simplified digitized structure comprising a few layers of variable thickness is feasible and could yield efficiencies ~50%.

Photon sieve fabrication

The salient features of the fabrication process for the silicon phase contrast sieves include the following steps. A 500 µm thick silicon handle wafer coated with silicon oxide and single crystal silicon layer is patterned by contact lithography to define the sieve holes. For binary amplitude

sieves, the silicon thickness is set to provide sufficient mechanical support while allowing for high aspect ratio etching of the sieve zones. Our standard fabrication process starts with commercially procured silicon-on-insulator wafers. These wafers offer the advantage of exceptionally uniform silicon thickness and repeatable material properties, which is important for optical repeatability and phase shift uniformity. The sieve holes are plasma etched down to the silicon oxide which serves as a chemical etch stop. For binary amplitude photon sieves of large area, fabrication is a balance between the membrane thickness required for mechanical integrity (in both handling and flight) and the ability to create high aspect ratio through-hole structures within the membrane. Figure 22 is a simplified illustration of the fabrication process.

Deep Reactive Ion Etching (DRIE) with aspect ratios as large as 40:1 (80 µm thick membrane, 2 µm diameter) have been demonstrated in the DDL up to diameters of 80 mm. For larger area sieves, the varying zone sizes presents a challenge to DRIE processing. This is due to the aspect ratio dependent etch rate [44] [42] and results in the wider center zones etching faster than the narrow outer zone structures. The result is that etch rate selectivity between the silicon, photomask, and etch stop layers needs to be carefully designed. Larger area sieves with minimal zone sizes as required for the Fe XVIII and Fe XIX lines will require additional process development but are well within current technology capabilities. The wafer is then bonded to a pyrex handle wafer with a high glass transition temperature polymer. The silicon handle wafer is patterned with thick photoresist, into a mesh pattern in the case of binary phase sieves or an open aperture in the case of a binary amplitude sieve, and etched by DRIE, again to the SiO_2 layer. The SiO_2 is removed in hydrofluoric acid solution and the polymer is dissolved releasing the sieve from the handle wafer and finishing the process.

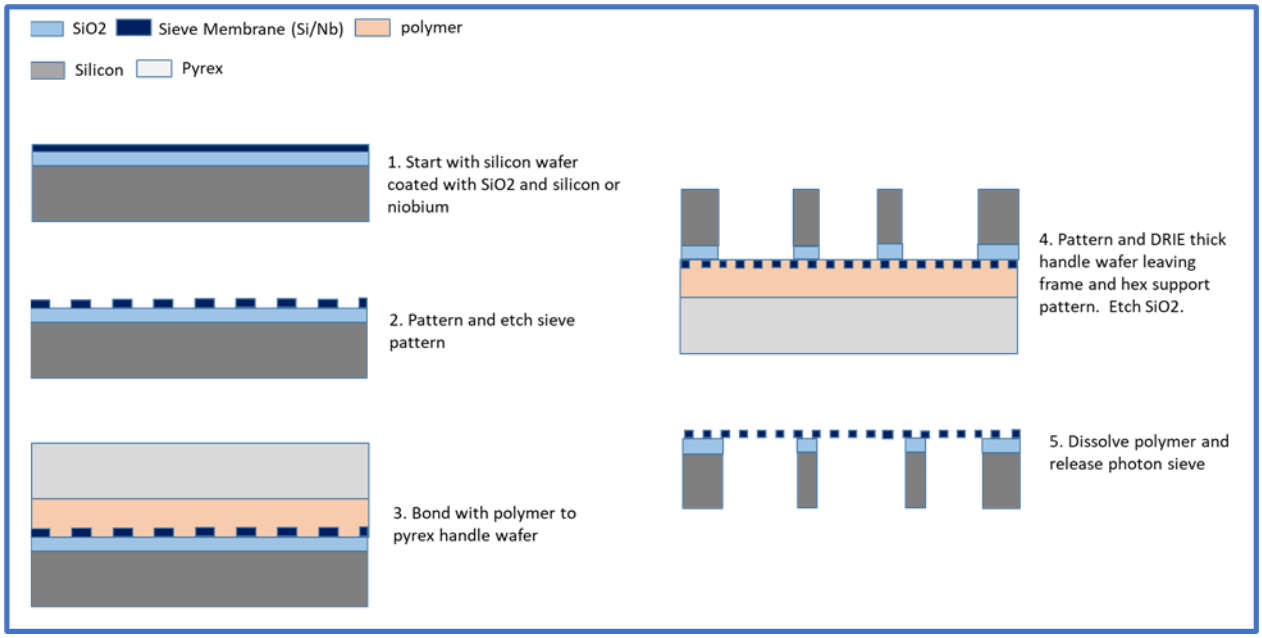

Figure 22. Simplified photon sieve fabrication process.

Appendix D. Relative Position Sensing System

The relative position sensing system (RPSS) continuously measures the position of one spacecraft relative to another. Data from the RPSS are used by the GNC system to command the TILE thrusters as needed to maintain alignment of the science instruments. For CMO, the "datum" spacecraft is SC2. The line of sight between the center of the occulting disk on SC2 and the center of the Sun forms the formation boresight as shown in Figure 5. The Extreme Ultraviolet Microscale Imaging Telescopes (EMIT) instrument is formed by the SC1/SC2 pair while the Multi-band Coronagraph (MBC) is formed by the SC2/SC3 pair. There are two full suites of RPSS sensors included on CMO, one for measuring the position of SC1 relative to SC2 and another for measuring SC3 relative to SC2. See Figure 8 for a diagram showing the distribution of the different RPSS components between the three spacecraft.

Each RPSS comprises three major subsystems (Table 24). Coarse longitudinal separation (range) and directional bearing are measured by the Radio Direction Finder (RDF). Fine resolution range measurement is given by the 3D Precision laser ranger (3DPLR). The 3DPLR also measures transverse linear offset from the boresight line and gives a coarse measurement of attitude relative to boresight. At the finest resolution, the Compact Astrometric and Alignment Sensor (CAAS) provides linear transverse offset from boresight and attitude relative to boresight.

Table 24. RPSS system performance and CMO instrument requirements

Subsystem	Operational Range	Longitudinal linear resolution	Transverse linear resolution	Attitude relative to boresight
RDF (1σ)	< 10 km	100 mm	---	1°
3DPLR (1σ) demonstrated	< 300 m	0.40 mm	0.40 mm	80 as
3DPLR (1σ) predicted	< 300 m	0.10 mm	0.10 mm	20 as
CAAS (1σ)	< 1 km	---	0.01 mm	1.5 as
EMIT knowledge requirement	100 m	5 mm	0.01 mm	2 as
MBC knowledge requirement	200 m	5 mm	0.30 mm	2 as

Radio Direction Finder

The technique of radio direction finding is a well established technology and is a key component of nearly all modern navigation systems. A variety of methods can be employed to enhance direction and range resolution, including the use of multiple antennas, phasing of signals, and timing of transmissions. Radio Acquired Detection and Ranging (RADAR) is one of the more sophisticated examples of RDF while wildlife tracking RDF systems are among the simplest. Modern RDF systems are compact, lightweight, robust, and have resolution proportional to the wavelength employed. At least one domestic provider of space qualified S-band radio systems has developed a prototype of an RDF system based on their own space qualified components for a defense customer. The vendor describes their prototype as being in the range of TRL4 or TRL5. The CMO team is currently communicating with that provider to understand their requirements for adapting their prototype system to CMO. The data provided in Table 24 are based on discussions with the vendor. Our baseline plan is to employ the S-band radio system

to provide both direction finding and interspacecraft communication. This minimizes the additional resources required for the RDF system, which will consist of additional S-band antennas and the added power consumption for RDF transmissions as opposed to communication transmissions. The PROBA-3 mission will use a similar radio direction finder system for coarse alignment and interspacecraft communication [45].

3D Precision Laser Ranger

The 3DPLR comprises a high-resolution laser ranger paired with a three dimensional retroreflective target. The laser ranger forming the basis of the system, the precision laser ranger (PLR), achieves finer range resolution than typical time-of-flight laser rangers by implementing signal analysis methods [46] (Figure 23). Instead of simple "pings", the PLR transmits a sequence of data packets or "frames". Each frame includes a header with an index number followed by a sequence of identical evenly spaced bits. The frames are transmitted to the target and reflected back to the origin where the return signal is analyzed. Since the frames are spaced evenly in time, comparison of the index number in the header data between the departing and arriving frames provides course range data. Intermediate resolution is achieved by comparing the elapsed bits in the arriving frame with the elapsed bits in the departing frame. Fine resolution is achieved through heterodyne phase analysis of the arriving bit with the departing bit. Thus, resolution can be measured down to a fraction of a single bit within the frame. The PLR employs telecommunications 1.5 µm diode laser transceivers with high reliability and low consumption of resources. Operational range of the single channel PLR is limited only by the strength of the return signal and spot size on the target. We have previously demonstrated 23 µm range resolution (1σ) with the PLR at a range of 150 m [47].

To achieve three dimensional sensing, we implement six separate PLR channels. Each channel is directed to a different face of a six-sided pyramid with 45° elevation faces coated with retroreflective material. The retroreflective coating is a suspension of millions of microscopic glass beads, each of which acts as a cats-eye retroreflector, as shown in Figure 24a. The incident laser beam is returned to the source, even though the coated surface is oriented 45° relative to the transmitted beam, as shown in Figure 24c. If the target spacecraft translates off

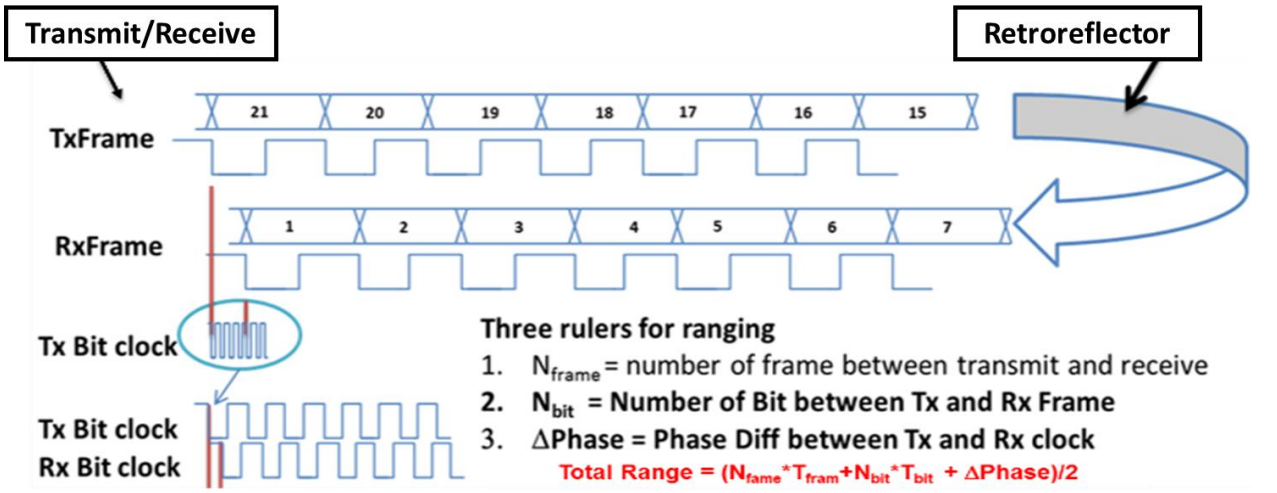

Figure 23. The PLR employs three levels of ranging accuracy through signal analysis. Evenly spaced packets of optical data or "frames" are transmitted to a retroreflector on the other spacecraft and returned to the transmitter. Each frame contains an index number and a sequence of identical bits. Course ranging compares the index number of the arriving frame with the departing frame. Intermediate ranging compares the number of bits that have elapsed in the arriving and departing frames. Fine ranging uses heterodyne phase analysis to measure the fractional difference in the arriving and departing bits (clock).

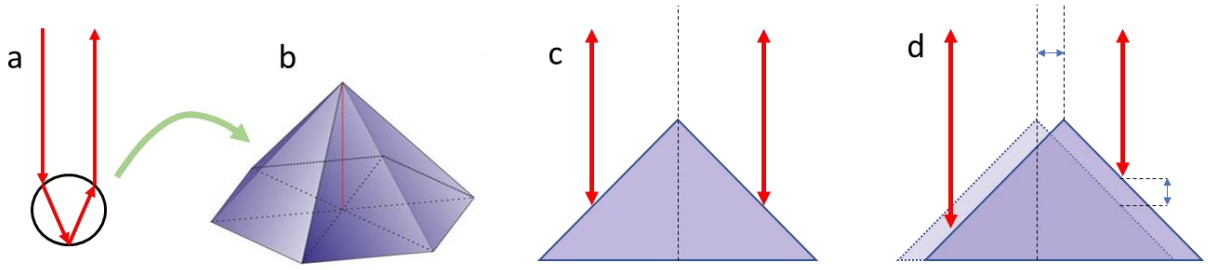

Figure 24. The 3DPLR employs retroreflective coating on a pyramidal target. The coating contains microscopic catseye retroreflectors (a), which are applied to a 6-sided pyramid with 45° elevation (b). Ranger beams originating on the other spacecraft are returned back to their origin by the retroreflective coating on the pyramid (c). If the target spacecraft shifts, the range values measured for each pyramid face will change (d). Comparing range values from all six faces enables measurement of all six degrees of freedom in relative position.

boresight, one PLR beam will descend its pyramid face (lengthening the range to target) while another beam will ascend its pyramid face (shortening the range to target). Because the pyramid has an elevation angle of 45°, the change in range is equal to the transverse movement, as can be seen in Figure 24d. Comparison of range values from all six faces enables full characterization of position and attitude relative to the transmitter. To direct the six beams to the pyramid, six transmit telescopes will be arranged in a hexagonal pattern around a single receiver telescope. The six channels will be time multiplexed to avoid confusion in the receiver channel.

Although the single-channel PLR has demonstrated 23 µm range resolution from a corner cube retroreflector, the use of the retroreflective material degrades the precision for both transverse and longitudinal sensing. The spot size of the laser beam results in an “uphill” return and a “downhill” return from different portions of the same laser spot, resulting in a time-broadened signal. Figure 25 shows the laboratory prototype for the single-channel PLR. Figure 26 shows experimental results for transverse sensing using a retroreflective target oriented at 45°. The data correspond to a transverse measurement sensitivity of 400 µm. We are currently working on improving the design of the transmit telescope to reduce the spot size on the target pyramid, which we predict will result in a transverse sensitivity of ~100 µm. Improving telescope design and transitioning to flight qualifiable packaging are key elements of our technology development plan (§4.2.2). The current 400 µm sensitive system is TRL 4.

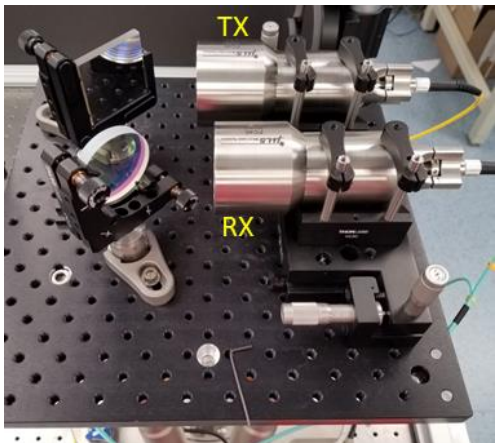

Figure 25. Transmit and receive telescopes of the 3DPLR laboratory prototype mounted on a hexapod.

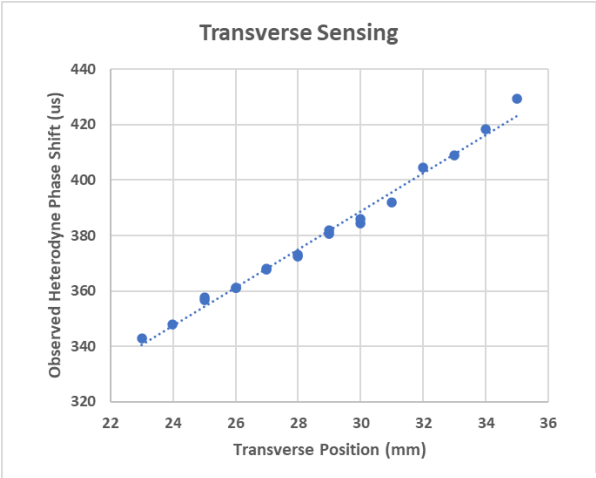

Figure 26. The PLR senses transverse motion of 45° angled target with 400 µm sensitivity.

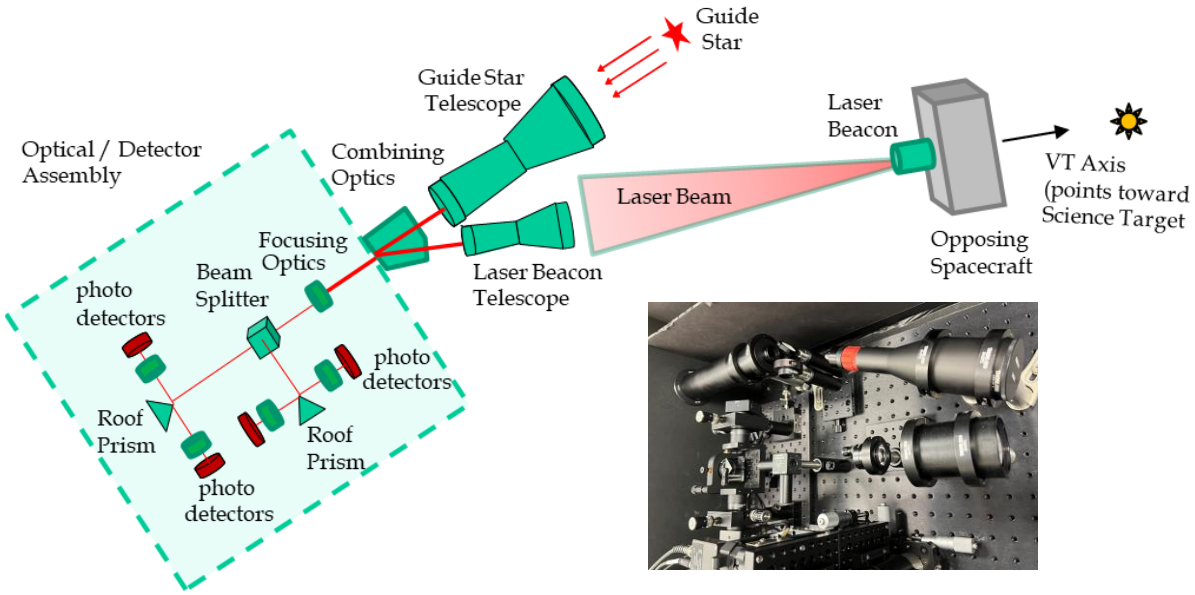

Figure 27. Optical layout of the Compact Astrometric Alignment Sensor and photo of the laboratory prototype.

Compact Astrometric Alignment Sensor

The Compact Astrometric Alignment Sensor (CAAS) provides a measurement of precision inertial alignment of each pair of spacecraft in the formation to ensure required astrometric alignment of the respective dual-spacecraft system. Receiver telescopes simultaneously focus the images of a guide star and a laser beacon mounted on the opposing spacecraft onto a common beam combining/dividing detector assembly to achieve ultra-precise milliarcsecond class alignment performance in a compact package. Figure 27 is a diagram of the CAAS laboratory prototype, illustrating the sensor's optical path for incoming light combined from the guide star and laser beacon. Focused images of guide star and laser beacon are combined optically and focused to diffraction-limited spot sizes through a beam splitter onto a set of knife edge prisms. The split light is refocused onto sensitive photodetectors to detect extremely low light level changes due to focused spot motion. When alignment is optimum, the images are split evenly, and each sensor records an equal intensity. Any shift in spacecraft alignment or inertial attitude results in the image translating relative to the knife edge and the two detectors receiving unequal fractions of the image. Flashing the laser beacon on/off provides a means to measure the spacecraft transverse alignment with respect to an inertial reference. Two pairs of prism/sensors mounted orthogonally provides both two-axis alignment measurements. The CAAS image dividing/detector assembly, based on the design of the Gravity Probe-B science telescope [48], provides a common measurement mechanism that eliminates systematic errors that would arise from using independent sensors to measure inertial attitude and transverse alignment.

The CAAS team has completed design and initial performance characterization of a fully functional, 2-axis laboratory prototype for PFF. Results of measured CAAS alignment sensitivity, shown in Figure 28, demonstrate system performance scalable to 0.045 as (for detector resolution = 6.5 fW), indicating TRL 4 maturity. The CAAS Engineering Model (EM) has been designed but is not yet built. The EM incorporates front end telescopes that use Cassegrain-type and folded optics to provide a flight-like model in a compact package (Figure 28). The CAAS EM features a separate optical assembly, with detector modules coupled to the CAAS EM optical assembly via fiber optic cables. This provides a means to locate the detector module

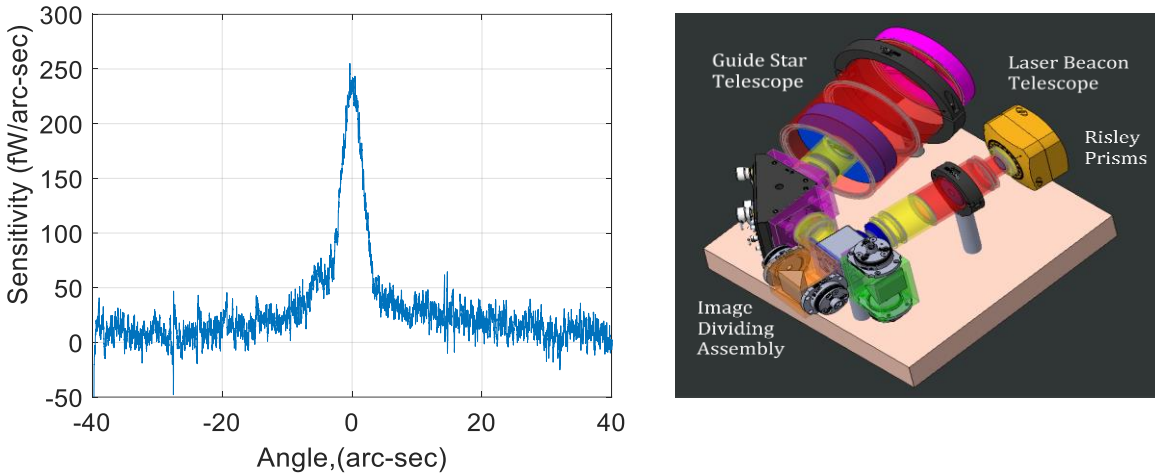

Figure 28. Measured sensitivity of the CAAS laboratory prototype.

in an environmentally stable location on the spacecraft bus, away from the optical assembly which is mounted on the exterior of the spacecraft. Additionally, the CAAS EM includes a set of Risley prisms on the front end of the laser beacon telescope to provide incoming beam scanning within a narrow field angle (2-3 deg). This is required for sensor acquisition and for solar tracking operations.

Our technology development plan (§4.2.2) will address development, comprehensive testing, and full performance characterization of the CAAS. We will demonstrate the full flight-like functionality of the system in a compact package. Testing of the sensor in a flight-like test environment will be used to evaluate the performance of the system in expected real-world conditions, such as those from stray light contamination of the guide star image from laser beacon light.

Precision Formation Software and Testbed

Standard guidance, navigation and control (GNC) software is generally not designed for precision formations. Each spacecraft has twelve degrees of freedom in its position, six with respect to inertial space, and six with respect to its datum spacecraft [49]. In addition to the sensors described, we are developing customized software that ingests the RPSS sensor data and then interfaces with the spacecraft GNC software to provide commanding for the TILE thrusters. Software development is not specifically identified in the Technology Development

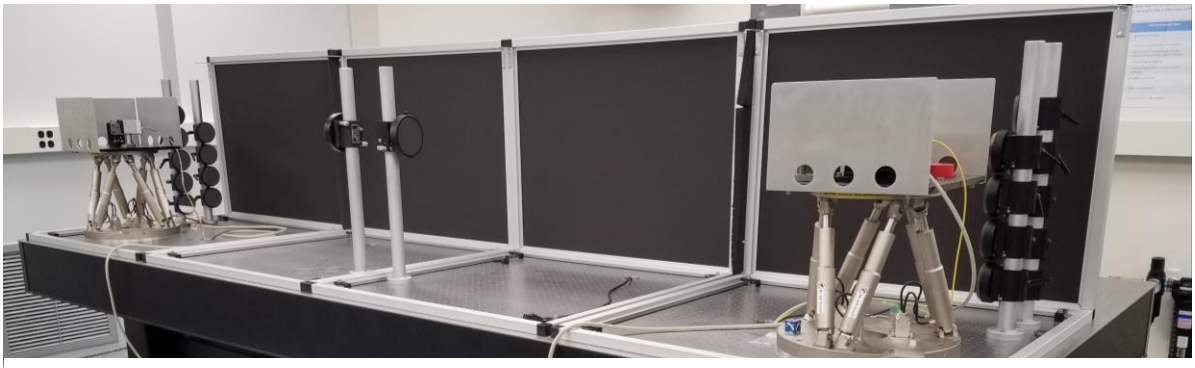

Figure 29. The Precision Formation Flying Testbed enables testing of RPSS subsystems. Two hexapod platforms with six degree of freedom motion simulate the two spacecraft while a series of 20 round mirrors provide a 100 m optical separation between the hexapods.

Plan (§4.2.2) because it is embedded in the sensor development. Sensors will undergo performance testing with the software on our Precision Formation Flying Testbed (Figure 29). The testbed includes two high precision hexapod platforms that simulate two separate spacecraft and can provide a range of positions and attitudes. A series of mirrors enable us to simulate an optical separation between the two “spacecraft” of up to 100 m. This testbed enables us to conduct performance tests during which the software is challenged to maintain alignment between the two hexapods when perturbed.

Appendix E. Spacecraft CAD Renderings and Functional Block Diagrams

To make the structure of the bus apparent, the CAD renderings intentionally do not show every flight system component or instrument component. The EFI instrument was not baselined at the time of the MDL study, so it is absent on the renderings and block diagram of SC1.

Spacecraft 1

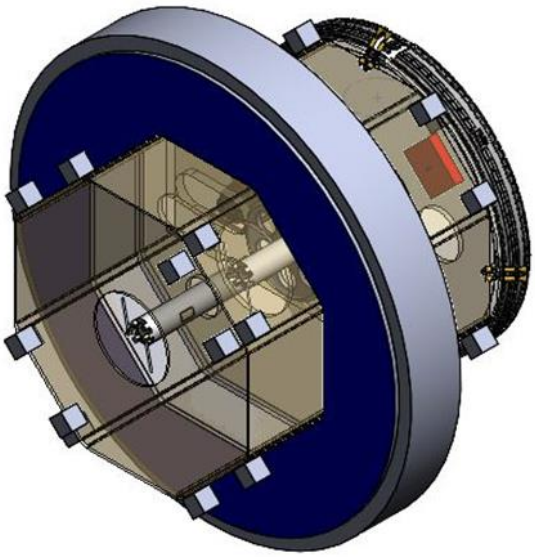

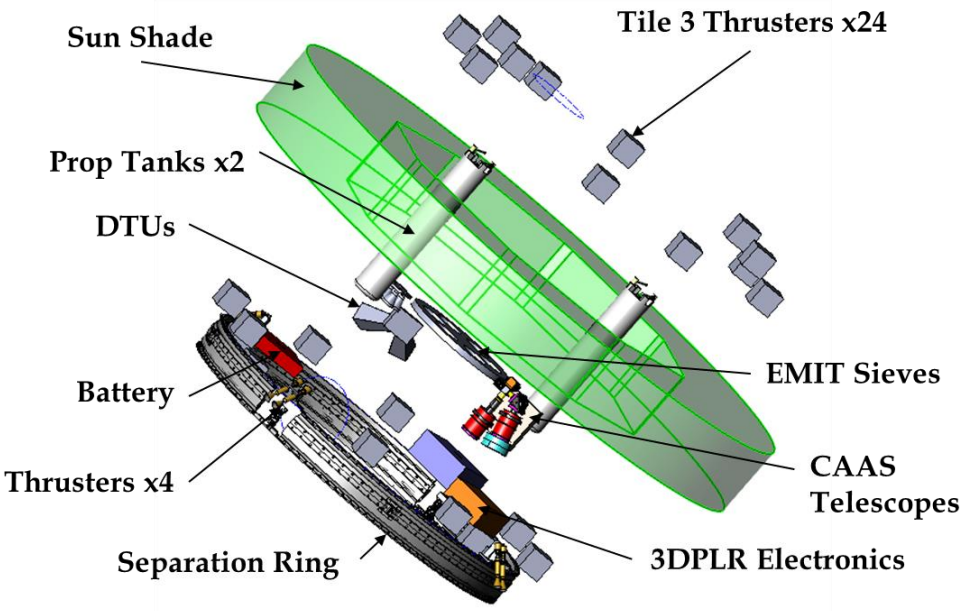

Spacecraft 2

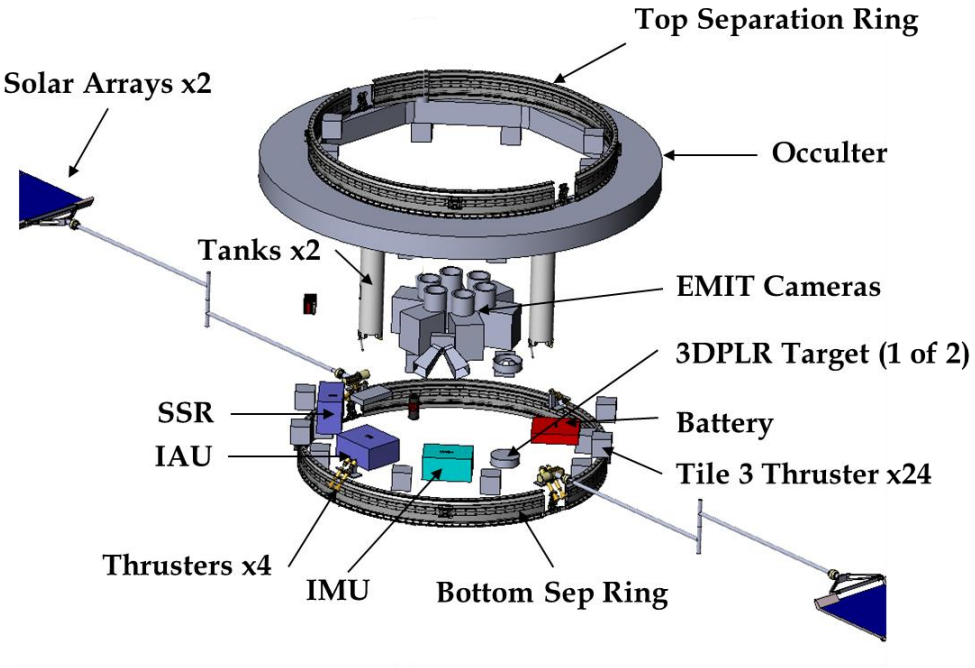

Spacecraft 3

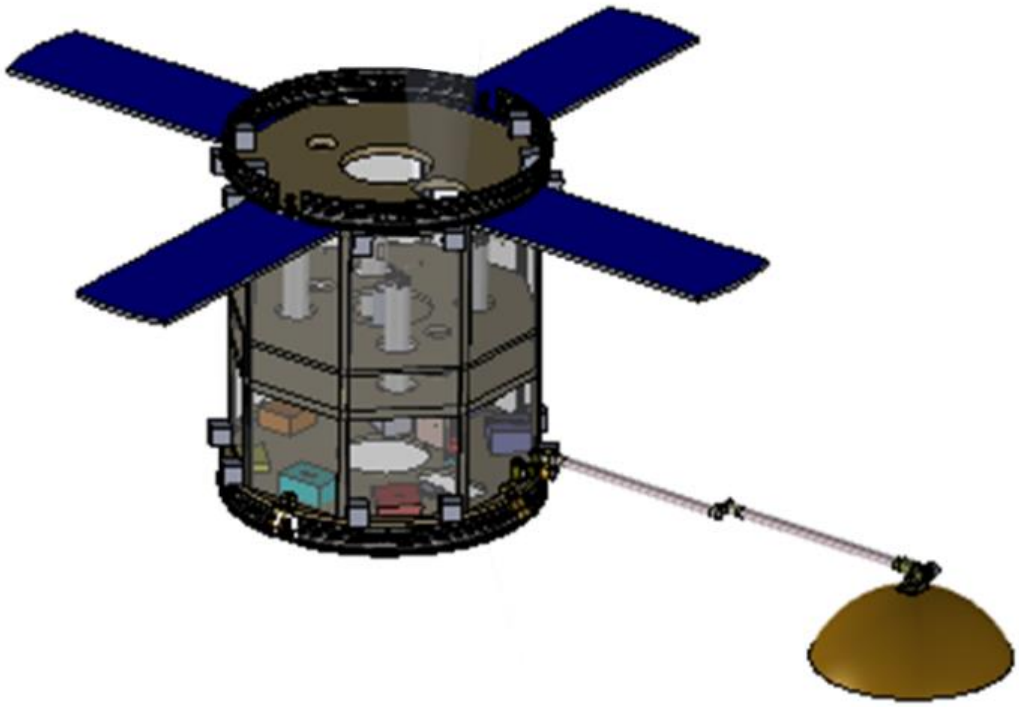

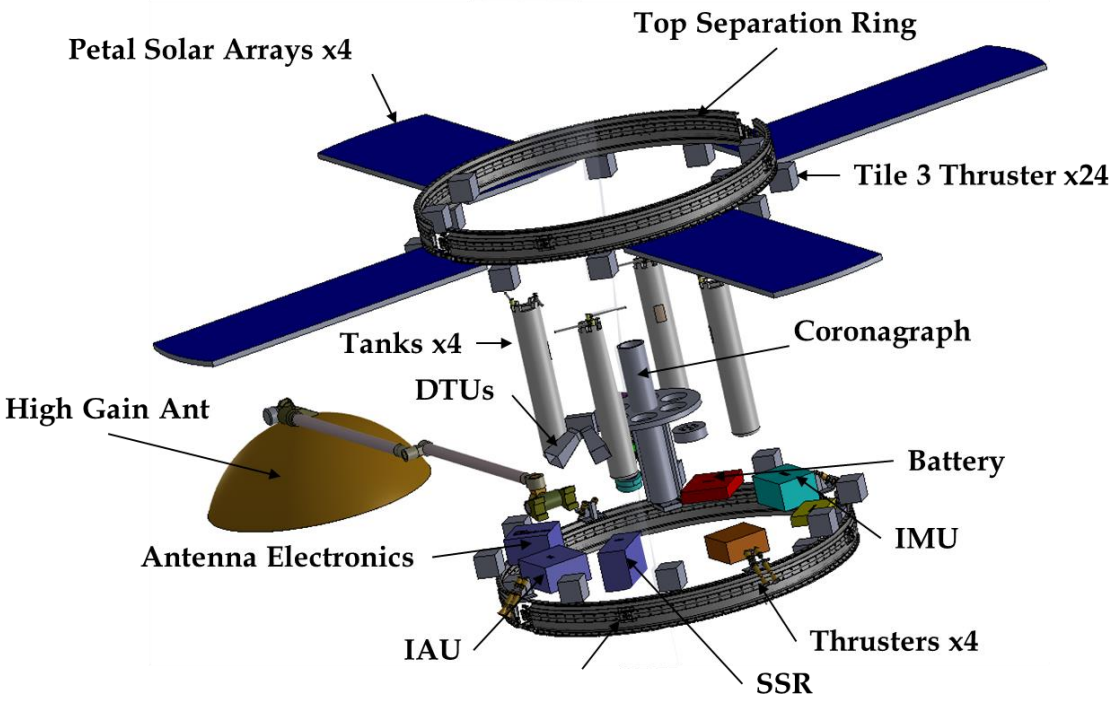

Spacecraft 1

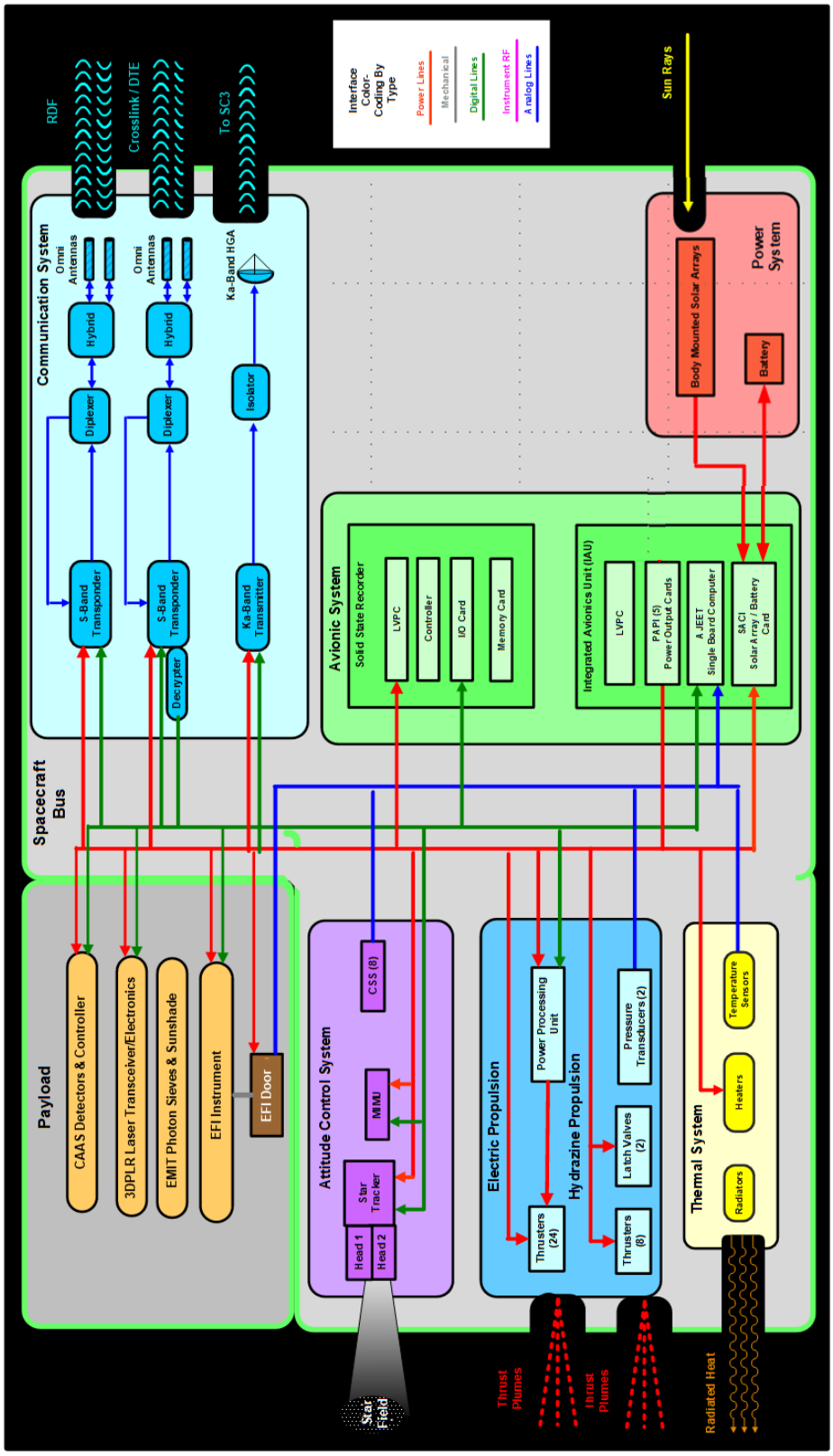

Spacecraft 2

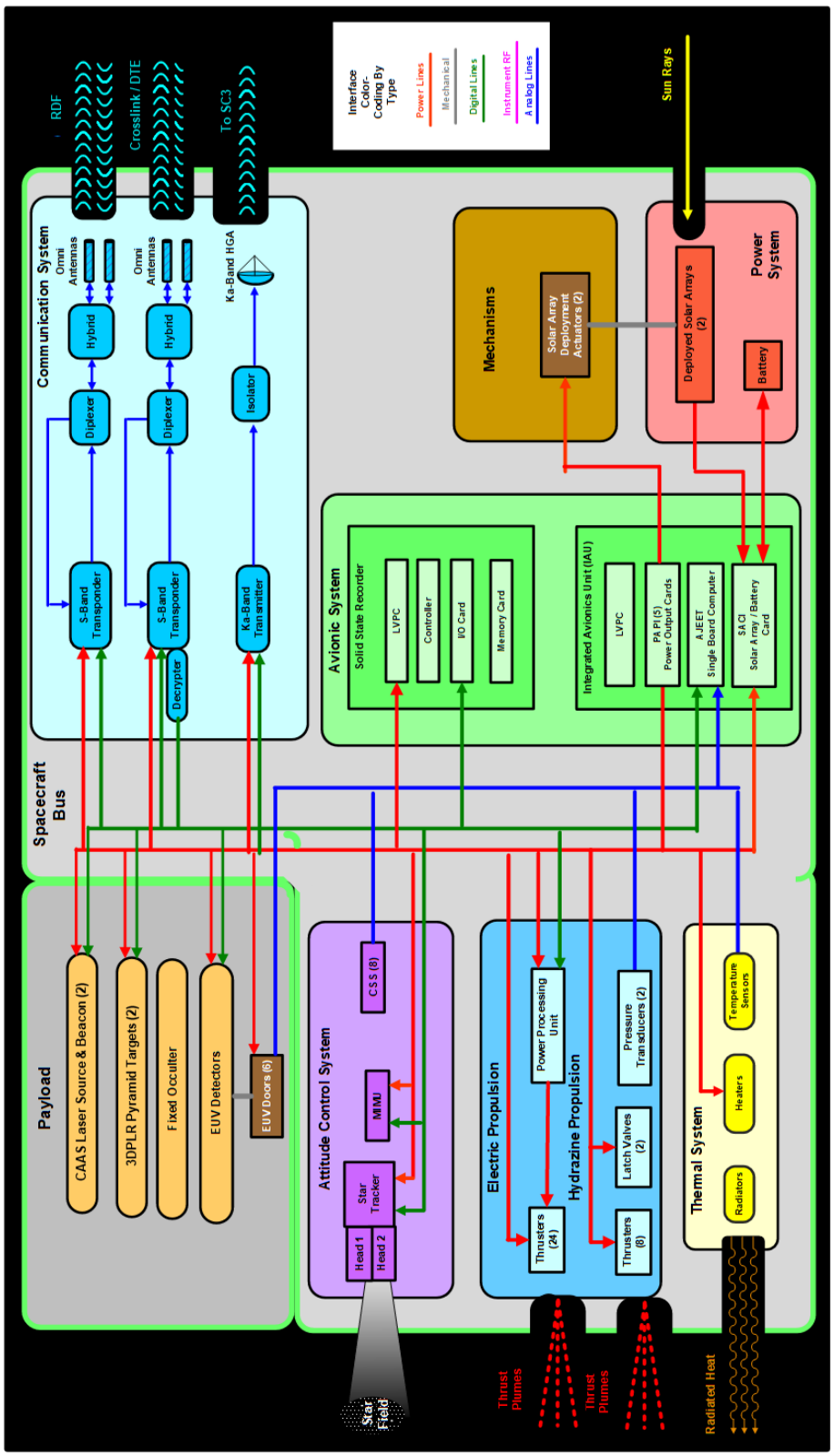

Spacecraft 3

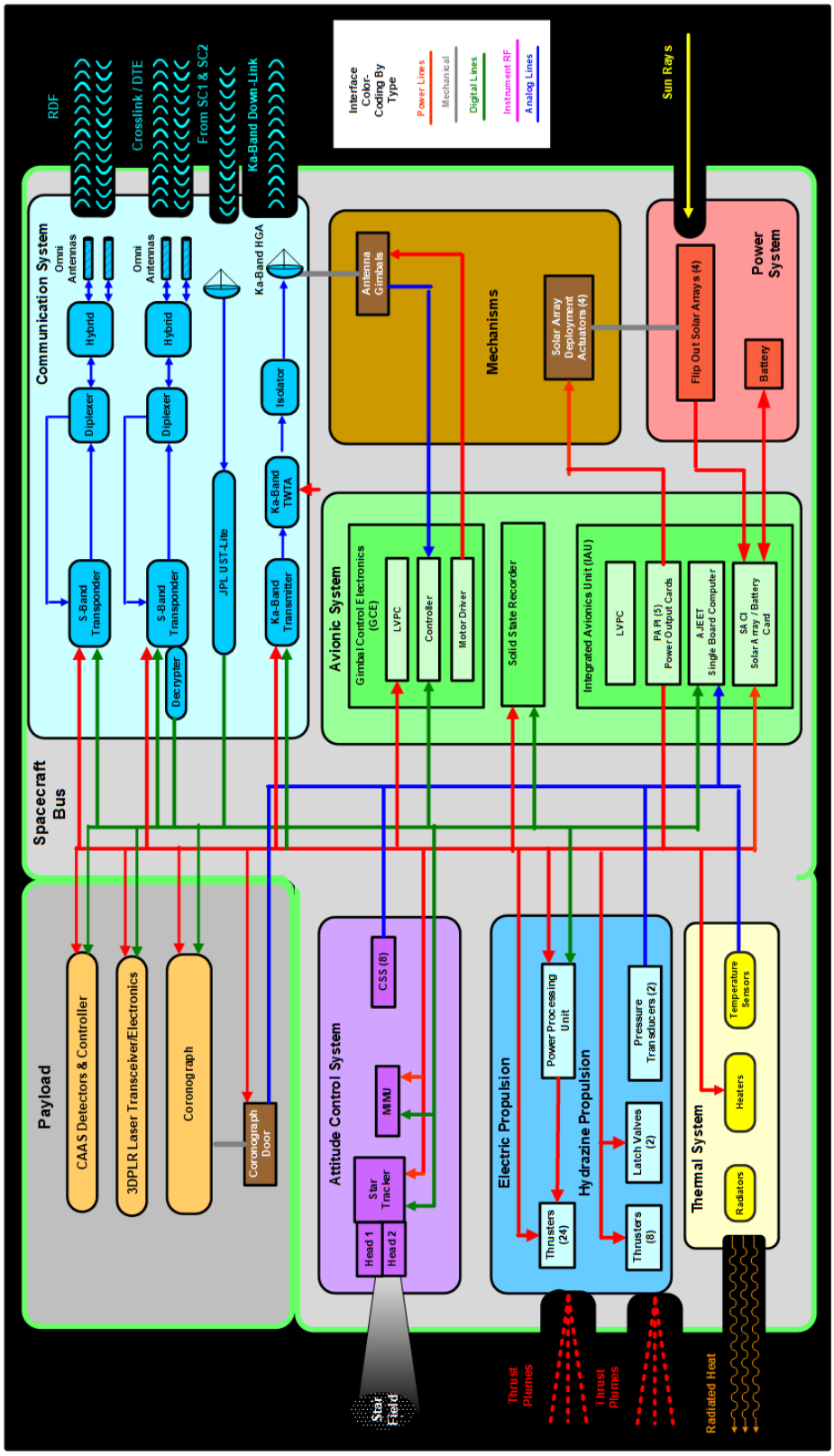

Appendix F. Optical Communications Option

Table 15 and the discussion in §3.3.1 summarize the potential scientific benefits of optical vs. radio frequency communications for CMO. This Appendix presents supporting details.

The key drivers of the optical advantage are simple: the optical data rate for both Intersatellite (ISC) and Direct-to-Earth (DTE) communications is 1.067 Gbps compared to 105 Mbps for S-band ISC and, constrained by onboard power, 315 Mbps for Ka-band DTE. There is also an operational benefit. In the RF baseline design, SC3 was the DTE communications satellite because of power constraints on SC2. Optical communications hardware reduces SWaP, particularly power: an estimated 86 W input power compared to amplified RF at 210 W. Consequently, SC2 (which generates the highest data volume because of EMIT), can be designated the DTE communications satellite. Figure 30 illustrates the optical communications architecture.

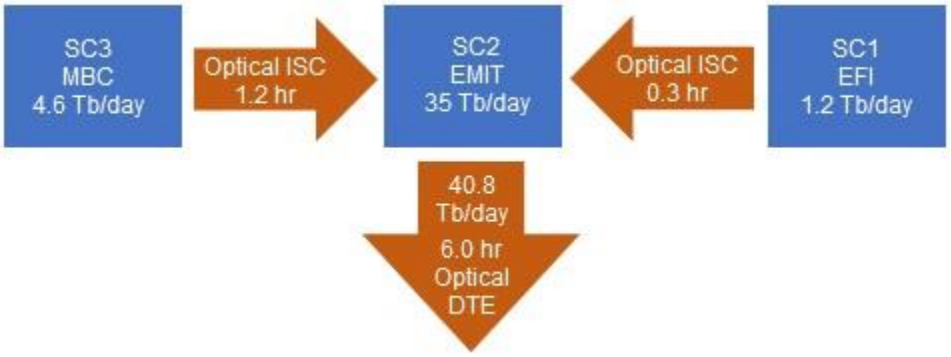

Figure 30. Data transfer architecture using optical links for both Intersatellite communications (ISC) and Direct to Earth (DTE) communications.

Requirements levied on the spacecraft bus by optical communications

R1: The bus shall provide 86 W of power for the optical communications subsystem while in communications mode (10 W in standby mode).

This requirement is a small increase compared to the 68 W in the baseline design of SC2 without the DTE function. R1 can be met by growing the area of the solar panels by 10%.

R2: The Sun-Earth L1 (SEL1) halo orbit shall be optimized so that the Sun Earth Vehicle Angle is greater than the minimum required.

The minimum SEV will be dictated by the Optical Ground Station (OGS) and is currently 12 deg. A 20-deg optimized halo orbit is comparable to the baseline SEL1 orbit, with the key difference that a second Lissajous Orbit Insertion (LOI) maneuver is needed about 1 year after launch. The magnitude of the LOI maneuver ranges within 20-60 m s^{-1} depending on the launch month. Station keeping (orbit maintenance) is minimal at 5-8 m s^{-1} over 4-5 years. These bounds contain contingency.

Figure 31 shows the optical contact duration to an OGS at DSN Goldstone during the CMO mission.

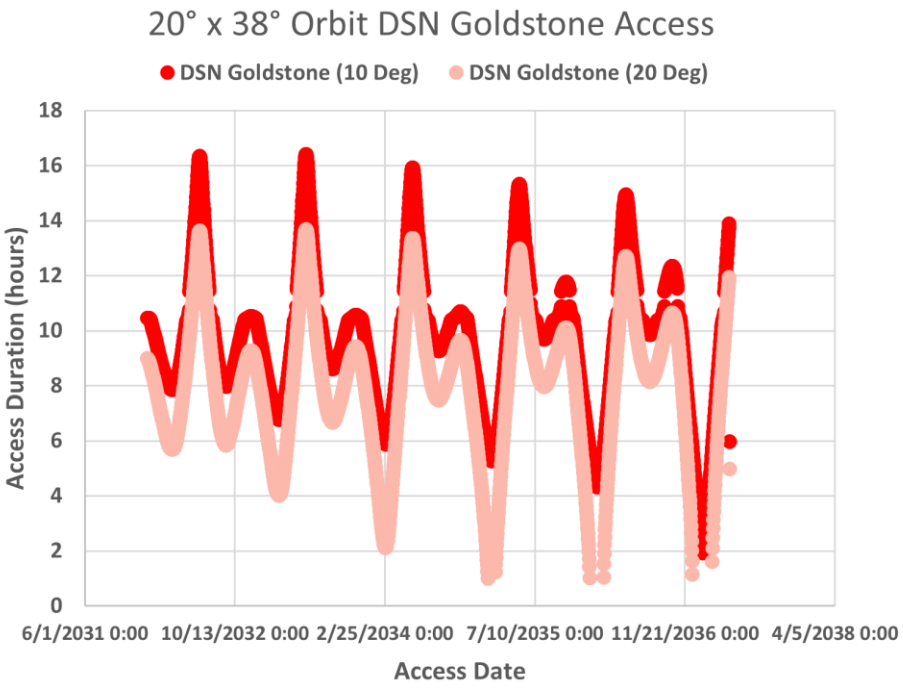

Figure 31. Connection duration (hr/day) to 8-m optical ground station at DSN Goldstone as a function of date for minimum required satellite elevation angles of 10° and 20°.

Optical System Architecture

The performance described above derives from hardware selected using the NASA Optical Communications Sustainment Study (OCSS, 2022). Fibertek components are the baseline because they have adequate power, aperture, and modem maturity, as well as the option of implementing Wavelength Division Multiplexing (WDM).

The Optical Space Terminal (OST) will utilize Wavelength-Division Multiplexing (WDM) to simultaneously transmit four PPM channels each operating at 267 Mbps. At the Ground Terminal (GT), the four channels will be received by the ground telescope, then spatially separated (demultiplexed) by filters downstream from the telescope with each channel directed to a Superconducting Nanowire Single Photon Detector (SNSPD). The electrical output from each SNSPD will be electronically processed (decoded) in a Ground Signal Processing Assembly (GSPA). In the final stage of the GSPA the four 267 Mbps data streams will be recombined into the original 1.067 Gbps data stream.

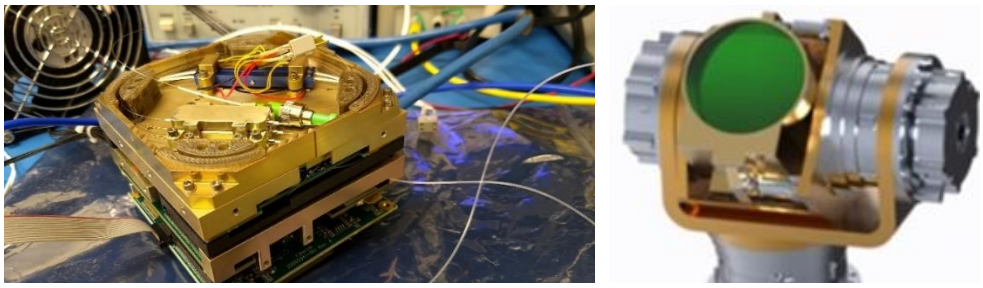

Figure 32. Fibertek “Trinity” Laser Electrical Module (LEM) (left) and Laser Optical Module (LOM) (right). LOM is 20.5 x 36.4 x 38.3 cm^3 and has a 10 cm telescope.

There is a trade between the SWaP of the OST and the size of the GT telescope aperture. Therefore, the GT telescope aperture and optics will be designed to receive enough optical signal power at each channel's SNSPD to receive data at 267Mbps under nominal conditions while maintaining low OST SWaP.

Optical Ground Station

The Optical Ground Station recommendation is the 8m hybrid DSN station estimated to be ready by early 2030s. This allows the power of the OST to be reduced, necessitating only a 2.5 W power amplifier. The use of a laser beacon array is assumed for acquisition and tracking on the ground.

The data rate and time needed to transmit remain unchanged with either OGS-OST combination. As the OGS size decreases, power needed on the spacecraft will increase. In case of the 34-m vs a 2-m ground telescope, the 34-m option provides more margin.

Radio Frequency (RF) communications are still required for command, ranging, and for the receipt of housekeeping and telemetry data. The 8-m hybrid antenna is the most optimal selection because it can simultaneously perform RF ranging, commanding, and receiving the CMO data via its optical segment.

The probability of all-day nominal weather increases from 68-79% for one OGS to ~97% with the addition of a second OGS in the southern hemisphere. Months with 10-15 hr links allow for missed data blocks to be re-transmitted. The long contact window also allows for scheduling around known climate patterns (e.g., showers at dusk). Margins are greatest with the 8-m OGS and range from 5 to 15 dB, sufficient to overcome partial cloudy cover. Recommended storage requirement is up to 3 days of science.

Table 25. Optical Ground Station trades

	DSN 8-m Hybrid Optical on 34-m RF	**3-4m class Astronomy Telescope rented**	**2-m LCOT-like build**
Electrical Power for OST on spacecraft	86 W in, 2.5W out	50 + 68 W in 8 W HPOA out	50 + 68 W in 8W HPOA out
Pros	The 8-m version is already planned to be completed by early 2030s. DSOC launching on Psyche in 2022 will validate 1.5-m segment.	Already built. "Bring your own receiver" concept can utilize DSOC copy with WDM mods. Rental is low cost.	Extension of a smaller proven aperture. Unconstrained time for loading.
Cons	Readiness can slip relative to CMO LOI.	Time needs to be negotiated. 3d party Sun keep-out angle must be enforced	Must be budgeted and built. Sun protection through a combination of sunshade and filter close to secondary mirror

Link Budget

Key Parameters:

- 1550nm band
- 4-channel WDM PPM
- 16-ary PPM
- CCSDS compliant
- 2.5 W TX total power for four channels
- 2 GHz slot rate
- 10-cm optical space telescope
- 8-m optical ground telescope
- SNSPD 64-array, reset < 50 ns
- WDM penalty: 1 dB

Table 26 presents the link budget. Table 27 gives the MEL and associated TRL levels for the baseline optical terminal.

Table 26. Optical communications link budget

L1 Range [km]	Atm. condition	FEC Code Rate	Each WDM Channel		WDM	
			Max. Data Rate (Mbps)	Link Margin [dB]	Max. Data Rate (Gbps)	Link Margin [dB]
1,130,000	Nominal	R 2/3	267	16.3	**1.07**	**15.3**
1,130,000	Stressed	R 2/3	267	10.9	**1.07**	**9.9**
1,470,000	Nominal	R 2/3	267	14.0	**1.07**	**13**
1,470,000	Stressed	R 2/3	267	8.6	**1.07**	**7.6**
1,810,000	Nominal	R 2/3	267	12.2	**1.07**	**11.2**

Table 27. FIbertek Trinity Flight Optical Terminal MEL and TRL

MASTER EQUIPMENT LIST (MEL)			
Subassembly / Component		Unit Mass [kg] (CBE)	Technology Readiness Level (TRL)
FiberTek-Trinity Flight Optical Terminal		**13.40**	5
Lasercom Electronics Module (LEM)			
1	LEM - Electronics Card Structural Assembly, fasteners	2.90	6
2	LEM - FPGA CLCT Controller Card	0.15	6
3	LEM - FPGA, Software Defined Modem, NASA GRC PPM Encoder	0.15	5
4	LEM - Transceiver TxRx, 3 cards, 6 Tx channels (2 spares), 1 RX channel	0.75	5
5	LEM- 28V Power DC-DC converter card	0.20	7
6	LEM - Fast Steering Electronics	0.10	6
7	LEM Backplane interface PWA	0.10	7
8	High Power Amplifier Card	0.15	7
Lasercom Optical Module (LOM)			
9	LOM - Structure Assy & Aft optics bench	1.50	6
10	LOM - Optical Telescope	1.00	6
11	LOM - Optical components	0.20	6
12	LOM - Laser Collimator Assembly	0.15	7
13	LOM - Fast Steering Mirror Assembly	0.20	7
14	LOM - PAT Camera	0.10	5
15	LOM - PAT Camera Electronics	0.15	4
16	LOM - Telescope Isolators	0.20	6
High Power Optical Amplifier (HPOA) 8W			
	Not needed. See item 8 instead		
Gimbal			
17	Gimbal Assembly	2.50	4
18	Yoke, Cable Wraps	2.40	4
19	Gimbal Controller	0.50	4

Appendix G. CEMA Cost-Risk Analysis

Figure 33 illustrates the Monte Carlo process used by CEMA to generate cost cumulative distribution functions (S-curves). Distributions are created for model input parameters based on CEMA best practices and MEL contingencies and margins.

Table 28–Table 30 show cost summaries (50% CL) and S-curves for the three CMO spacecraft.

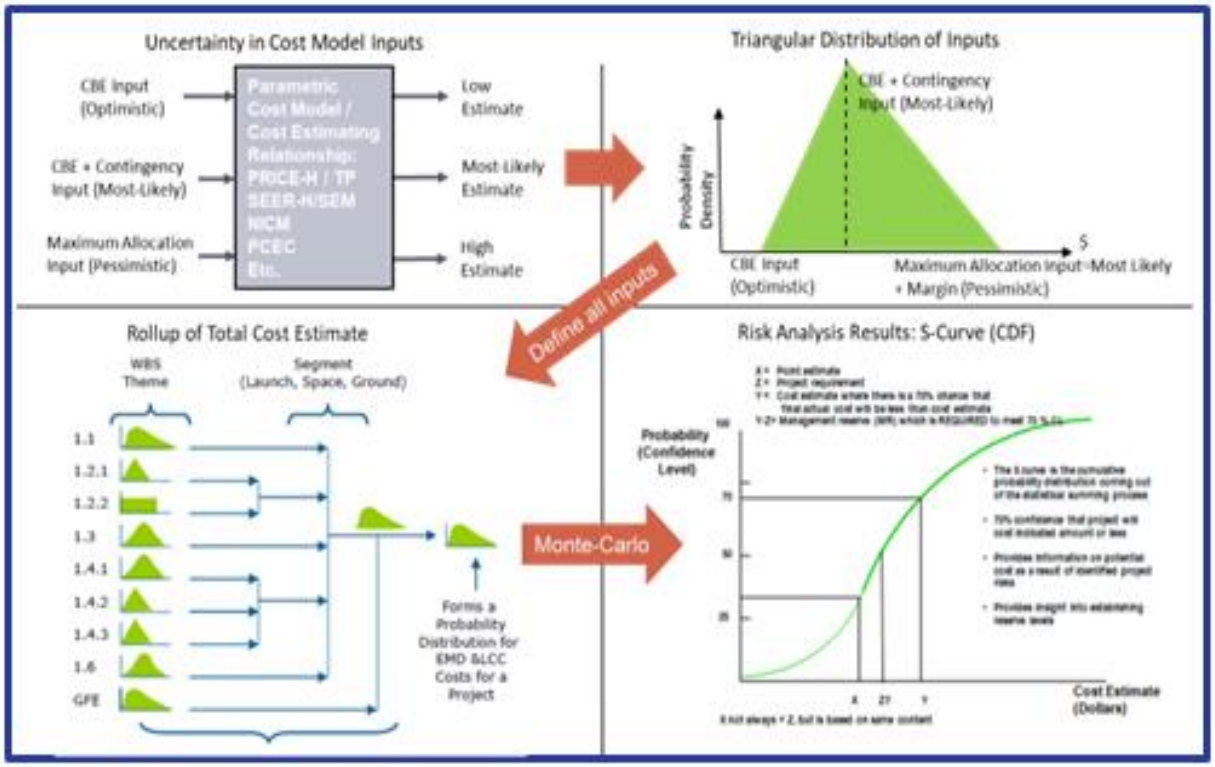

Figure 33. CEMA cost risk analysis process. Adapted from NASA Cost Estimating Handbook v4.0.

Table 28. Cost summary and S-curve for SC1.

MDL CMO Spacecraft #1 CEMA Independent Cost Risk Analysis (Development and Production Costs)	50% CL FY27$M	
Cost Model Summary **04-Oct-21**		
CMO Spacecraft #1	**$115.9**	
Attitude Control System		*$88.0*
Avionics System		*$10.3*
Communication System		*$2.3*
Mechanical System		*$9.4*
Propulsion System		*$13.8*
Electrical Power System		*$25.5*
Thermal System		*$6.5*
Management, Systems Engineering, Assembly, Integration & Test		*$19.3*
Additional Costs	**$31.6**	
FPGA Development		*$0.7*
Flight Software		*$10.1*
FSW Test Bed		*$0.5*
Flight Spares & Engineering Test Units		*$10.1*
Environmental Test		*$5.1*
Ground Support Equipment		*$5.1*
CMO Spacecraft #1 TOTAL	**$131.2**	

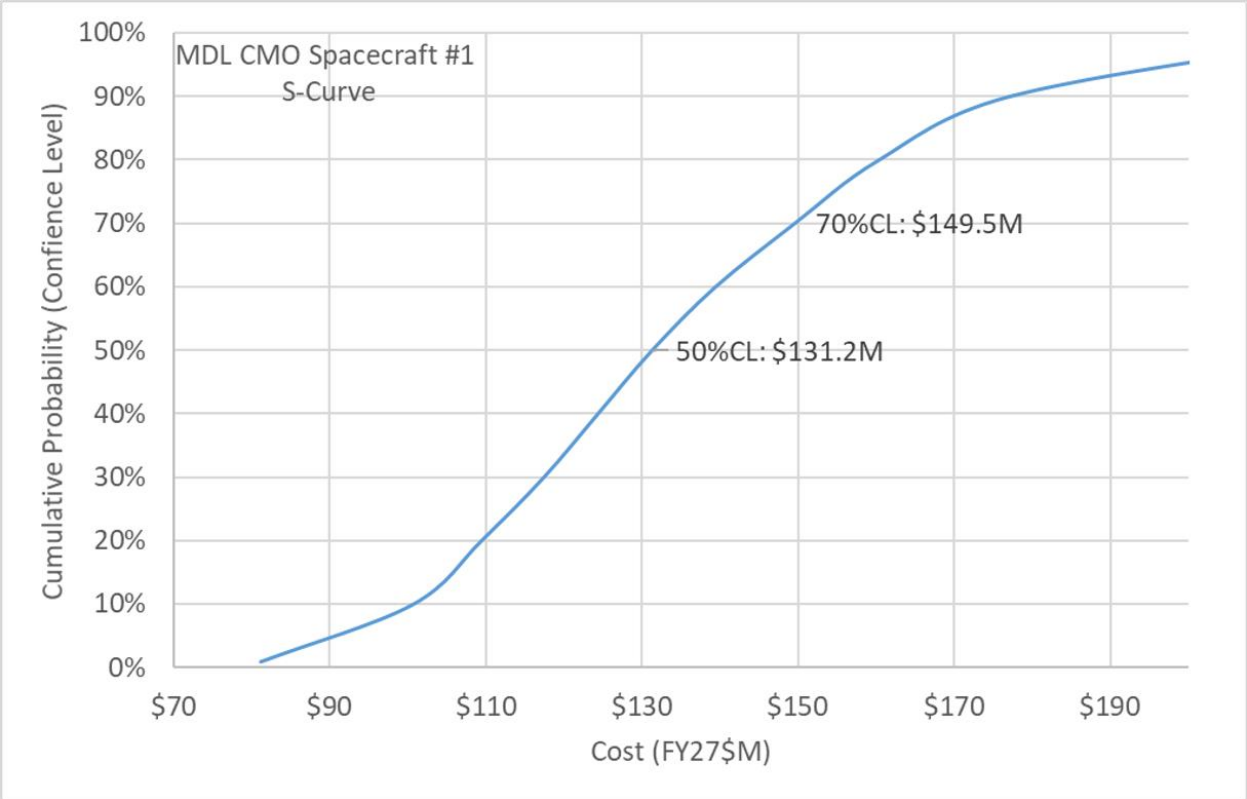

Table 29. Cost summary and S-curve for SC2.

MDL CMO Spacecraft #2 CEMA Independent Cost Risk Analysis (Development and Production Costs)	50% CL FY27$M	
Cost Model Summary **04-Oct-21**		
CMO Spacecraft #2	**$113.2**	
Attitude Control System		*$11.7*
Avionics System		*$7.2*
Communication System		*$15.8*
Mechanical System		*$19.6*
Propulsion System		*$24.5*
Electrical Power System		*$12.8*
Management, Systems Engineering, Assembly, Integration & Test		*$21.6*
Additional Costs	**$36.7**	
FPGA Development		*$1.6*
Flight Software		*$11.5*
FSW Test Bed		*$0.6*
Flight Spares & Engineering Test Units		*$11.5*
Environmental Test		*$5.8*
Ground Support Equipment		*$5.8*
CMO Spacecraft #2 TOTAL	**$149.9**	

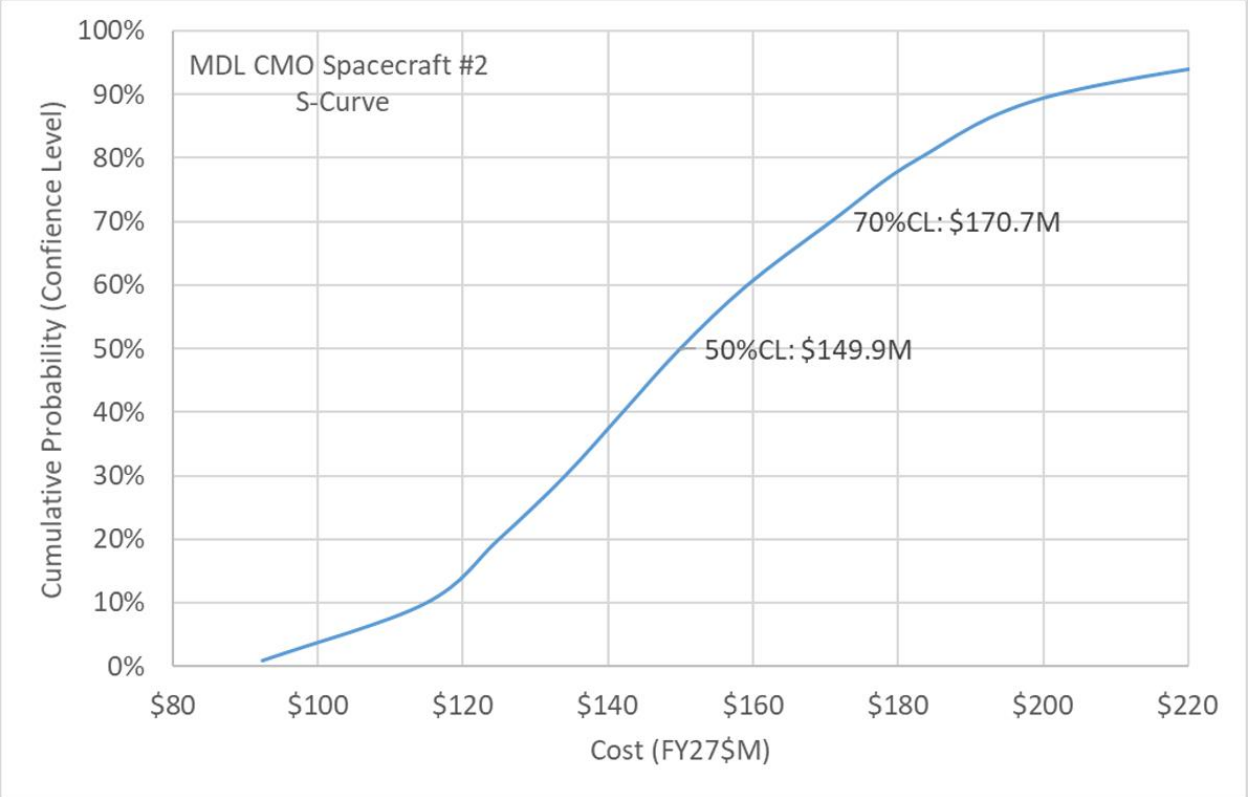

Table 30. Cost summary and S-curve for SC3.

CMO Spacecraft #3 CEMA Independent Cost Risk Analysis (Development and Production Costs)	50% CL FY27$M	
Cost Model Summary **04-Oct-21**		
CMO Spacecraft #3	**$130.4**	
Attitude Control System		*$11.7*
Avionics System		*$6.8*
Communication System		*$23.7*
Mechanical System		*$19.2*
Propulsion System		*$26.7*
Electrical Power System		*$21.0*
Thermal System		*$0.9*
Management, Systems Engineering, Assembly, Integration & Test		*$20.4*
Additional Costs	**$42.8**	
FPGA Development		*$2.2*
Flight Software		*$13.3*
FSW Test Bed		*$0.7*
Flight Spares & ETUs		*$13.3*
Ground Support Equipment		*$6.6*
Environmental Test		*$6.6*
CMO Spacecraft #3 TOTAL	**$173.2**	

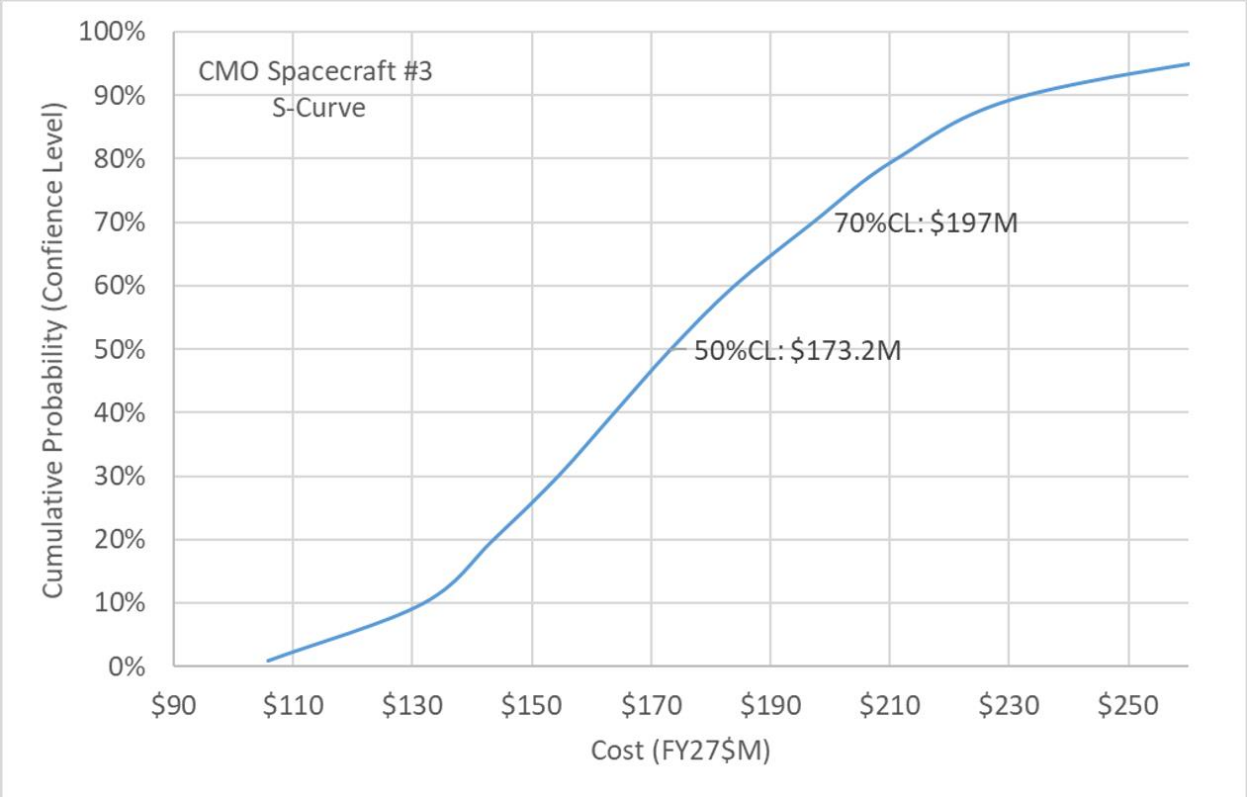

References

[1] D. Rabin, A. Novo-Gradac, A. Daw, J. Klimchuk, N. Viall, K. Denis, J. Newmark, S. Christe, E. Peretz, F. Kamalabadi, P. Chamberlin, L. Golub, I. De Moortel, A. Winebarger, D. Seaton, M. West, E. Mason and N. Reginald, "Observing Coronal Microscales and their Connection with Mesoscales," White paper for 2024 Decadal Survey of Solar and Space Physics (National Academy of Sciences), 2022.

[2] NASA, "Solar Terrestrial Probes Program (STP)," [Online]. Available: https://stp.gsfc.nasa.gov/program_details.html.

[3] J. Klimchuk, "Key aspects of coronal heating," *Philosophical Transactions of the Royal Society A,* vol. 373, no. 2042, pp. 20140256-20140256. doi:10.1098/rsta.2014.0256, 2015.

[4] K. Yang, D. Longcope, M. Ding and Y. Guo, "Observationally quantified reconnection providing a viable mechanism for active region coronal heating," *Nature Communications,* Vols. 9. doi:10.1038/s41467-018-03056-8 , 2018.

[5] N. Viall and J. Borovsky, "Nine outstanding questions of solar wind physics," *Journal of Geophysical Research Space Physics,* vol. 125, no. 7. doi:10.1029/2018JA026005, 2020.

[6] E. N. Parker, "Topological dissipation and the small-scale fields in turbulent gases," *Astrophysical Journal,* pp. 499-510. doi:10.1086/151512, 1972.

[7] J. Klimchuk, "Heating of the magnetically closed corona and physical models of solar and stellar spectral irradiances," White paper for 2024 Decadal Survey of Solar and Space Physics, 2022.

[8] A. Vourlidas, A. Caspi, Y.-K. Ko, M. Laming, J. Mason, M. Miralles, N.-E. Raouafi, J. Raymond, D. Seaton, L. Strachan, N. Viall, J. Vievering and M. West, "The critical coronal transition region: a physics-framed strategy to uncover the genesis of the solar wind and solar eruptions," White paper for 2024 Decadal Survey in Solar and Space Physics, 2022.

[9] L. Kepko, S. Merkin, N. Viall, A. Vourlidas and S. McIntosh, "Mesoscale dynamics - the key to unlocking the universal physics of multiscale feedback," White paper for 2024 Decadal Survey of Solar and Space Physics, 2022.

[10] J. Klimchuk, *private communication,* 2021.

[11] P. Antolin, I. De Moortel, T. Van Doorsselaere and T. Yokoyama, "Observational signatures of transverse magnetohydrodynamic waves and associated dynamic instabilities in coronal flux tubes," *Astrophysical Journal,* vol. 836, no. 2. doi:10.3847/1538-4357/aa5eb2, 2017.

[12] S. Habbal, M. Druckmüller, N. Alzate, A. Ding, J. Johnson, P. Starha, J. Hoderova, B. Boe, S. Constantinou and M. Arndt, "Identifying the coronal source regions of solar wind streams from total solar eclipse observations and in situ measurements extending over a solar cycle," *Astrophysical Journal Letters,* vol. 911, pp. L4. doi:10.3847/2041-8213/abe775, 2021.

[13] S. Tomczyk, E. Landi, B. Berkey, J. Burkepile, M. Cotter, D. Gallagher, M. Galley, R. Graves, P. Oakley, L. Perez-Gonzalez, S. d. T. G. Sewell and P. Zmarzly, "AGU Fall Meeting 2021 SH15G-2089," [Online]. Available: https://agu.confex.com/agu/fm21/meetingapp.cgi/Paper/986704.

[14] NASA Office of the Chief Technologist, "Technology Readiness Assessment Best Practices Guide (SP-20205003605)," NASA, 2020.

[15] NSF, "VISORS," [Online]. Available: https://ssdl.gatech.edu/research/projects/visors-virtual-super-resolution-optics-using-reconfigurable-swarms.

[16] L. Kipp, M. Skibowski, R. Johnson, R. Berndt, R. Adelung, S. Harm and R. Seeman, "Sharper images by focusing soft X-rays with photon sieves," *Nature,* vol. 414, pp. 184-188. doi:0.1038/35102526, 2001.

[17] L. Penin and others, "Proba-3: ESA's small satellites precise formation flying mission to study the Sun's inner corona as never before," in *Proceedings 34th Annual Small Satellite Conferece*, 2020.

[18] J. Jorgensen and M. Benn, "VBS - The Optical Rendezvous and Docking Sensor for PRISMA," *NordicSpace,* pp. 16-19, 2010.

[19] V. Noce and others, "Metrology on-board PROBA-3: The shadow position sensors subsystem," *Advances in Space Research,* vol. 67, no. 11, pp. 3807-3818. doi:0.1016/j.asr.2020.08.004., 2021.

[20] J. Ma, S. Masoodian, D. Starkey and E. Fossum, "Photon-number-resolving megapixel image sensor at room temperature without avalanche gain," *Optica,* vol. 4, no. 12. doi:10.1364/OPTICA.4.001474, 2017.

[21] B. De Pontieu and others, "Probing the physics of the solar atmosphere with the Multi-slit Solar Explorer (MUSE). I. Coronal heating," *Astrophysical Journal,* vol. 926, no. 1. doi:10.3847/1538-4357/ac4222, 2022.

[22] H. Futrell and others, "Key components of the Next Generation Solar Physics Mission (NGSPM)," 29 04 2022. [Online]. Available: https://ntrs.nasa.gov/search?q=euvst%20AND%20muse.

[23] K. Kobayashi and others, "The high-resolution coronal imager (Hi-C)," *Solar Physics,* vol. 289, pp. 4393-4412. doi:10.1007/s11207-014-0544-4, 2014.

[24] L. Rachmeler and others, "The high-resolution coronal imager, flight 2.1," *Solar Physics,* Vols. 294. doi:10.1007/s11207-019-1551-2, 2019.

[25] E. Renotte and others, "Design status of ASPIICS, an externally occulted coronagraph for PROBA-3," *Proceedings of SPIE,* vol. 9604. doi:10.1117/12.2186962, 2015.

[26] S. Shestov, A. Zhukov, B. Inhester, L. Dolla and M. Mierla, "Expected performances of the PROBA-3/ASPIICS solar coronagraph: Simulated data," *Astronomy and Astrophysics,* Vols. 652. doi:10.1051/0004-6361/202140467, 2021.

[27] C. Galy and others, "Straylight analysis on ASPIICS, PROBA-3 coronagraph," *Proceedings of SPIE,* vol. 11180. doi:10.1117/12.2536008, 2019.

[28] N. Reginald, J. Davila, O. C. St. Cyr and D. Rabin, "Electron temperature maps of the low solar corona: ISCORE results from the total solar eclipse of 1 August 2008 in China," *Journal of Geophysical Research: Space Physics,* vol. 122, no. 6, pp. 5856-5869. doi:10.1002/2017JA024014, 2017.

[29] N. Gopalswamy and others, "The balloon-borne investigation of temperature and speed of electrons in the corona (BITSE): mission description and preliminary results," *Solar Physics,* vol. 296, no. 1. doi:10.1007/s11207-020-01751-8., 2021.

[30] S. Shestov and others, "Scientific processing pipeline for ASPIICS coronagraph," *Proceedings of SPIE,* vol. 11443. doi:10.1117/12.2560164, 2020.

[31] T. RImmele and others, "The Daniel K. Inouye Solar Telescope – observatory overview," *Solar Physics,* Vols. 295. doi:10.1007/s11207-020-01736-7, 2020.

[32] W. Cao, N. Gorceix, R. Coulter, K. Ahn, T. Rimmele and P. Goode, "Scientific instrumentation for the 1.6 m New Solar Telescope in Big Bear," *Astronomische Nachrichten,* vol. 331, no. 6, pp. 636-639. doi:10.1002/asna.201011390, 2010.

[33] C. Denker, C. Kuckein, M. Verma, S. Gonzalez Manrique, A. Diercke, H. Enke, J. Klar, H. Balthasar, R. Louis and E. Dineva, "High-cadence imaging and imaging spectroscopy at the GREGOR Solar Telescope," *Astrophysical Journal,* vol. 236, no. 5. doi:10.3847/1538-4365/aab773, 2018.

[34] S. Tiraplegui, D. Serrano, L. Penin, R. Contreras, G. Rodriguez, J. Villa, D. Galano, R. Rougeot and K. Mellab, "Proba-3: challenges and needs for sub-millimetre autonomous formation flying," in *8th European Conference for Aeronautics and Aerospace Sciences (EUCASS)*, doi:10.13009/EUCASS2019-764, 2019.

[35] G. Marr, "Orbit Determination (OD) Error Analysis Results for the Triana Sun-Earth L1 Libration Point Mission," in *Big Sky, MT 2003AAS/AIAA Astrodynamics Specialist Conference*, 2003.

[36] N. Pokrupa, N. Ahlgren, T. Karlsson, P. Bodin and R. Larsson, "One year of in-flight results from the Prisma formation flying demonstration mission," in *25th Annual AIAA/USU Conference on Small Satellites*, 2011.

[37] G. Andersen, "Large optical photon sieve," *Optics Letters,* vol. 30, no. 2, pp. 2976-2978. doi:10.1364/OL.30.002976, 2005.

[38] J. Davila, "High-resolution solar imaging with a photon sieve," *Proceedings SPIE,* vol. 8148. doi:10.1117/12.898956, 2011.

[39] F. Laermer and A. Schilp, "Method of anisotropically etching silicon". US Patent 5501893, 26 March 1996.

[40] D. Goldfarb, "Fabrication of a full-size EUV pellicle based on silicon nitride," *Proceedings SPIE,* vol. 9635. doi:10.1117/12.2196901, 2015.

[41] C. Hou, "Novel diffractive optical element: binary photon sieve," *Optical Engineering,* vol. 50. doi:10.1117/1.3589294, 2011.

[42] M. Blauw, T. Zijlstra and D. van der Drift, "Balancing the etching and passivation in time-multiplexed deep dry etching of silicon," *Journal of Vacuum Tecnology B,* vol. 19. doi:10.1116/1.1415511, 2001.

[43] K. Keskinbora, C. Grevent, M. Hirscher, M. Weigand and G. Schutz, "Single-Step 3D Nanofabrication of Kinoform Optics via Gray-Scale Focused Ion Beam Lithography for Efficient X-Ray Focusing," *Advanced Optical Materials,* vol. 3, no. 6. doi:10.1002/adom.201400411, 2015.

[44] J. Yeom, Y. Wu, J. Selby and M. Shannon, "Maximum achievable aspect ratio in deep reactive ion etching of silicon due to aspect ratio dependent transport and the microloading effect," *Journal of Vacuum Science & Technology B,* vol. 23. doi:10.1116/1.2101678, 2005.

[45] "PROBA-3 (Project for On-Board Autonomy-3)," [Online]. Available: https://www.eoportal.org/satellite-missions/proba-3.

[46] G. Yang, L. W., X. Sun, J. Chen and M. Krainak, "Innovative free space optical communication and navigation system with high data rate communication, precision ranging, range rate measurements, and accurate spacecraft pointing," *Proceedings SPIE,* vol. 9739. , no. doi:10.1117/12.2197923, 2016.

[47] A. Novo-Gradac, G. Yang, S. Li and J. Davila, "Relative position sensing for a precision formation flying space telescope," in *9th International Workshop on Satellite Constellations and Formation Flying (IWSCFF)*, Boulder, CO, 2017.

[48] S. Wang, R. Farley, ,. J. Goebel, M. Heifetz, ,. J. Lipa and J. Turneaure, "Science telescope for Gravity Probe B," *Proceedings SPIE,* vol. 5172, pp. 108-118. doi:10.1117/12.513934, 2003.

[49] P. Calhoun, A. Novo-Gradac and N. Shah, "Spacecraft alignment determination and control for dual spacecraft precision formation flying"," *Acta Astronautica,* vol. 153, pp. 349-356. doi:10.1016/j.actaastro.2018.02.021, 2018.